**UNIVERSITY OF CATANIA**

**Department of Chemistry**

**International PhD in Chemical Sciences XXX cycle**

---

**NICOLETTA FRANCESCA**

# Design and synthesis of new processable materials for application in organic devices

Final thesis

Coordinator:

Prof. S. Sortino

Tutor:

Prof. C. Fortuna

---

**ACADEMIC YEAR 2016-2017**

*I have not failed,*
*I have only discovered*
*10.000 ways that didn't work!*

*Thomas Edison*

# Table of contents

Introduction ..... 7
1. Energy demand from alternative sources ..... 8
2. Organic polyconjugated compounds: new materials for optoelectronic devices ..... 9
3. Organic solar cells ..... 12
3.1 Architecture of organic photovoltaic devices ..... 17
4. Demand of alternative materials in transistors production ..... 20
4.1 Organic field effect transistors ..... 21
5. Compounds with diketopyrrolopyrrole structure ..... 23
Results and discussion ..... 28
6. New triazole-diketopyrrolopyrrole derivatives with tunable solubility ..... 29
6.1 Synthesis of small molecules ..... 31
6.2 Solubility of the small molecules ..... 33
6.3 UV-Vis characterization in solution and in the solid state ..... 34
6.4 Determination of HOMO and LUMO levels ..... 38
6.5 Preliminary tests in solar cells ..... 40
7. New conjugated polymers for bulk heterojunction solar cells ..... 43
7.1 GPC characterization of the polymers ..... 47
7.2 UV-Vis characterization of the polymers ..... 48
7.3 Thermal treatment of polymers **TegDPPK** and **TegDPPK1** ..... 50
7.4 Determination of HOMO and LUMO levels of the polymers ..... 53
7.5 Tests in BHJ solar cells ..... 55
7.6 Tests in organic field-effect transistor ..... 59
8 Synthesis of **TegDPPBDT-HMW** and **EHDPPBDT** ..... 61

8.1 GPC characterization of the polymers ..... 62
8.2 UV-Vis characterization in solution and in the solid state ..... 63
8.3 Determination of HOMO and LUMO levels ..... 65
8.4 Tests in organic field-effect transistor ..... 66
Conclusions ..... 68
Experimental section ..... 72
9 Solvents and reagents ..... 73
9.1 Instruments ..... 73
10 Synthesis of **2a** ..... 75
10.1 Synthesis of **TegDPP** ..... 76
10.2 Synthesis of **TegDPPBr$_2$** ..... 77
10.3 Synthesis of **2c** ..... 78
10.4 Synthesis of **3a** ..... 80
10.5 Synthesis of **3b** ..... 81
10.6 Synthesis of **3c** ..... 82
10.7 Synthesis of **4a** ..... 84
10.8 Synthesis of **4b** ..... 85
10.9 Synthesis of **4c** ..... 86
10.10 Synthesis of **5a** ..... 87
10.11 Synthesis of **5b** ..... 88
10.12 Synthesis of **5c** ..... 90
10.13 Synthesis of **5d** ..... 91
10.14 Synthesis of **5e** ..... 93
10.15 Synthesis of **5f** ..... 94
11 Fabrication of **5a** in BHJ solar cells ..... 96
12 Synthesis of the copolymer **TegDPPV** ..... 97

12.1 Synthesis of the copolymer **TegDPPT** ..... 98
12.2 Synthesis of the copolymer **TegDPPBDT**..... 99
12.3 Synthesis of 2-(2-(2-methoxyethoxy)ethoxy)ethyl 2,5-dibromothiophen-3-carboxylate ..... 100
12.4 Synthesis of the polymer **TegDPPTegES** ..... 101
12.5 Synthesis of 4-(2,3-bis(tert-butyldimethylsilyloxy) propoxy)-2-methylbutan-2-yl 2,5-dibromo-thiophene-3-carboxylate ..... 102
12.6 Synthesis of the polymer **TegDPPK**..... 104
12.7 Deprotection of the hydroxyl groups in the **TegDPPK** ..... 105
12.8 Synthesis of the polymer **TegDPPK1**..... 106
12.9 Deprotection of the hydroxyl groups in the **TegDPPK1** ..... 107
13 Fabrication of **TegDPPBDT** in BHJ solar cells..... 108
13.1 Fabrication of **TegDPPBDT** in OFETs ..... 108
14 Synthesis of the polymer **TegDPPBDT-HMW**..... 110
14.1 Synthesis of the polymer **EHDPPBDT**..... 111
Appendix spectra ..... 112
Bibliography ..... 131

# Introduction

# 1. Energy demand from alternative sources

The growing energy demand and the gradual exhaustion of fossil fuels have, in recent years, pushed the national governments to adopt energy policies aimed at the exploitation of so-called renewable energy, energy that is derived from unlimited energy sources over time, in order to restrict emissions of pollutants or greenhouse gases. Some examples are hydroelectric, wind, marine, geothermal, solar and biomass produced energy.

Big investments have been devoted to study photovoltaic energy and to development of photovoltaic cells more efficient and economical.

Photovoltaic energy exploits the photovoltaic effect that occurs at the interface of a junction between a p-doped and an n-doped semiconductor (p-n junction).

To date, the monocrystalline, polycrystalline or amorphous silicon form the majority of the photovoltaic modules on the market, with an efficiency of power conversion of the solar spectrum into electrical energy, up to 20-25%. However, the production costs are still thus leading to a cost per watt/hour higher than that supported by burning fossil fuels. Therefore, the only way to make photovoltaic competitive should focus on increasing production volumes and efficiency or on introducing new technologies and new materials.

The organic photovoltaic (**OPV**) cells have emerged to meet these needs, a thin film of just a few microns constitutes them, but they have efficiencies slightly lower, compared to classical silicon cells. The costs are significantly

lower, thanks to the reduction of high temperature processes, lower than the melting temperature of silicon (1414 °C), and to the use of lower amounts of semiconductor material. Against a lower efficiency, this shows the significant advantages both as regards the costs, that the versatility of the applications.

The versatility of organic solar cells resides in: i) low-cost technology of production, ii) possibility to be realized with flexible substrates and iii) more easy processability than silicon[1]. Besides, these materials can be printed easily on large areas using them as inks, dissolved in organic solvents. The structures can be cut and realized in any size and shape. Furthermore, they form colored and semitransparent films.

# 2. Organic polyconjugated compounds: new materials for optoelectronic devices

The classical inorganic semiconductors are characterized by conduction bands, however also a simple organic molecule it is characterized by the **HOMO** and **LUMO** orbitals. Numerous studies show that the formation of a polymer chain[2] determines the approach between them of the empty orbitals, and in the same way of those full. In this way, the energy gap between HOMO and LUMO levels decreases (figure 2.1).

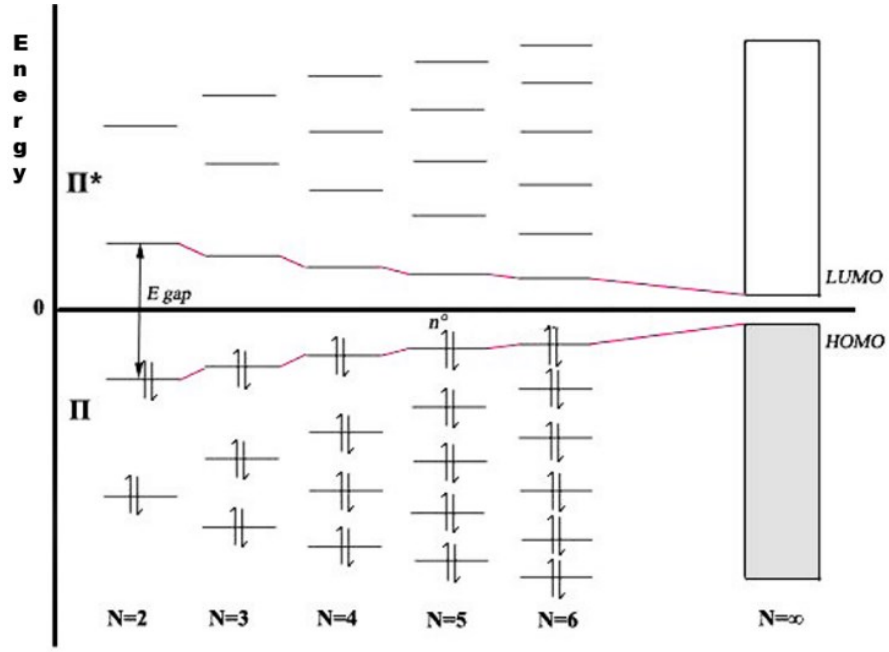


**Figure 2.1:** Energy levels calculated for oligomers and polymers.

To behave as semiconductor, an organic molecule must possess a sequence of planar carbon atoms ($sp^2$ or **sp** hybridization) and each carbon atom bears a $p_z$ orbital able to give overlap with the adjacent orbitals.

The energy gap ($E_g$) is the energy range between the lowest unoccupied molecular orbital (**LUMO**) and the higher occupied (**HOMO**): this is one of the most important chemico-physical parameters in determining the opto-electronic properties of a semiconductor, since it is strongly connected to the structure of the polyconjugated molecules.

The many structural changes, allow the fine-tuning of the optical and electronic properties over a wide range, which is currently unthinkable for inorganic materials. Figure 2.2 shows some polyconjugated structures and their band gap values.

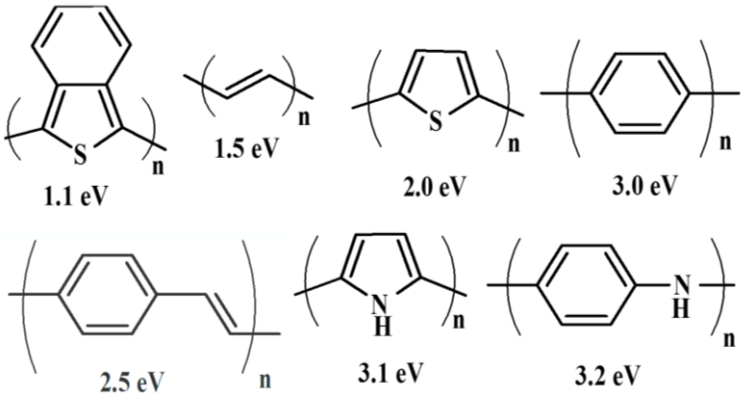


**Figure 2.2:** Examples of polyconjugated polymers.

The main factors that allows to modulate the band gap in the polyconjugated compounds are listed below:

1. Structure of the conjugate skeleton
2. Length of the conjugated system
3. Presence of electronic substituents
4. Presence of distortion
5. Inter-chain interactions.

Roncalì[3] rationalizes these effects in the following equation:

$$E_g = E_{res}+E_{\delta r}+E_{sub}+E_{\theta}+E_{int}$$

where the terms $E_{res}$ and $E_{\delta r}$ refer to the structure and length of the conjugated system, the $E_{sub}$ is the electronic effect of substituents, the $E_{\theta}$ is related to the effect of deviation from the flatness and the $E_{int}$ is about the effect of interchain interaction in the solid state.

The electronic effect, electron-donor or electron-withdrawing, of the substituents on the conjugate skeleton causes a variation of the energy gap as figure 2.3 shows.

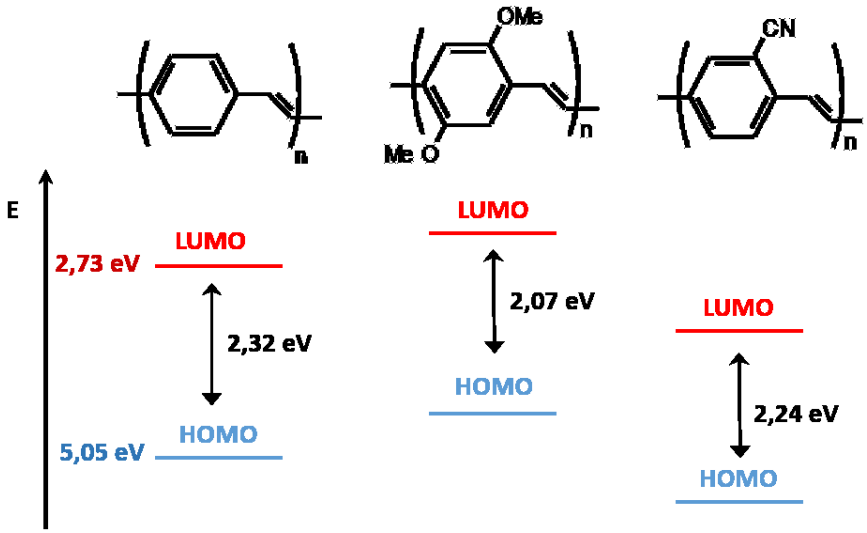


**Figure 2.3:** Electronic effect of the substituents.

In the case of Poly(p-phenylene vinylene) (PPV), for example, the introduction of electron-donor groups destabilizes both the level HOMO and LUMO. The effect, however, is much more pronounced on the HOMO level so the band gap is reduced. The reduction in the band gap is then due to an asymmetrical destabilization of HOMO and LUMO levels.

## 3. Organic solar cells

The use of active organic layers, based on donor-acceptor polymers plays a very important role, given their easiness of synthesis. The thin organic semiconductor films, show high absorption coefficients ($10^5$ $cm^{-1}$) and low oxidation potential of the excited state; these properties make them efficient donors in the generation of photo-induced charge separation within the solar cells. Usually films with thicknesses of about 100 nm are sufficient to obtain an operating solar cell.[4]

Generally, the mobility of holes and electrons for a single material are not the same, and the work functions of the cathodes, commonly used, do not match perfectly with **LUMO** orbital of most of the organic semiconductor polymers.[5] Consequently, a single polymer will hardly be able to generate the charge separation and to ensure the migration to the electrodes without recombination. The blending of polymers with different conjugated systems (i.e. electron acceptors, such as fullerene $\mathbf{C_{60}}$), is a very efficient method to achieve the separation of excitons into free carriers, through a photo-induced electron transfer from the polymer to the fullerene (figure 3.1).

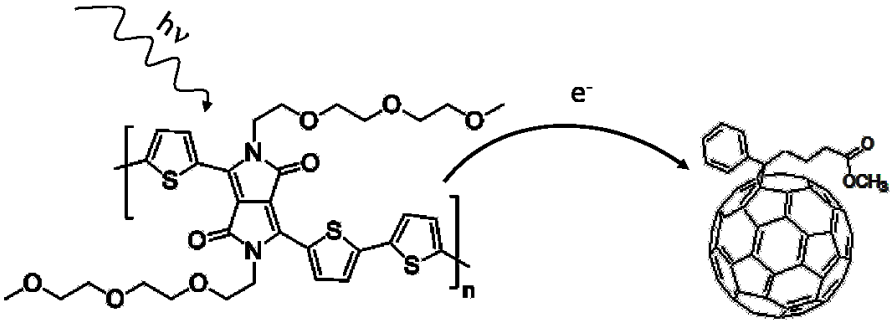


**Figure 3.1**: Photo-induced electron transfer from organic polymer to fullerene.

The charge transfer from the excited state of the polymer towards the **LUMO** of an acceptor material, which is located at a lower energy level, is thermodynamically favorable[6]. In figure 3.2, it is reported a scheme for the photo-induced charge transfer process of the polymer/fullerene system.

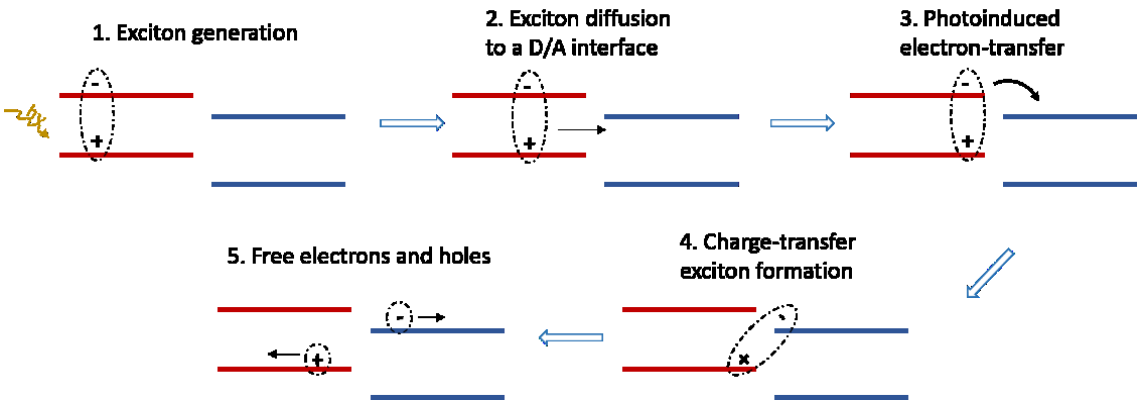


**Figure 3.2:** Schematization of the photo-induced charge separation between donor and acceptor.

The best performance for an organic solar cell is obtained through the so-called bulk heterojunction (**BHJ**): two different materials are used as carriers of holes and electrons, as well as different doping of silicon that generate the p-n junctions, which are the basis of the inorganic photovoltaic systems. Double-layer devices (donor-acceptor) can therefore be used as classic p-n junctions.[3]

The following steps describe the process of conversion of light into electricity via an organic solar cell:

1) absorption of a photon that leads to the formation of an exciton along the polymeric chain, this generate the electron-hole pair;
2) the exciton diffuses along the material until it reaches a region where its dissociation can take place (charge separation): generally the interface between the two materials where the separation of charge is favored;
3) charge transport within the organic semiconductor to the respective electrodes.[7]

The first step in the photovoltaic mechanism, which converts light energy into electrical energy, involves the absorption of sunlight by the

photoactive materials. The maximum of absorption of sunlight is around 700 nm, which correspond at a low band gap of about 1.77 eV, therefore is necessary to design polymers that adsorbed in the red and near-infrared ranges. To date, the better strategy to model the polymers $\mathbf{E_g}$, is the alternation of a conjugated electron-rich donor (D) unit and a conjugated electron-deficient acceptor (A) unit in the same backbone.[8,9]

In order to avoid a rapid decay (radiatively or non-radiatively), the exciton must be formed at a distance, from the interface, lower its diffusion length (typically 5-14 nm).[10,11] Therefore, the ideal situation occurs when the donor and acceptor phases form a bicontinuous interpenetrating network at nanometer level. This is the case of the **BHJ**, which exhibits a separation of the donor-acceptor phases ranging between 10 and 20 nm (figure 3.3). In this network, each interface is at a distance, from the site of absorption, lower than the length of exciton diffusion. In this way, it is also considerably increased the interfacial area between the donor and acceptor phases which results in higher efficiencies of the solar cells. The **BHJ** may be obtained by deposition of donor-acceptor mixtures from solution.[12]

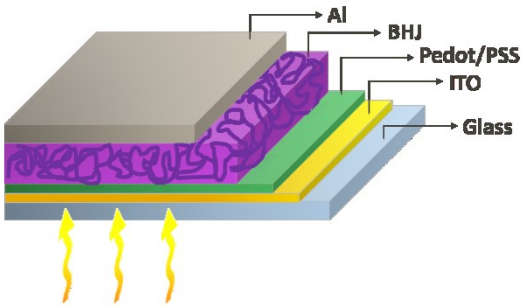


**Figure 3.3:** Schematic view of a bulk heterojunction solar cell.

The poly(p-phenylenevinylene) (PPV), polythiophenes (PT) and polyfluorene (PFO) are among the materials commonly used in organic photovoltaics. We can also mention the poly [2-methoxy-5-(3',7'-dimethyloctyloxy)-1,4-phenylenevinylene] (MDMO-PPV) and the poly (3-hexylthiophene) (P3HT) (figure 3.4).

The Buckminster fullerene (**$C_{60}$**),[13] has the **LUMO** orbital energetically close to the work function of the cathode (aluminum coated with LiF or calcium). Given the limited solubility of **$C_{60}$**, Wudl synthesized a soluble derivative of the **$C_{60}$**, the 1-(3-methoxycarbonyl) propyl-1-phenyl [6,6] $C_{61}$ (**$PC_{60}BM$**)[6] (figure 3.4), which is widely used as acceptor in the solar cell polymer/fullerene. For its structural symmetry, the PCBM, has an insufficient absorption in the visible region so this determined a low efficiency of **BHJ** devices, but the situation can be further improved by replacing acceptor **$C_{60}$ PCBM** with its higher fullerene analogue **$C_{70}$ PCBM** (**$PC_{71}BM$**), which has lower symmetry and allows more transitions.[14,15]

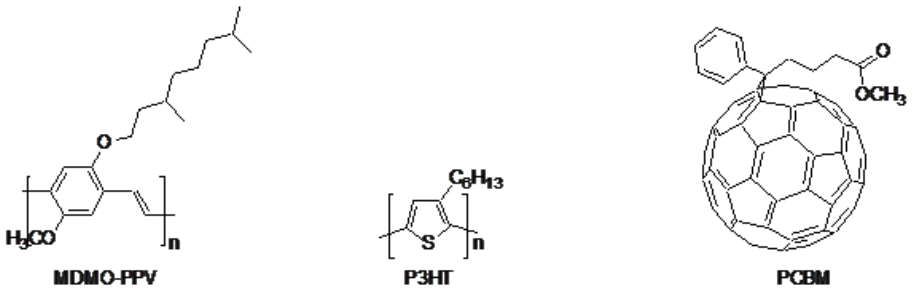


**Figure 3.4:** MDMO-PPV, P3HT and PCBM.

## 3.1 Architecture of organic photovoltaic devices

The techniques of deposition from solution are the methods of preparation of thin films most commonly used in the production of **BHJ** solar cells. In fact, the polymers should decompose if subjected to excessive heat and have molar masses too large to be evaporated under vacuum. The most commonly used techniques are the methods of spin-coating, doctor blading and screen-printing. This is a significant point in favor of fabrication of such devices, given that the techniques adopted are simple to realize and low cost.

The general structure used for organic solar cells is similar to that of the organic light emitting diodes (**OLED**). The devices are manufactured by means of a sandwich geometry.

Figure 3.5a shows a schematic representation of a solar cell. The substrates used are transparent and conductor electrodes, such as glass or plastic coated with ITO.

The electrodes in ITO are transparent, conductor but expensive. The support of ITO can be previously structured by means of chemical etching. The support is then coated with PEDOT:PSS; (poly(EDOT) doped with, a polystyrene sulfonate (PSS).

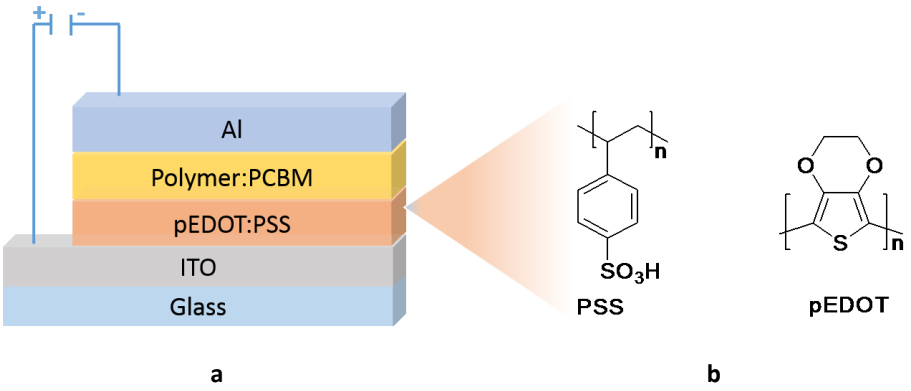


**Figure 3.5:** a) Scheme of a bulk heterojunction solar cell in the sandwich geometry; b) chemical structure of PEDOT (poly (3,4-ethylenedioxythiophene)) and PSS (polystyrene sulfonate).

This layer improves the surface quality of the electrode of ITO (reducing the probability of short circuits) and facilitates the extraction of holes. Deposition of the active layer is made using solution techniques, as mentioned above. In the case of small molecules, it is also possible to use the evaporation under high vacuum. Finally, the top metal electrode is evaporated thermally on the active layer under high vacuum (typically $10^{-7}$-$10^{-6}$ mbar).

To evaluate experimentally the efficiency of a solar cell a series of electrical measurements are carried out on the device, in order to draw a diagram of density current/voltage (J/V) in different experimental conditions. Figure 3.6 shows the J/V characteristics related to a generic photovoltaic cell in dark or under illumination.

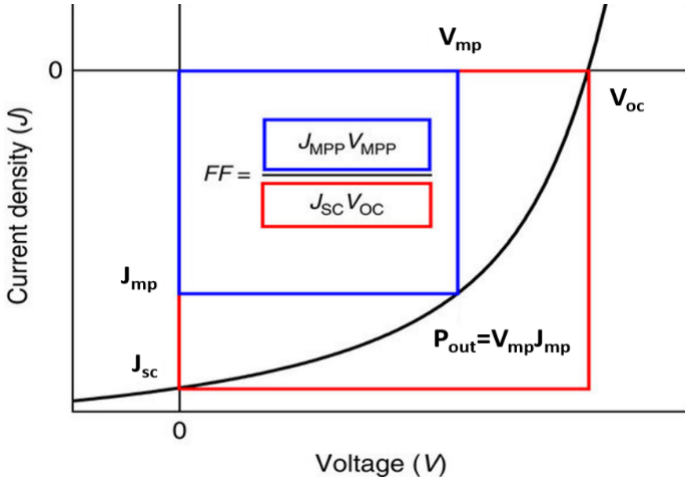


**Figure 3.6:** Characteristic curve current-voltage of a solar cell.

The efficiency $\eta$ of the cell is determined by the ratio between the maximum power delivered by the device and the incoming power $\mathbf{P_{in}}$:

$$\eta = \frac{P_{out}}{P_{in}} = \frac{J_{mp} \cdot V_{mp}}{P_{in}} = \frac{FF \cdot J_{sc} \cdot V_{oc}}{P_{in}}$$

In this expression the output power ($\mathbf{P_{out}t=J_{mp} \cdot V_{mp}}$) is estimated by evaluating the point of the curve where the product of the current density for the voltage is maximum (area red). While the fill factor (**FF**) represents the ratio between the maximum measured power $P_{out}$ and the maximum theoretical $\mathbf{P_{th}=J_{sc} \cdot V_{oc}}$ (ratio of the area of the blue rectangle and red rectangle in figure 3.6).

# 4. Demand of alternative materials in transistors production

In the last decades, the increasing demand of high-performance electronic devices, bearing unexpected and sophisticated characteristics, such as flexibility and lightness, has pushed the development of new technologies enabling the fabrication of electronic components with such particular features. The transistor is a landmark in the development of modern electronics, and is the key enabling technology in virtually every electronic device today. In a field-effect transistor (FET), the current flowing between two terminals, the so called source and drain electrodes, is amplified by a third electrode, the gate.

During the years, silicon transistors have shown high charge-carrier mobilities and their sizes have progressively been reduced according to the well-known Moore's law[16]. However, further improvements could soon be hampered by the increasing sophistication of the miniaturization process[17]. Therefore, to satisfy the increasing requests of the electronics market, the introduction of new materials, such as organic semiconductors, showing good performances but also additional advantages, can be a possible alternative.

With respect to silicon, organic semiconductors can be easily processed from solution on flexible substrate,[18] opening new paths to a vast array of applications ranging from flexible displays and circuits,[19] to radiofrequency identification (RFID) tags,[20] as well as to artificial skin for biomedical electronics.[21] The use of organic semiconductors for the fabrication of FETs leads to several important advantages such as the low costs of production,

because of they can be processed from solution using printing, ink-jet or roll-to-roll techniques, and the high scalability on large area deposition.[22,23]

## 4.1 Organic field effect transistors

Organic donor-acceptor polymers exhibit excellent properties in charge-carriers transport within organic field effect transistors[24,25] and their high mobility can be attributed to the particular architecture and to the strong interactions between the polymeric chains, in fact the reduction of the intermolecular distance increase the charge transport.[26]

The field effect is a phenomenon in which the conductivity of a semiconductor changes due to the application of an electric field.

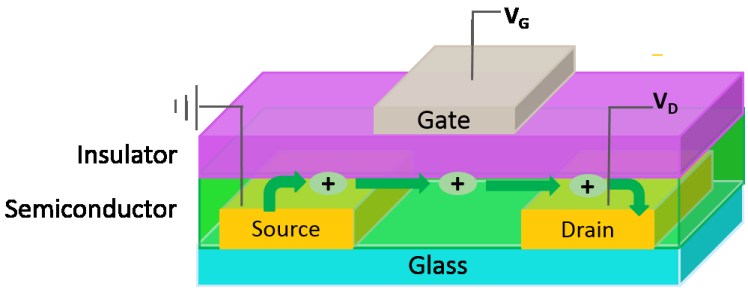


**Figure 4.1:** Schematic view of an organic field effect transistor.

Figure 4.1 shows a generic top gate structure, in which source and drain electrodes are deposited on glass (or on flexible) substrate, the organic semiconductor layer is deposited on top and it is separated from the gate by the insulating.

By applying a voltage bias between the gate and the source electrodes ($V_G$), charge accumulate at the semiconductor/insulator interface. When a bias

is applied between the source and the drain electrodes ($V_D$), a current ($I_D$) will flow between these two contacts. The $I_D$ is modulated by the applied gate.

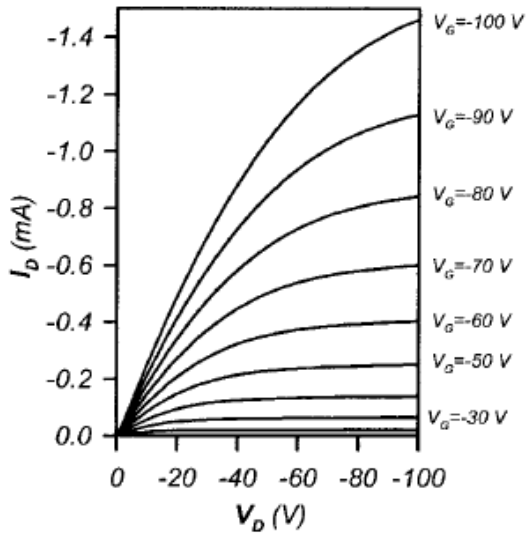


**Figure 4.2:** Typical current-voltage behavior

The curves reported in figure 4.2, show the typical $I_D$ behavior of an OFET, output drain current increases as the $V_D$ increases, until the saturation point that depends on the applied $V_G$.

The main features that characterize an OFET are the field-effect mobility and the $I_{ON}/I_{OFF}$ ratio, the mobility is function of the semiconductor properties, while the $I_{ON}/I_{OFF}$ ratio is the ratio between the saturation value when $V_G$ is high and the leakage current when $V_G$ is zero.

# 5. Compounds with diketopyrrolopyrrole structure

Donald Farnum and his collaborators at the University of Michigan, in the United States of America, accidentally synthesized the first compound with diketopyrrolopyrrole structure (DPP) in 1974. They reacted ethyl bromoacetate with benzonitrile in the presence of zinc, in the Reformatsky conditions, with the intention of synthesizing the β unsaturated lactam 1,

instead the product 2 was obtained, although in a very modest yield (scheme 5.1). For the properties exhibited by the compound 2, such as the bright red colour and low solubility, it was thought that this could be a new organic pigment.[27]

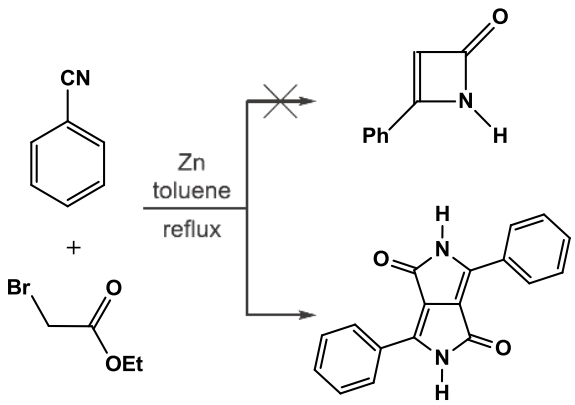


**Scheme 5.1:** Synthesis of the **DPP**.

Currently, the compounds in **DPP** structure are synthesized through a condensation reaction between an aromatic nitrile and the succinic ester (scheme 5.2).

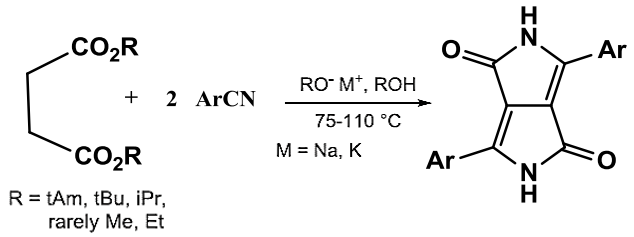


**Scheme 5.2:** Succinic method for the synthesis of **DPP**.

This method allows the synthesis of pigments in which the **DPP** unit is conjugated to different aromatic groups (i.e., phenyl, thienyl, furyl) in good yields. Furthermore, these derivatives may undergo various synthetic modifications that allow modulating the properties. For example, the alkylation of the lactam units allows increasing the solubility in organic solvents, while by means of electrophilic aromatic substitution reactions it is possible to functionalize the aryl unit. A frequent functionalization is represented by halogenation, which allows obtaining useful intermediates in the synthesis of molecules to more complex structures.[28]

Compounds containing the **DPP** units are widely used as industrial pigments for paints, inks, varnishes and plastics due to their exceptional photochemical, thermal and mechanical stability. In recent years, the derivatives with **DPP** structure have attracted great attention for their applications in organic electronic. In fact, the **DPP** unit works as an excellent electron-acceptor unit in copolymers with low bandgap used as semiconductors both in solar cells and in organic transistors.[29,30]

The 3,6-di(thiophene-2-yl)pyrrolo[3,4-c] pyrrole-1,4 (2H, 5H)-dione (**dithienyl DPP**) has attracted particular interest because of its high planar structure more flat than the **diphenyl DPP**. This causes a red shift of the

absorption maxima and favours the π-π stacking, which in turn, influences the charge transport abilities.

Many polymers and small molecules, containing the unit **dithienyl DPP**, were incorporated as donors in organic solar cells, having high efficiency. Efficiencies up to 8% were reported by Jannsen[31] for solar cells containing a terpolymer (figure 5.1, a) as donor and the **$PC_{71}BM$** as acceptor, and by Hwang[32] for solar cells containing the polymer (figure 5.1, b) in which the **dithienyl DPP** unit is alternated with triisopropyl silil etinil-benzodithiophene.

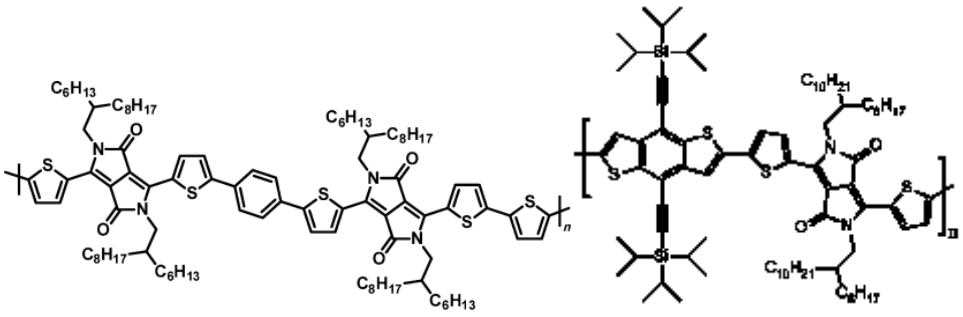

**a** **b**

**Figure 5.1**: Examples of polymer with TDPP structure in OPV cells.

Winnewisser[33] reported a polymer with **dithienyl DPP** unit (figure 5.2, a) for application in field-effect transistor that shows ambipolar charge transport properties, reaching ~0.1 $cm^2\ V^{-1}s^{-1}$and ~0.09 $cm^2\ V^{-1}s^{-1}$ for holes and electrons, respectively. Similar copolymer possessing **dithienyl DPP** unit (figure 5.2, b) was reported by Janssen[34] exhibiting ambipolar transport around 0.01 $cm^2\ V^{-1}s^{-1}$ both for electrons and holes mobility.

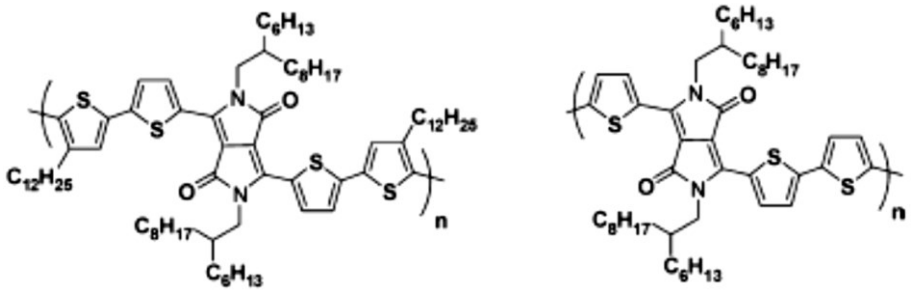

a b

**Figure 5.2**: Examples of polymer with TDPP structure in OFET.

Most applied compounds in organic electronics, which possess the DPP moiety, contain alkyl substituents on the lactam units. The introduction of such group not only increases the solubility in organic solvents but also allows the modulation of the optoelectronic properties. Recent literature reports on examples of **dithienyl DPP** derivatives containing hydrophilic polyether chains, able of the self-assembly in the solid state.[35] For example, Patil[36,37] reported a copolymer in which the alkylated **dithienyl DPP** units are alternated to **dithienyl DPP** units functionalized with triethylen glycol chains (polymer a, Figure 4.5) for applications in transistor with high mobility (electron mobility up to 3 $cm^2V^{-1}s^{-1}$ ). Yang[38] showed that the strong effect exerted by triethylen glycol chains in the self-assembling improves the efficiency of polymer systems (efficiencies from 6.2% to 7.0% with triethylen glycol modification, polymer b, figure 5.3).

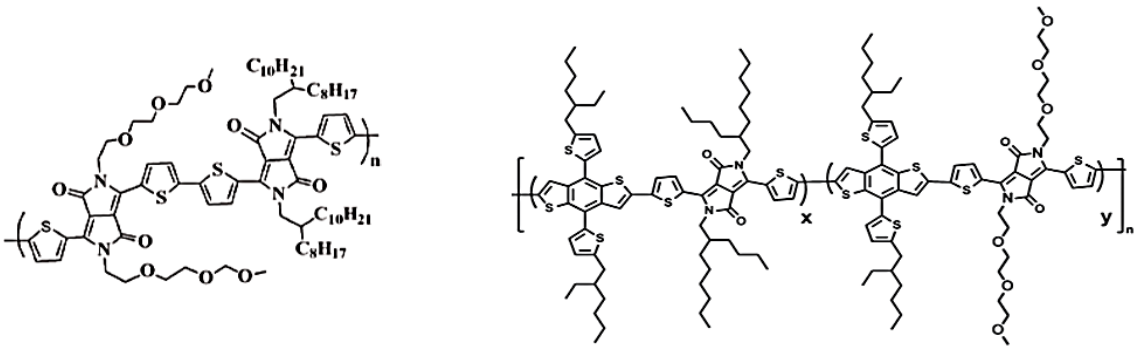

a b

**Figure 5.3:** Examples of materials with **TDPP** structure functionalized with hydrophilic chains.

Finally, in the last years several jobs in the literature describe the use of **DPP** derivatives as fluorescent probes for the detection of different analytes, such as, anions ($F^-$, $CN^-$), cations ($Zn^{2+}$, $Hg^{2+}$, $Cu^{2+}$), ROS ($H_2O_2$, $^{\cdot}OH$, $^{-}OCl$) and thiols.[28,39] The interest is justified by the fact that, compared to other classes of compounds, they have high absorption and high quantum yields of fluorescence together to high thermal and light stability. The revelation comes from changes in the photophysical properties of the probes, indicated by an increase or quenching of fluorescence, together with a red or blue shift in the absorption or emission band. The high fluorescence quantum yields have also allowed the use of **DPP** derivatives in bioimaging techniques.

# Results and discussion

# 6. New triazole-diketopyrrolopyrrole derivatives with tunable solubility

One of the critical aspects in the production of organic photovoltaic cells is the use of toxic and pollutant solvents. The introduction of polyethylenglycolic chains can improve the solubility in environmentally friendly solvent, the self-assembly of the **BHJ** and therefore the charge transfert.[36,38]

To date, the reverse phase photovoltaic cell proposed by Krebs,[40] which is fully processed by hydroalcoholic mixture, represents the state of the art. The active layer was formed by a fullerene derivative, functionalized with a triethyleneglycol chain (acceptor), and a polythiophene with removable hydrophilic chains (donor). After the deposition from hydroalcoholic solvents, the active layer was heated at about 300°C to remove the hydrophilic chains present on the polymer, generating a film insoluble in water, upon which it is possible to deposit the following layer (scheme 6.1). Although the efficiency of the cell obtained is modest (PCE = 0.7%), the result is interesting because it represents a first step towards the realization of sustainable organic solar cells.

In the scheme 6.1 are reported the structures of organic materials used in the solar cell.

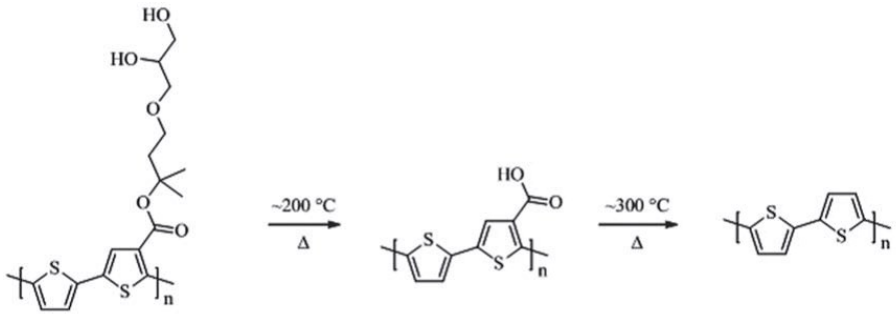


**1** **P$_3$CT** **PT-Insoluble**

**Scheme 6.1:** Structures of organic materials used in the cell proposed by Krebs.

My work was aimed at the design and synthesis of new systems with tunable solubility. DPP was used as the central core and the solubility of the final compounds will be modulated both by the introduction of different side chains on the N atoms of the lactam ring and by conjugation of some 1,2,3-triazole moieties at the central core.

The connection of the triazole units was carried out through a cycloaddition reaction that is an interesting example of “click chemistry”. The reaction takes place between 1,3-dipolar azides and alkynes in presence of a copper catalyst, it is regioselective and shows good reproducibility. Using different organic azides we aim to modulate the solubility of the molecules.[41]

## 6.1 Synthesis of small molecules

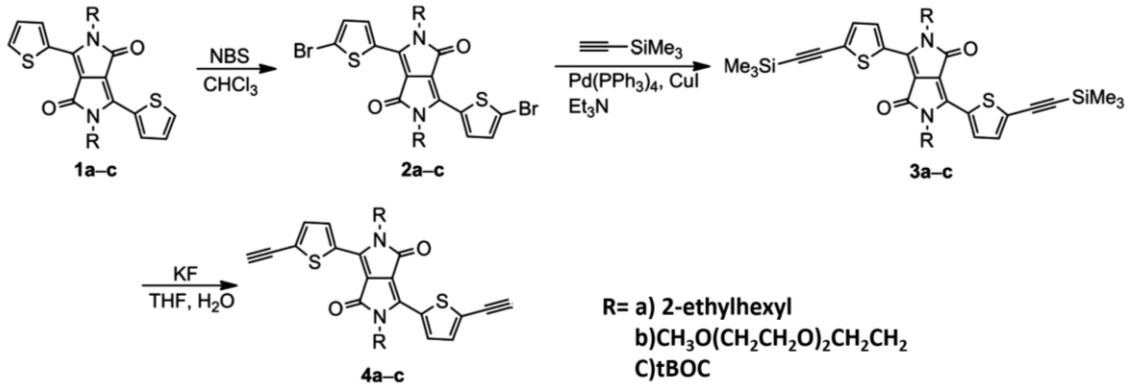


**Scheme 6.2:** Synthetic route to compounds **4a-c**.

The precursors **1a-c** are treated with N-bromosuccinimide to obtain the brominated derivatives; these undergo to silylation, through reaction with trimethylsilylacetylene in presence of $Pd(PPh_3)_4$, CuI and trimethylamine, to give the intermediates **3a-c**. The protecting silyls groups were removed by reaction with potassium fluoride to provide the alkynes **4a-c**. They contain solubilizing groups with different properties on the lactam rings of DPP core, namely the hydrophobic 2-ethylhexyl chains for **4a** or the hydrophilic 2-(2-(2-methoxethoxy)ethoxy)ethyl chains for **4b** and *t*-BOC groups for **4c**, respectively.

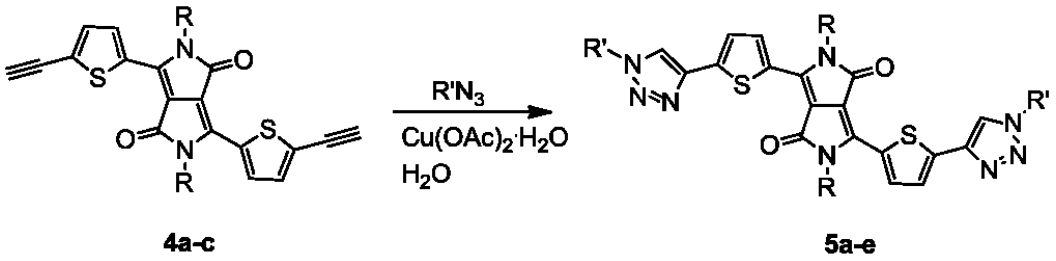


**Scheme 6.3:** Synthetic route to compounds 5a-f.

Finally, the compounds **4a-c** have been reacted with organic azides in presence of $Cu(OAc)_2.H_2O$, in water, to introduce various substituents in the terminal position of the conjugated backbone. The molecular structures of the obtained small molecules are reported in table 6.1.

**Table 6.1:**. Structures of compounds **5a-f**.

| Entry | Alkynes 4 | Azides | Products 5 |
|---|---|---|---|
| **1** | **4a** | *n*-octyl | 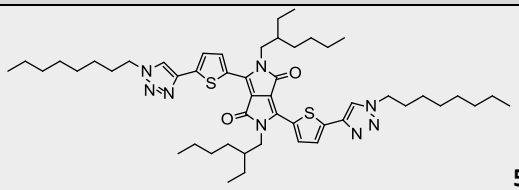 **5a** |
| **2** | **4b** | *n*-octyl | 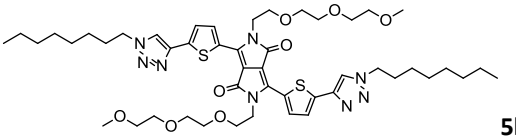 **5b** |
| **3** | **4c** | *n*-octyl | 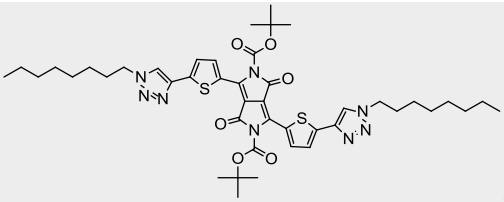 **5c** |
| **4** | **4b** | *n*-hexadecyl | 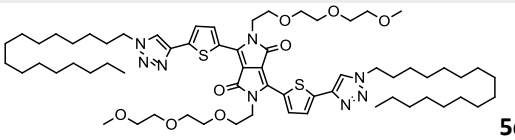 **5d** |
| **4** | **4a** | $HOCH_2CH_2(OCH_2CH_2)_3$ | 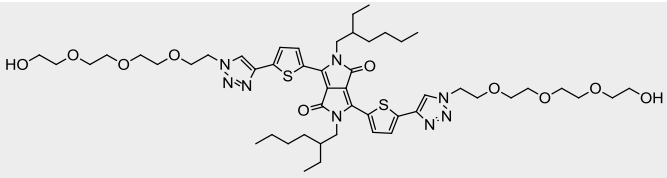 **5e** |
| **5** | **4b** | $HOCH_2CH_2(OCH_2CH_2)_3$ | 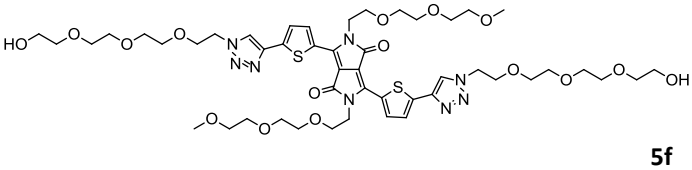 **5f** |

## 6.2 Solubility of the small molecules

The solubility of the synthetized compounds was qualitatively tested in solvents with different polarities. The tests were carried out mixing 1mg of each molecules with 0.5 ml of solvent at room temperature and if the solubilization was not complete the mixture was heated. In table 6.2 are reported the results.

**Table 6.2:** Solubility of compounds **5a-f** in solvents of different polarity.

| Solvent | 5a | 5b | 5c | 5d | 5e | 5f |
|---|---|---|---|---|---|---|
| *n*-Hexane | - | - | - | - | - | - |
| Toluene | + | ++ | ++ | ++ | ++ | ± |
| *o*-Dichlorobenzene | ++ | ++ | ++ | ++ | ++ | ++ |
| $CH_2Cl_2$ | ++ | ++ | ++ | ++ | ++ | ++ |
| $CHCl_3$ | ++ | ++ | ++ | ++ | ++ | ++ |
| THF | ++ | ++ | ++ | ++ | ++ | ++ |
| Isopropanol | - | ++ | + | + | + | + |
| Ethanol | - | ++ | + | + | + | ++ |
| Acetone | + | ++ | ++ | ++ | ++ | ++ |
| Methanol | - | ++ | + | ± | + | ++ |
| $H_2O$ | - | - | - | - | - | ++ |

++ soluble at room temperature; + soluble on heating; ± partly soluble; - insoluble.

All compounds are insoluble in hexane but they are soluble in halogenated solvent as *o*-dichlorobenzene, dichloromethane and chloroform, as well as in tetrahydrofuran, in acetone and in toluene (only the **5f**, is partly soluble upon heating).

Additionally their solubility in alcohols increases as the number of hydrophilic oligoether chains increase. Compound **5f**, possessing oligoether chains on both the DPP core and the triazole units, is soluble in water at room temperature. Singularly, only few water-soluble DPP derivatives have been reported so far.[42,43,44]

## 6.3 UV-Vis characterization in solution and in the solid state

The molecules were characterized through UV-Vis spectroscopy; the absorption and emission spectra are recorded in chloroform (see figure 6.1).

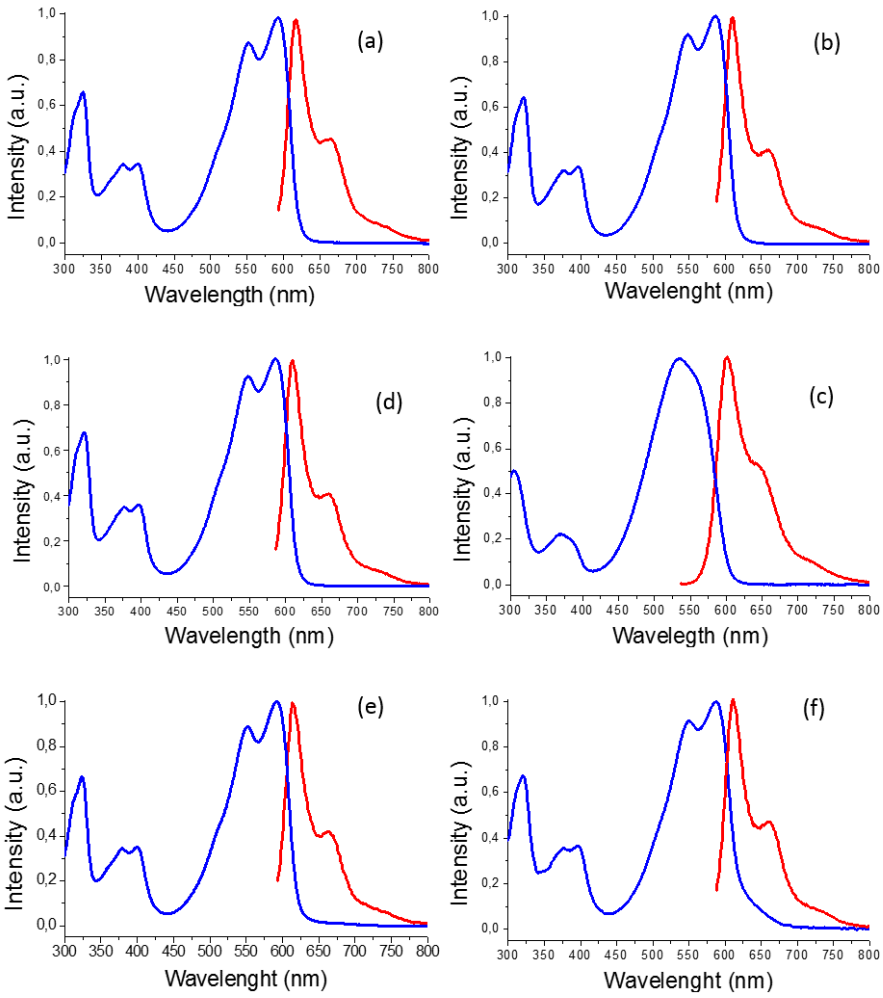


**Figure 6.1:** Normalized UV-Vis absorption (blue line) and emission (red line) spectra of compounds (a) **5a**, (b) **5b**, (c) **5c**, (d) **5d**, (e) **5e**, and (f) **5f** in solution ($CHCl_3$, $10^{-5}$ M).

All compounds exhibit similar absorption and emission maximum with the exception of **5c** that shows a blue shift of about 50 nm, probably due to the higher steric hindrance of the *t*-BOC groups on the DPP core, which reduces the planarity/conjugation of the molecules. The higher planarity of compounds **5a**, **5b**, and **5d–f** with respect to compound **5c** allowed us to visualize resolved vibronic structure.

Furthermore molar extinction coefficients (ε) have been calculated and all molecules manifest similar and high values ranging from $3.39 \times 10^4$ to $5.36 \times 10^4$ $M^{-1}$ $cm^{-1}$.

**Table 6.3:** Optical data of the compounds 5a-f in chloroform solution.

| Compound | $\lambda_{max\ abs}$ (nm)[a] | ε ($M^{-1}cm^{-1}$) | $\lambda_{max\ PLem}$ (nm)[a] | $\lambda_{onset}$ (nm)[a] |
|---|---|---|---|---|
| **5a** | 592 | $5.36x10^4$ | 616 | 620 |
| **5b** | 586 | $4.19x10^4$ | 610 | 618 |
| **5c** | 535 | $4.16x10^4$ | 600 | 610 |
| **5d** | 586 | $3.30x10^4$ | 610 | 616 |
| **5e** | 592 | $3.39x10^4$ | 614 | 625 |
| **5f** | 587 | $4.43x10^4$ | 611 | 625 |

[a] $10^{-5}$ M $CHCl_3$ solution. [b] Optical bandgap evaluated as $E_g = 1240/\lambda_{onset}$.

All compounds were also characterized at the solid state, as thin spin-coated films (1000 rpm/60 sec, then 2000 rpm/60 sec) from chloroform solution (10mg/ml), on glass plates. The UV-Vis absorption curves at the solid state, exhibit a broadening of the absorption band and a red shift of the absorption onset when compared to the data acquired in solution. This is a clear indication of an increment of the structural order.

From the absorption spectra, the optical energy gaps in solution and in film have been calculated; all compounds exhibit low values of the optical bandgap at the solid state, as summarized in table 6.4.

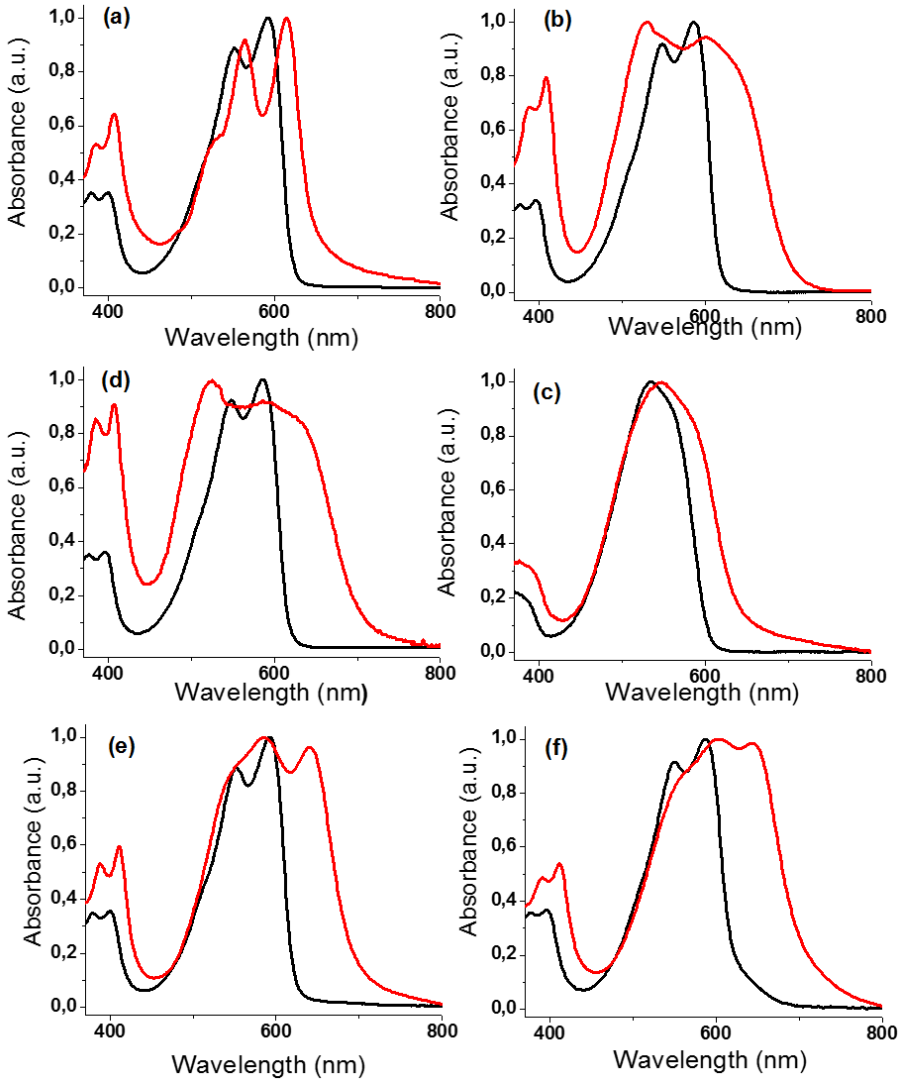


**Figure 6.2:** Normalized UV-Vis absorption in solution (black line) and UV-Vis absorption at the solid state (red line) spectra of compounds (a) **5a**, (b) **5b**, (c) **5c**, (d) **5d**, (e) **5e**, and (f) **5f**.

**Table 6.4:** Optical data of the compounds 5a-f in chloroform solution and in film.

| Compound | $\lambda_{max\ sol}$ (nm)[a] | $\lambda_{onset\ sol}$ (nm) [a] | $E_{g\ sol}$ (eV)[c] | $\lambda_{max\ film}$ (nm) [b] | $\lambda_{onset\ film}$ (nm) [b] | $E_{g\ film}$ (eV) [c] |
|---|---|---|---|---|---|---|
| **5a** | 592 | 620 | 2.00 | 616 | 652 | 1.85 |
| **5b** | 586 | 618 | 2.01 | 529 | 703 | 1.76 |
| **5c** | 535 | 610 | 2.03 | 548 | 644 | 1.92 |
| **5d** | 586 | 616 | 2.01 | 525 | 706 | 1.76 |
| **5e** | 592 | 625 | 1.98 | 586 | 702 | 1.77 |
| **5f** | 587 | 625 | 1.98 | 601 | 715 | 1.73 |

[a] $10^{-5}$ M $CHCl_3$ solution. [b] 10mg/ml (1000 rpm/60s) $CHCl_3$ solution [c] Optical bandgap evaluated as $E_g = 1240/\lambda_{onset}$.

## 6.4 Determination of HOMO and LUMO levels

Electrochemical properties and HOMO and LUMO levels were estimated through CV, using a platinum working electrode, a platinum counter electrode and an $Ag/Ag^+$ reference electrode. While the tetrabutylammonium hexafluorophosphate was used as supporting electrolyte and the ferrocene/ferrocenium ($Fc/Fc^+$) redox couple as external standard. CV curves of all compounds show two reversible oxidation and one irreversible reduction waves (figure 6.3).

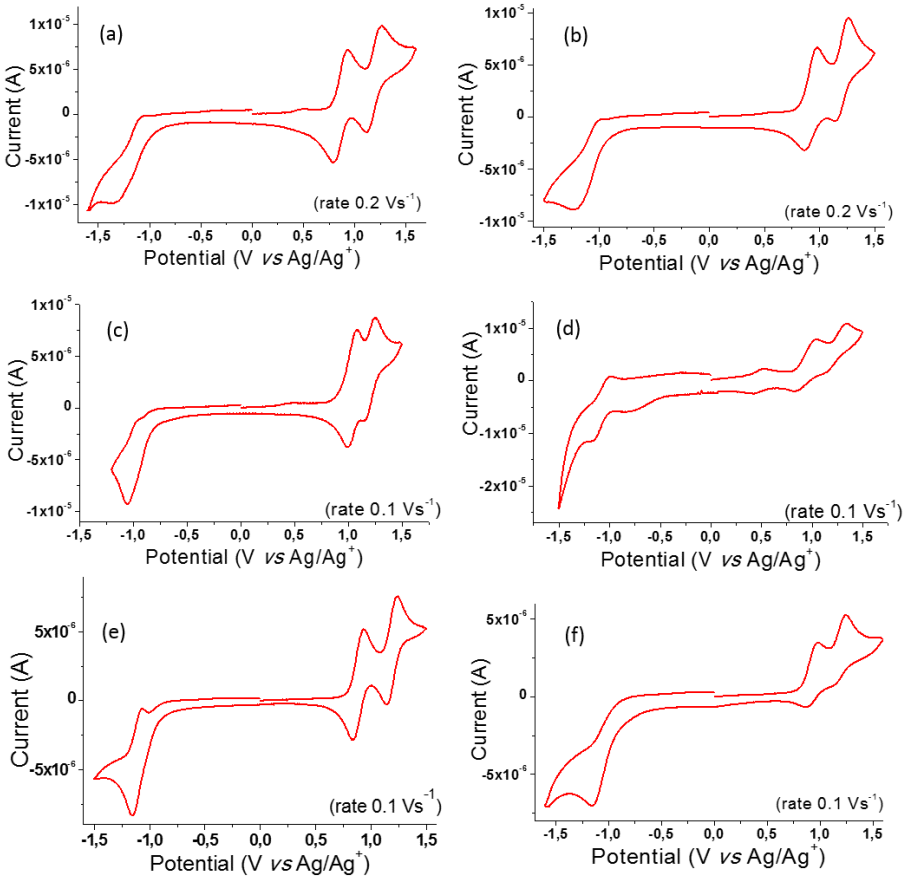


**Figure 6.3:** Cyclic voltammograms on a Pt working electrode in 0.1M n-$Bu_4NPF_6$/ anhydrous dichloromethane at room temperature for compounds **5a** (a), **5b** (b), **5c** (c), **5d** (d), **5e** (e) and **5f** (f).

The HOMO energy levels were estimated, for each molecule, according to the empirical equation: HOMO = - ($E_{ox}$ + 5.1V), where $E_{ox}$ is the onset of the first peak potential versus $Fc/Fc^+$ reference and -5.1eV is the position of the formal potential of the $Fc/Fc^+$ redox couple in the Fermi scale.[45] While the LUMO energy levels were calculated as follows: LUMO = HOMO + $E_g^{opt}$. The electrochemical data of compounds **5a-f** in $CH_2Cl_2$ solution are reported in table 6.5.

**Table 6.5:** Electrochemical data of the compounds **5a-f** in dichloromethane solution

| Compound | $E_{ox}$ (V) | $E_{red}$ (V) | HOMO (eV) | LUMO (eV) |
|---|---|---|---|---|
| **5a** | 0.38 | -1.78 | -5.48 | -3.48 |
| **5b** | 0.41 | -1.74 | -5.51 | -3.50 |
| **5c** | 0.55 | -1.52 | -5.65 | -3.62 |
| **5d** | 0.42 | -1.69 | -5.52 | -3.51 |
| **5e** | 0.37 | -1.67 | -5.47 | -3.49 |
| **5f** | 0.41 | -1.65 | -5.51 | -3.53 |

Compounds **5a-b, d-f** possessing alkyl and/or oligoether chains show similar electrochemical properties, suggesting that the variations in the side-chains do not cause any noticeable difference of electronic behavior. For all these molecules, the HOMO and LUMO levels are approximately the same ranging from -5.5 and -3.5, respectively. Otherwise, the introduction of the more electronegative *t*-BOC groups on the DPP core produces a small lowering of HOMO-LUMO energy levels of compound **5c**.

## 6.5 Preliminary tests in solar cells

All small molecules were tested in BHJ solar cells, using they as donor (D) materials and [6,6]-Phenyl-$C_{61}$-butyric acid methyl ester ($PC_{60}BM$) as acceptor (A) material. The cells were fabricated using **small molecule**/$PC_{60}BM$, in ratio D/A 1:1 (wt/wt), as active layer in order to obtainer solar cell devices in the direct architecture[44]: ITO/PEDOT:PSS(50nm)/**small molecule**:$PC_{60}BM$ (200nm)/ Ca (5nm)/ Al

(100nm). The architecture used in fabrication of solar cells is schematized in figure 6.4:

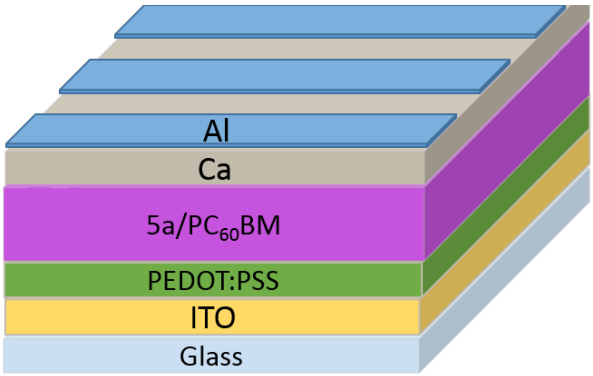


**Figure 6.4:** The architecture used for solar cell device.

The active layer was spin coated from chloroform solution, at two different rates, at 500 or 1000 rpm, and then annealed on hotplate at 130°C under inert atmosphere for 10 min.

In table 6.6 are reported the performance data of the cells prepared with different spinning rate for the molecule **5a**.

**Table 6.6:** Photovoltaic parameters for ITO/PEDOT:PSS/**5a**:$PC_{60}BM$/Ca/Al solar cells under AM1.5G, 1000 W/$m^2$ illumination.

| Devices | rpm | $J_{sc}$ (mA/$cm^2$) | $V_{oc}$ (V) | FF (%) | PCE (%) |
|---|---|---|---|---|---|
| **5a**/$PC_{60}BM$ | 500 | -0.544±0.020 | 0.571±0.021 | 20.01±0.32 | - |
| **5a**/$PC_{60}BM$ | 1000 | -0.0444±0.06 | 0.713±0.299 | 17.9±6.07 | - |

In figure 6.6 is reported the external quantum efficiency curve (EQE) of the solar cell and it shows a broad spectrum in the visible and NIR region with

a peak at 520 nm. For comparison, the absorption spectrum of the solar cell device was also recorded (figure 6.7).

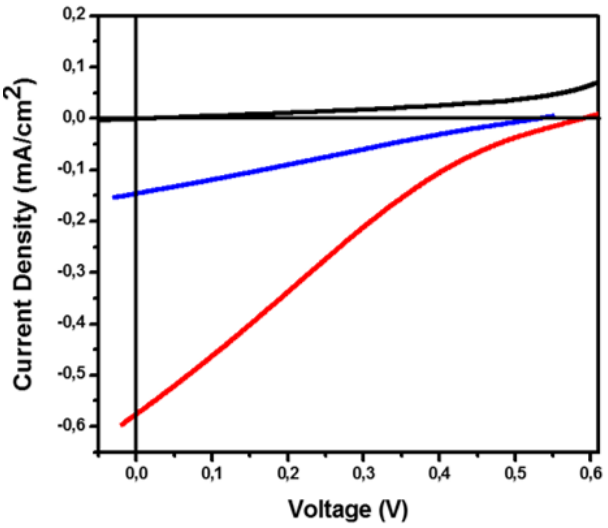


**Figure 6.5:** J-V characteristics of **5a**/$PC_{60}BM$ based solar cell device in the dark (black line) and under AM1.5G, 1000 $W/m^2$ illumination (500 rpm in red line and 1000 rpm in blue line).

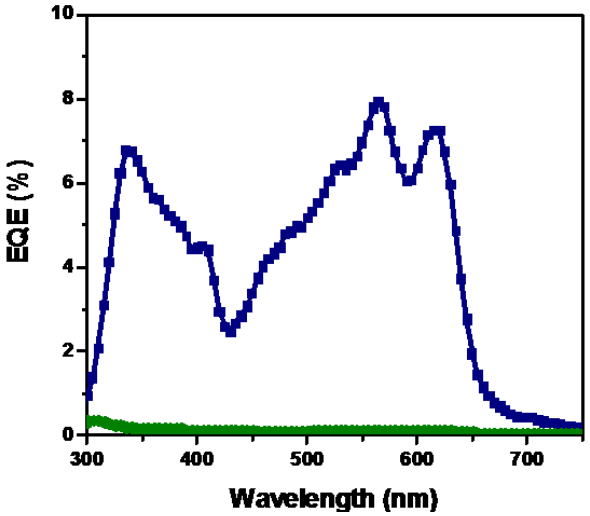


**Figure 6.6:** EQE spectrum of the ITO/PEDOT:PSS/**5a**:$PC_{60}BM$/Ca/Al solar cell (500 rpm in blue line and 1000 rpm in green line).

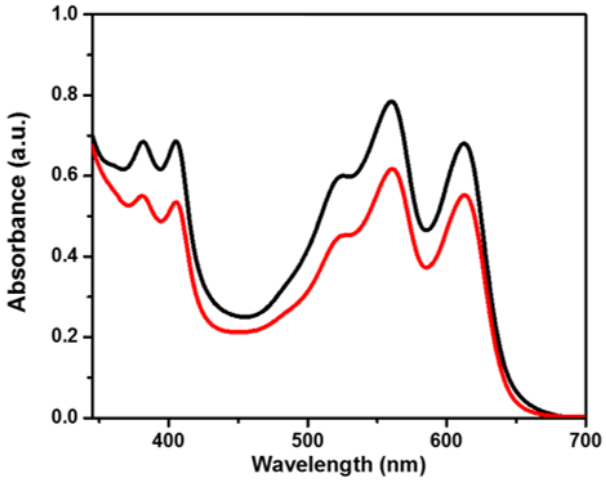


**Figure 6.7:** Absorption spectrum of the ITO/PEDOT:PSS/**5a**:$PC_{60}BM$/Ca/Al solar cell (500 rpm in black line and 1000 rpm in red line).

The investigated systems show very low values of FF, $J_{sc}$ and PCE, but the $V_{OC}$ is considerably high. Comparing the EQE and the absorbance spectrum of the solar cell, is evident that the charge generation is rather balanced between the fullerene than the molecule. Probably the reason of these poor results could be attributed to the low conjugation of the backbone.

# 7. New conjugated polymers for bulk heterojunction solar cells

In view of the results obtained with the small molecules I focused my attention on the synthesis of different polymers functionalized with hydrophilic groups. The polymers possess a **DPP** core-unit functionalized whit triethyleneglycol chains, with the aim of improving the solubility of the polymers in polar solvents.

Initially, three copolymers characterized by alternating **DPP** units functionalized with triethyleneglycol chains (**TegDPP**) on the lactam cycle,

and a vinyl (**TegDPPV**), a thiophene ring (**TegDPPT**) or a (ethylhexyloxy) benzodithiophene group, (**TegDPPBDT**) were synthetized through the efficient Stille cross coupling involving $Pd(PPh_3)_4$ as catalyst, and purified by Soxhlet extraction. Furthermore the molecular weight of the polymers was estimated through GPC analysis while the optical and the electrochemical properties were investigated by UV-Vis spectroscopy and CV, respectively.[46]

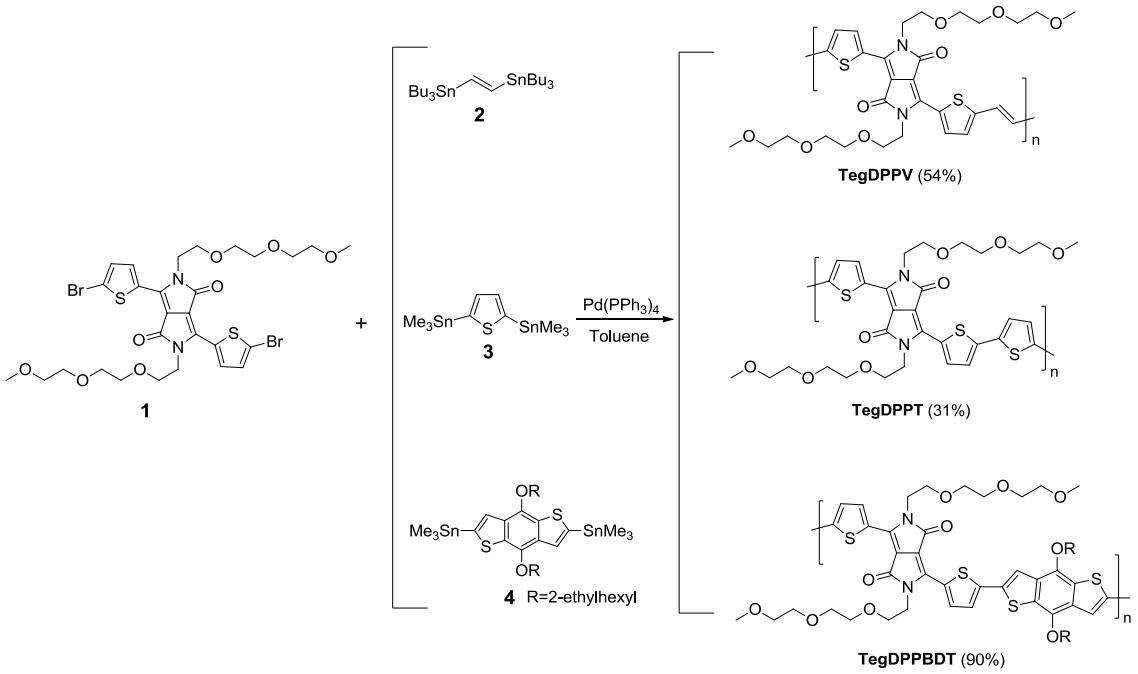


**Scheme 7.1:** Synthesis of **TegDPPV**, **TegDPPT** and **TegDPPBDT**.

Solubility tests show that synthetized polymers are soluble only in halogenated solvents, in order to improve the solubility of my systems in polar solvent, **TegDPP** units was linked to a thiophene unit, functionalized with a triethyleneglycol chain, in a random terpolymer (**TegDPPTegES**) carried out by Stille cross-coupling. The polymer was purified by Soxhlet extraction and characterized through GPC to determine the molecular

weight, UV-Vis spectroscopy to analyze the optical properties and CV to investigate HOMO and LUMO energy levels.

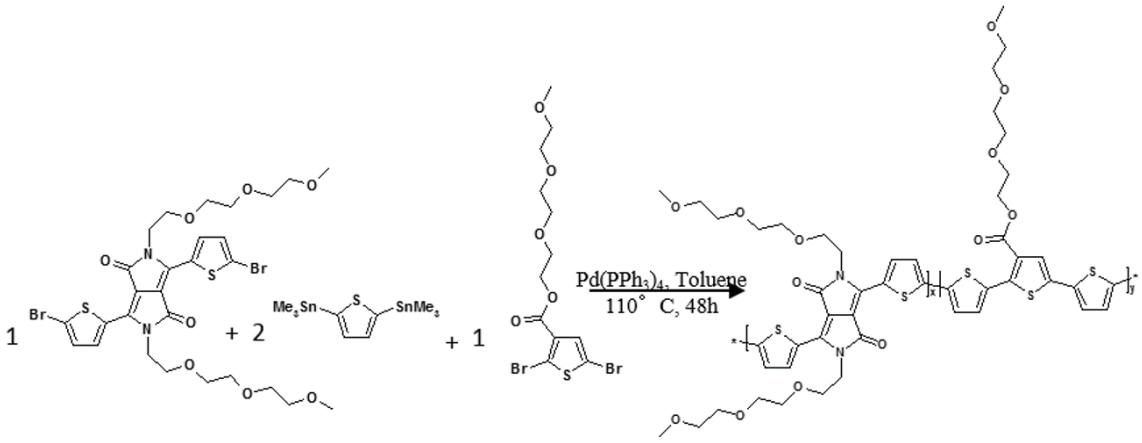


**1** **3** **5** **TegDPPTegES.**

**Scheme 7.2:** Synthesis of **TegDPPTegES**.

Also, the polymer **TegDPPTegES** is soluble only in halogenated solvents and to obtain new polymers soluble in polar solvents, the synthesis of **TegDPPK** was designed, in addition, this polymer shows a side chain removable by thermal treatment, to modulate the solubility. To synthetize the polymer I used the Stille reaction and it was isolated by Soxhlet extraction, also this polymer was characterized through GPC, UV-Vis and CV.

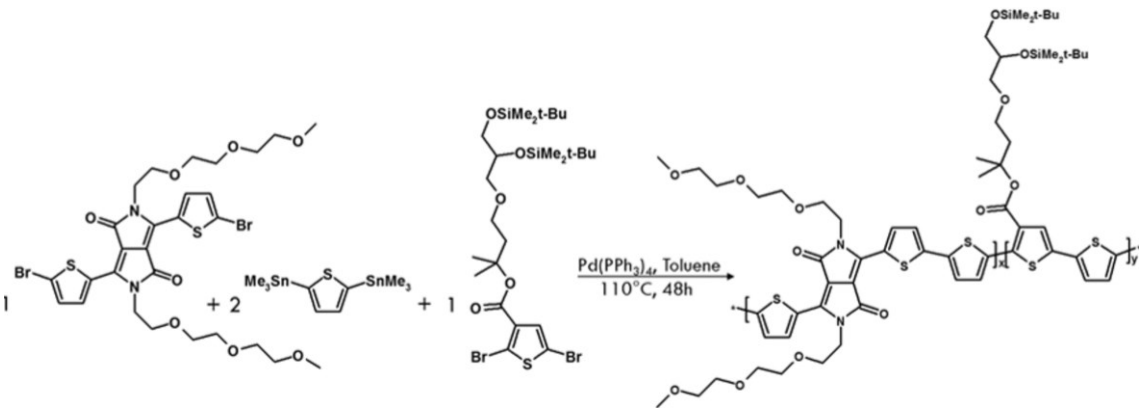


**1** **3** **6** **TegDPPK**

**Scheme 7.3:** Synthesis of **TegDPPK**.

Considering that **TegDPPK** is not soluble in polar solvents, in order to simplify the polymeric structure, **TegDPPK1** was synthesized, which shares some similarities with **TegDPPK**, but I realized the direct connection between **TegDPP** unit and the thiophene functionalized with the ester group. Furthermore to obtain the polymer a different synthetic procedure was employed: the Direct Heteroarylation Polymerization (**DAHP**).[47,48,49] With this procedure, it is not necessary to synthesize any stannylated reagent, but I took advantage of the reaction between the halogenated thiophene derivate and the **TegDPP** monomer. Also this polymer was purified through Soxhlet extraction and characterized by GPC, UV-Vis and CV to investigate the molecular weight, the optical and the electrochemical properties, respectively.

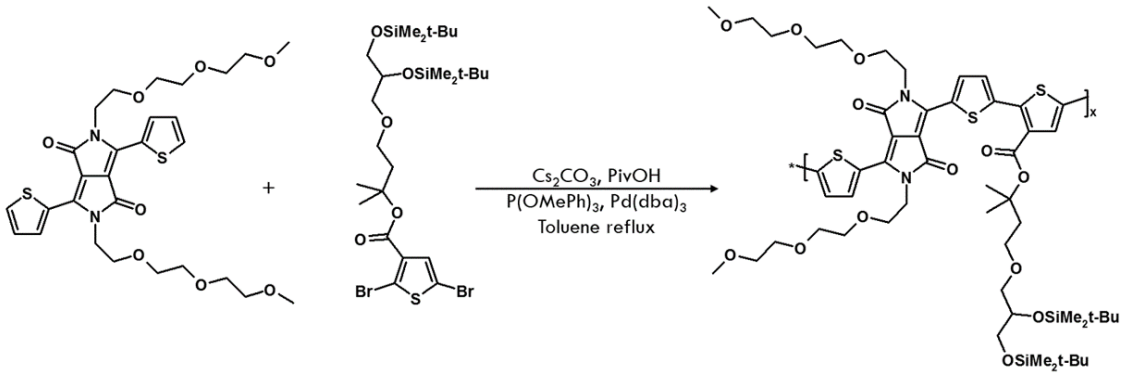


**1** **6** **TegDPPK1**

**Scheme 7.4:** Synthesis of **TegDPPK1**.

Like **TegDPPK,** also **TegDPPK1**, possesses a side chain thermally removable to modulate the solubility of the polymer.

## 7.1 GPC characterization of the polymers

The polymers were analyzed by GPC in order to determine the molecular weight and the polydispersity. The analyses were carried out using the polystyrene as standard and a mixture of chloroform and DMF (1:0.2 v/v) as eluent to facilitate the elution of the polymers. It was not possible to use pure chloroform because the polymers were not eluted, reasonable due to establishing strong interactions with the stationary phase. For polymers **TegDPPTegES** and **TegDPPV,** the GPC analysis showed the presence of polymeric and oligomeric species with molecular weights ($M_n$) markedly different. **TegDPPT**, **TegDPPBDT**, **TegDPPK** and **TegDPPK1** have similar molecular weight and a polydispersity index (PDI) ranging from 1.6 and 3.2 as reported in table 7.1.

**Table 7.1:** GPC data for **DPP**-based polymers.

| Polymer | $M_n$ (kDa) | $M_w$ (kDa) | PDI |
|---|---|---|---|
| TegDPPTV[a] | 20.3/1.1 | 29.4/1.3 | 1.4/1.2 |
| TegDPPT | 16.1 | 25.4 | 1.6 |
| TegDPPBDT | 18.5 | 42.9 | 2.3 |
| TegDPPTegES[a] | 21.5/1.2 | 28.4/1.8 | 1.3/1.5 |
| TegDPPK | 13 | 41.3 | 3.2 |
| TegDPPK1 | 14.7 | 31.3 | 2.1 |

[a] Bimodal molecular-weight distribution was observed.

## 7.2 UV-Vis characterization of the polymers

All polymers were characterized through UV-Vis analysis; the spectra were registered both in chloroform solution and in the solid state. For each polymer, the optical energy gap was calculated in solution and in film. The calculation takes account of the absorption onset in the UV-Vis spectra using the eq4uation:

$$E_g = 1240/\lambda_{onset}$$

Polymers **TegDPPV**, **TegDPPBDT**, **TegDPPTegES**, **TegDPPK** and **TegDPPK1** were solubilized in chloroform and then spin-coated (1000 rpm/60 sec, then 2000 rpm/60 sec) films, on glass plates, while for **TegDPPT**, it was not possible to obtain the film due to wettability problems. The overlapping of the normalized spectra in solution and in films for all polymers, were reported in figure 7.1 with exception of **TegDPPT** for which it is available only the spectrum in solution.

The polymers **TegDPPV**, **TegDPPBDT** and, especially, **TegDPPK1**, show a red shift of the absorption onset in the solid state: that is a clear indication of an increment of the structural order.

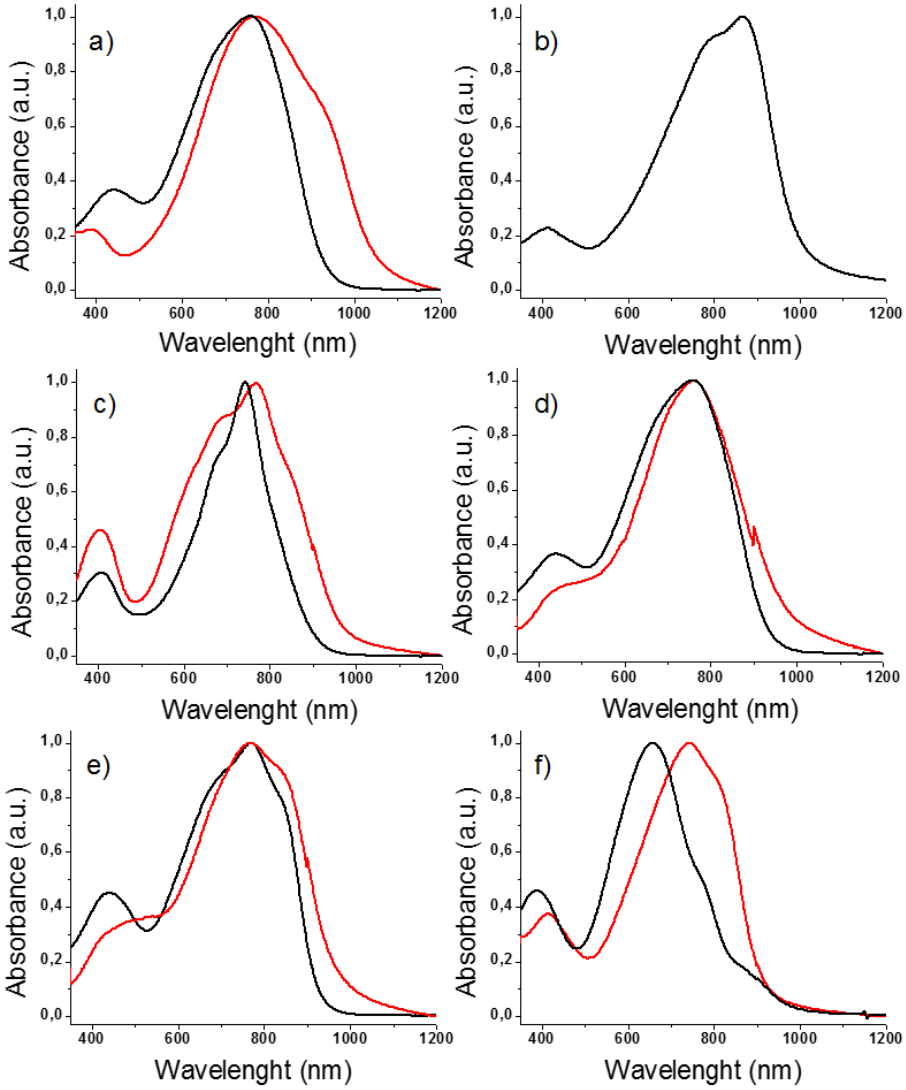


**Figure 7.1:** UV-Vis normalized spectra of **TegDPPV** (a), **TegDPPT** (b), **TegDPPBDT** (c), **TegDPPTegES** (d), **TegDPPK** (e), and **TegDPPK1** (f) in $CHCl_3$ solution (black line) and in film (red line).

**Table 7.2:** Optic properties of the synthesized polymers.

| Polymers | $\lambda_{max\ sol}$ (nm)[a] | $\lambda_{onset\ sol}$ (nm) [a] | $\lambda_{max\ film}$ (nm) [b] | $\lambda_{onset\ film}$ (nm) [b] | $E_g^{opt}$ (eV) [c] |
|---|---|---|---|---|---|
| TegDPPV | 756 | 935 | 777[d] | 1053 | 1.19 |
| TegDPPT | 869 | 1000 | -[e] | -[e] | -[e] |
| TegDPPBDT | 743 | 900 | 765[f] | 971 | 1.28 |
| TegDPPTegES | 758 | 941 | 760[g] | 982 | 1.27 |
| TegDPPK | 771 | 912 | 777[h] | 975 | 1.27 |
| TegDPPK1 | 651 | 880 | 741[i] | 918 | 1.35 |

[a] Measured in dilute $CHCl_3$ solution. [b] Films deposited by spin-coating from $CHCl_3$ solution. [c] Optical band-gap evaluated as $E_g = 1240/\lambda_{onset\ film}$. [d] Film from $CHCl_3$ solution (10 mg/ml). [e] For **TegDPPT** it was not possible to acquire the UV/Vis/NIR spectrum in the solid state due to its poor wettability. [f] Film from $CHCl_3$ solution (6 mg/ml). [g] Film from $CHCl_3$ solution (5 mg/ml). [h] Film from $CHCl_3$ solution (3.5 mg/ml). [i] Film from $CHCl_3$ solution (5 mg/ml).

The optical band-gaps ($E_g^{opt}$) of the polymers in the solid state was estimated from the onset of the thin-film absorptions, (Table 7.2). Low optical band-gaps, ranging from 1.19 to 1.28, were calculated for **TegDPPV TegDPPBDT**, **TegDPPTegES** and **TegDPPK**. The polymer **TegDPPK1** is characterized by a larger $E_g^{opt}$ if compared to **TegDPPK,** due to the smaller network of polythiophene donor blocks.

## 7.3 Thermal treatment of polymers TegDPPK and TegDPPK1

Considering that polymers **TegDPPK** and **TegDPPK1** possess thermally cleavable tertiary ester groups, to study their thermal decomposition, the spin-coated films obtained from chloroform solutions, were heated on a

hotplate at 300°C in air for 2 minutes. IR spectra show a decrease of the band at about 1700 $cm^{-1}$ related to the carboxylic group stretching (Figure 7.2), suggesting their decomposition.

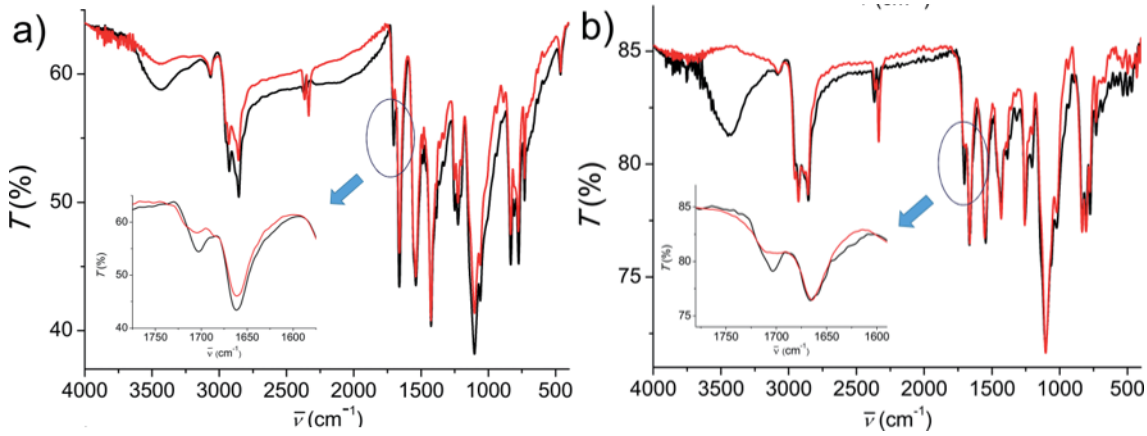


**Figure 7.2:** FT-IR spectra of **TegDPPK** (a) and **TegDPPK1** (b) before (black) and after (red) thermal cleavage at 300 °C for 2 min.

The cleavage causes a drastic reduction of solubility in chloroform improving the resistance of polymers to solvent attack leading, consequently, to morphologically stable films. Furthermore, the removal of the side chains, increase the charge transport properties of the polymers.[50] Thermal gravimetric analyses (TGA) confirm the thermal cleavage of the side chains. Thermograms curves in figure 7.3 shows a loss in weight of 25 % and 28 % for **TegDPPK** and **TegDPPK1**, respectively, ranging from 220 and 400 °C due to the thermolysis of the ester side chains.

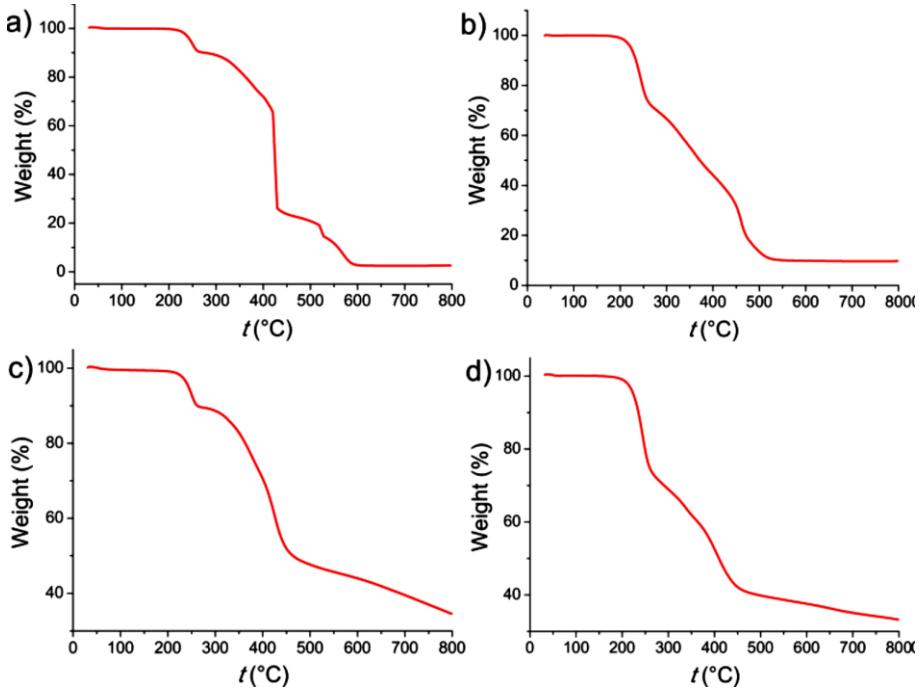


**Figure 7.3:** TGA analysis of **TegDPPK** in air (a) and under nitrogen (c); TGA analysis of **TegDPPK1** in air (b) and under nitrogen (d).

Furthermore, after thermal treatment, the UV-Vis spectra show absorption profiles very similar to the initial polymers, as reported in figure 7.4.

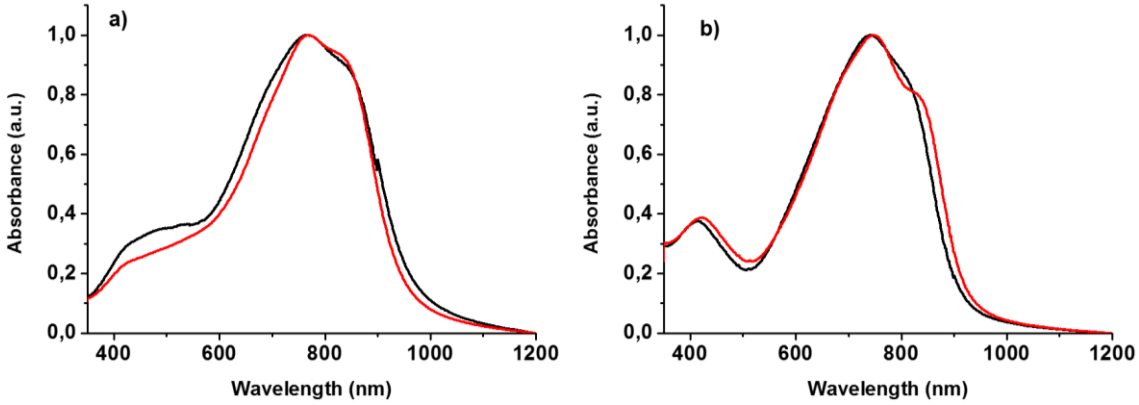


**Figure 7.4:** UV-Vis normalized spectra of **TegDPPK** (a) and **TegDPPK1** (b) films before (black line) and after thermal treatment at 300 °C for 2 min (red line).

## 7.4 Determination of HOMO and LUMO levels of the polymers

Electrochemical properties of the polymers were investigated through cyclic voltammetry (CV). The CV curves (figure 7.5) were obtained after the deposition of a thin film on the platinum working electrode in 0.1 M tetrabutylammonium hexafluorophosphate ($nBu_4NPF_6$)/acetonitrile solution. The $Fc/Fc^+$ redox couple was used as an external standard to calibrate all the measurements. The HOMO and LUMO energy levels were calculated employing the following empirical equations:

$$\mathbf{E_{HOMO} = -(E_{ox} + 5.1\ V)} \quad \text{and} \quad \mathbf{E_{LUMO} = -(E_{red} + 5.1\ V)}$$

where $E_{ox}$ and $E_{red}$ are the onset oxidation and reduction potentials vs $Fc/Fc^+$, respectively, while -5.1 eV is the position of the formal potential of the $Fc/Fc^+$ redox couple on the Fermi scale.[45]

The electrochemical data reported in table 7.3, shows values of electrochemical band gaps larger than the optical ones. The reason of this phenomenon is probably due at the presence of an energy barrier at the interface between the working electrode surface and the polymeric film.[51] The current intensity for the reduction curves is lower than that of oxidation ones, therefore the synthetized polymers are good holes transporters, but they are not good transporters of electrons. The same observations have been made for N-alkylated DPP polymers.[29]

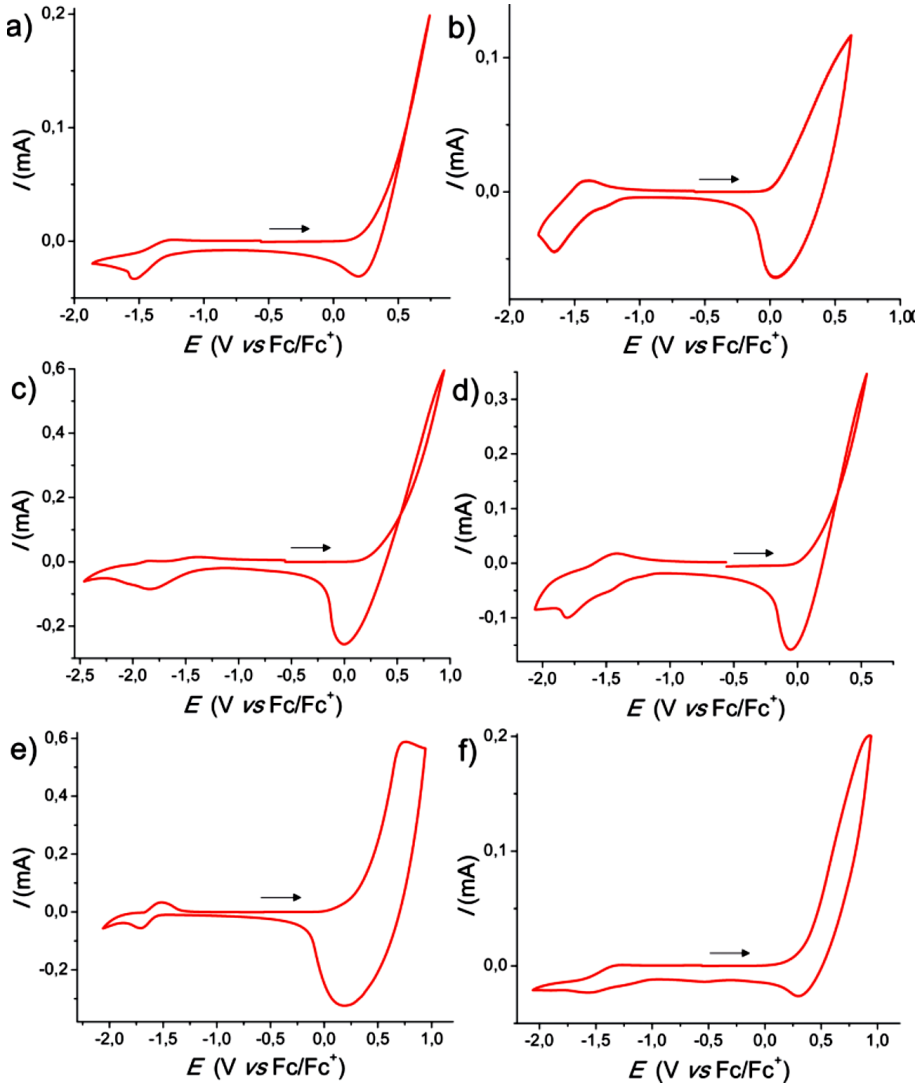


**Figure 7.5:** Cyclic voltammograms of **TegDPPV** (a), **TegDPPT** (b), **TegDPPBDT** (c), **TegDPPTegES** (d), **TegDPPK** (e) and **TegDPPK1** (f) films on a Pt working electrode in 0.1 M $nBu_4NPF_6$/acetonitrile at room temperature.

**Table 7.3:** Electrochemical data of **TegDPP**-based polymers.

| Polymer | $E_{ox}$ (V) [a] | HOMO (eV)[b] | $E_{red}$ (V)[a] | LUMO (eV)[b] | $E_g^{el}$ (eV)[c] |
|---|---|---|---|---|---|
| TegDPPV | 0.30 | –5.40 | –1.25 | –3.85 | 1.55 |
| TegDPPT | 0.06 | –5.16 | –1.31 | –3.79 | 1.37 |
| TegDPPBDT | 0.25 | –5.35 | –1.38 | –3.72 | 1.63 |
| TegDPPTegES | 0.12 | –5.22 | –1.38 | –3.72 | 1.50 |
| TegDPPK | 0.25 | –5.35 | –1.51 | –3.59 | 1.76 |
| TegDPPK1 | 0.40 | –5.50 | 1.35 | –3.75 | 1.75 |

[a] Onset oxidation and reduction potentials vs $Fc/Fc^+$. [b] HOMO–LUMO energy levels evaluated as $E_{HOMO} = -(E^{ox}_{onset} + 5.1\ V)$ and $E_{LUMO} = -(E^{red}_{onset} + 5.1\ V)$ where $E_{onset}$ is measured vs $Fc/Fc^+$ reference, and –5.1 eV is the position of the formal potential of the $Fc/Fc^+$ redox couple on the Fermi scale.[45] [c] Electrochemical band-gap calculated from $E_g = -(E_{ox} - E_{red})$.

## 7.5 Tests in BHJ solar cells

All polymers were tested in BHJ solar cells, using them as donor (D) materials and [6,6]-Phenyl-$C_{71}$-butyric acid methyl ester ($PC_{70}BM$) as acceptor (A) material.

The cells were prepared using the direct configuration: ITO/PEDOT-PSS/**Polymer**:$PC_{70}BM$/Ca/Al. The composition of the active layer is D/A 1:2 (wt/wt) and after the deposition, from ortho-dichlorobenzene solution, it undergoes to thermal annealing (testing the treatment at both 150 and 290°C) under inert atmosphere for 2 minutes.

The efficiency of these cells was very low and, for this reason, the compounds were also tested in BHJ solar cells with an inverted configuration.[52] The architecture: ITO/ZnO/**Polymer**:$PC_{70}BM$/$MoO_3$/Ag (see

figure 7.6) was used, and the active layer composed by D/A in ratio 1:2 (wt/wt), was annealed at 290°C under inert atmosphere for 2 minutes (see table 7.4). All polymers exhibit very poor photovoltaic parameters with exception for **TegDPPBDT** that exhibits the most promising results and for which I report the obtained values.

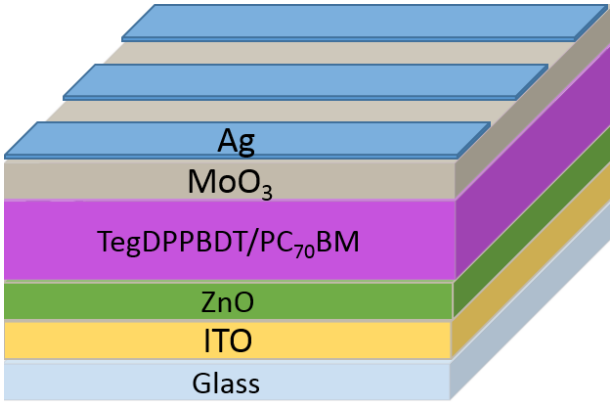


**Figure 7.6:** The architecture used for solar cell device.

In table 7.4 are reported the photovoltaic values both for the average and the best cell in the reverse phase.

**Table 7.4:** PV parameters for ITO/ZnO/**TegDPPBDT**:$PC_{70}BM$/$MoO_3$/Ag solar cells under AM1.5G, 1000 W/$m^2$ illumination.

| Device | $J_{sc}$ (mA/$cm^2$)] | $V_{oc}$ (V) | FF (%) | PCE (%) |
|---|---|---|---|---|
| Average | 5.45 ± 0.30 | 0.598 ± 0.01 | 41.1 ± 3.1 | 1.34 ± 0.18 |
| Best | 5.71 | 0.616 | 44.4 | 1.56 |

It was also investigated the possibility to use a lower annealing temperature (at 150°C), but the efficiency and the other photovoltaic parameters ($J_{sc}$=

2.36 mA/cm$^2$, $V_{oc}$ = 0.523 V, FF = 42.9 %, efficiency = 0.53 %) were less satisfactory.

The I/V curves under dark conditions and under illumination (AM1.5G, 1000 W/m$^2$) are shown in figure 6.7 for the best performing device. The external quantum efficiency curve (EQE) of the solar cell was also reported and it shows a broad spectrum in the visible and NIR region with a peak at 520 nm (figure 7.8). For comparison, the absorption spectrum of the solar cell device was also recorded (figure 7.9).

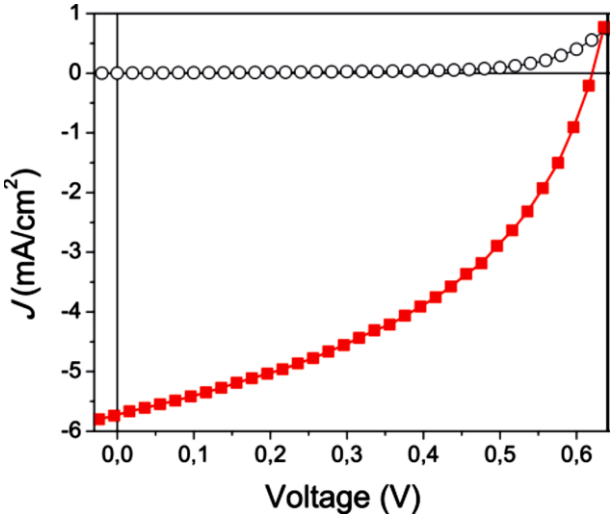


**Figure 7.7:** J–V characteristics of a **TegDPPBDT**:$PC_{70}BM$-based inverted solar cell device in the dark (black open circles) and under AM1.5G, 1000 W/m$^2$ illumination (red solid squares).

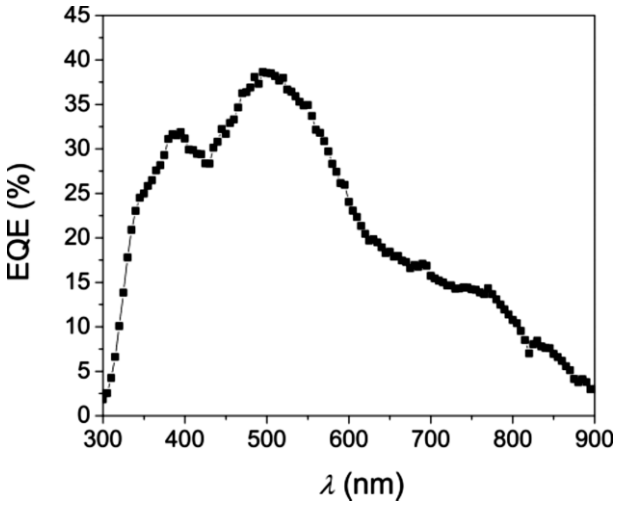


**Figure 7.8:** EQE spectrum of the ITO/ZnO/**TegDPPBDT**:$PC_{70}BM$/$MoO_3$/Ag solar cell.

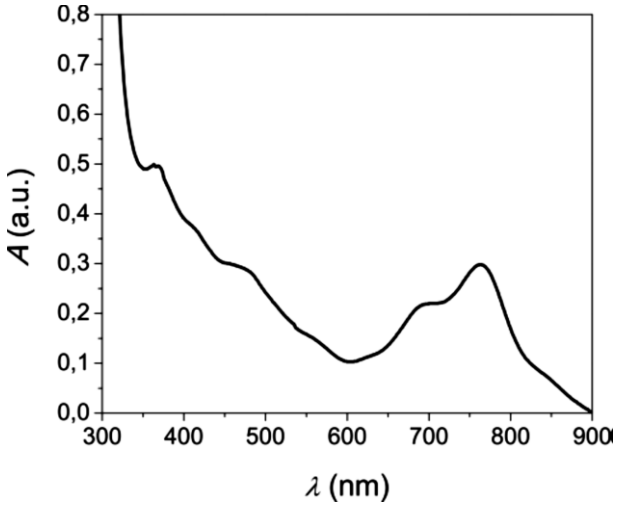


**Figure 7.9:** Absorption spectrum of the ITO/ZnO/**TegDPPBDT**:$PC_{70}BM$/$MoO_3$/Ag solar cell.

Although **TegDPPBDT** adsorbs very well in the NIR region, the photocurrent in this part of the spectrum is very poor, because most of the charge generation comes from the fullerene rather than the polymer. Changing the ratio between donor and acceptor materials, the performance of the device could improve.

## 7.6 Tests in organic field-effect transistor

During my visiting period in the Northwestern University, all polymers were tested in a bottom-contact, top-gate field-effect transistor configuration, using the CYTOP, a fluoropolymeric material, as dielectric layer. Gold source and drain contacts are used as the injecting/extracting electrodes, while aluminum is used here as the top gate electrode. The active layer was deposited from chloroform solution and thermally annealed at 150°C on hotplate under inert atmosphere for 15 minutes. Also in this case, the only polymer exhibiting the most promising performances is **TegDPPBDT** whose performance data, both for the average and for the best device, are summarized in table 7.5.

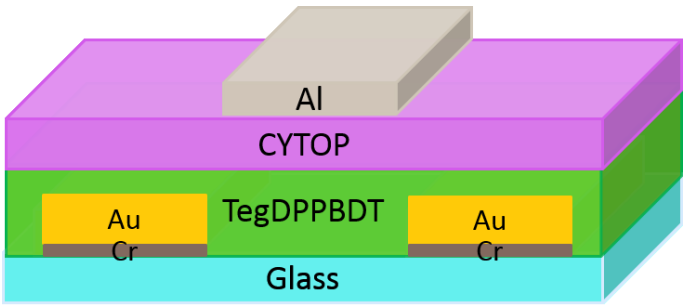


**Figure 7.10:** The architecture used for organic field-effect transistor.

**Table 7.5:** Parameters for top gate OFET.

| Device | $\mu_h$ ($cm^2 V^{-1} s^{-1}$) | $V_{th}$ (V) | $I_{on}/I_{off}$ |
|---|---|---|---|
| Average | 0,011 | -8/+11 | $10^4$ |
| Best | 0,013 | -2/+17 | $10^4$ |

The output curves (figure 7.11) were registered applying different gate voltages, ranging from -20 V to -100 V, while the reported transfer curve (figure 7.12) was registered applying a drain voltage of -80 V.

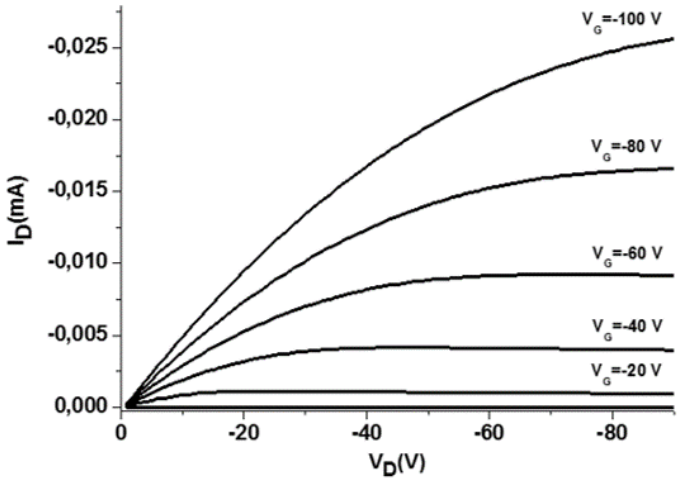


**Figure 7.11:** Plot of drain current $I_D$ versus drain voltage $V_D$ at various gate voltages $V_G$.

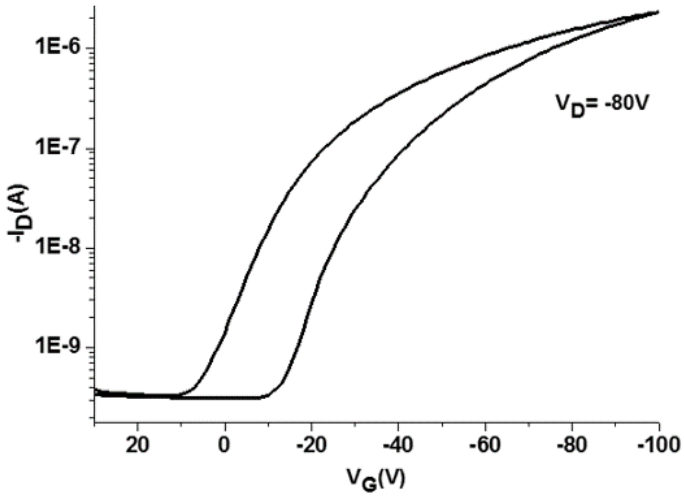


**Figure 7.12:** Plot of drain current $I_D$ versus gate voltages $V_G$.

The $I_D/V_G$ curve shows a hysteresis probably due to the presence of charge trapping site in the semiconductor material or at the OSC/insulator interface.

# 8 Synthesis of TegDPPBDT-HMW and EHDPPBDT

One the main features that influences power conversion efficiency in organic solar cells as well as channel currents and field-effect mobilities in OFETs is the molecular weight of the involved polymer, in particular high molecular weight improves the performance of organic devices.[53,54] Therefore, in order to increase the performances in organic devices, I repeated the synthesis of **TegDPPBDT** polymer to obtain a new polymer (**TegDPPBDT-HMW**) with higher molecular weight. With this aim, a different combination between catalyst and ligand has been used, and in particular $Pd_2(dba)_3$ and $P(o\text{-}tol)_3$ were employed.

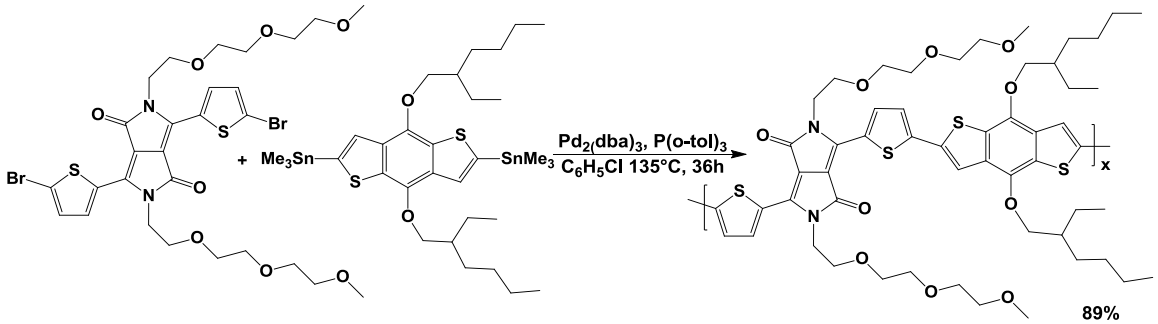


**1** **4** **TegDPPBDT-HMW**

**Scheme 8.1:** Synthesis of **TegDPPBDT-HMW**.

Also, the side chains of conjugated polymers affect the performances of organic devices, therefore, to investigate the different contribution of

hydrophilic and hydrophobic side chains, the know polymer, **EHDPPBDT**[55,56] was synthetized. This last possesses the same backbone of **TegDPPBDT-HMW**, but the N atoms of the DPP core has been functionalized with ethylhexyl chains (**EHDPP**).

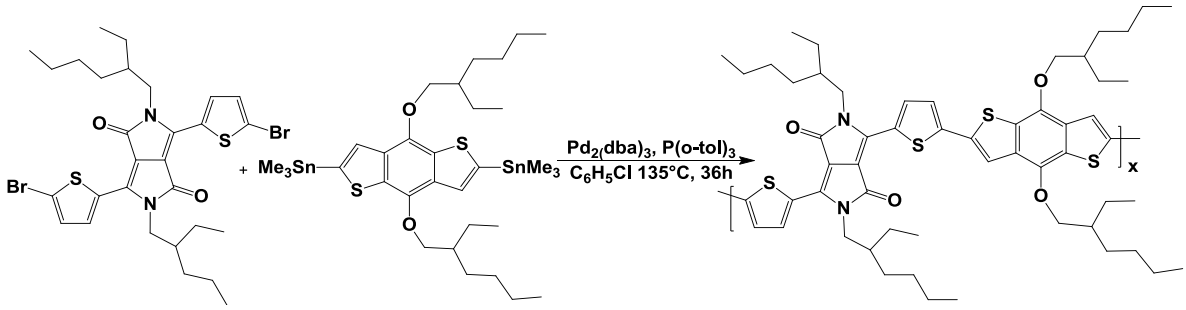


**EHDPP** **4** **EHDPPBDT**

**Scheme 8.2:** Synthesis of **EHPPBDT**.

Both the polymers were synthetized using the same reaction conditions and purified by Soxhlet extraction with methanol, acetone, hexane and chloroform. The two polymers have been obtained in good yield.

## 8.1 GPC characterization of the polymers

The molecular weight of the polymers was estimated through GPC analysis carried out at 150°C, using trichlorobenzene as eluent and polystyrene as standard. Both the polymers exhibit high molecular weight ranging from 77.3 and 68.7 (KDa) as reported in table 8.1, furthermore **TegDPPBDT-HMW** shows a $M_n$ value four time higher than polymer **TegDPPBDT**.

**Table 8.1:** GPC data.

| Polymer | $M_n$ (kDa) | $M_w$ (kDa) | PDI |
|---|---|---|---|
| TegDPPBDT-HMW | 77.3 | 278.3 | 3.6 |
| EHDPPBDT | 68.7 | 158.0 | 2.3 |

## 8.2 UV-Vis characterization in solution and in the solid state

The two polymers were characterized through UV-Vis spectroscopy both in chloroform solution and at the solid state as thin spin-coated films (1000 rpm/60 sec) from chloroform solution (6mg/ml).

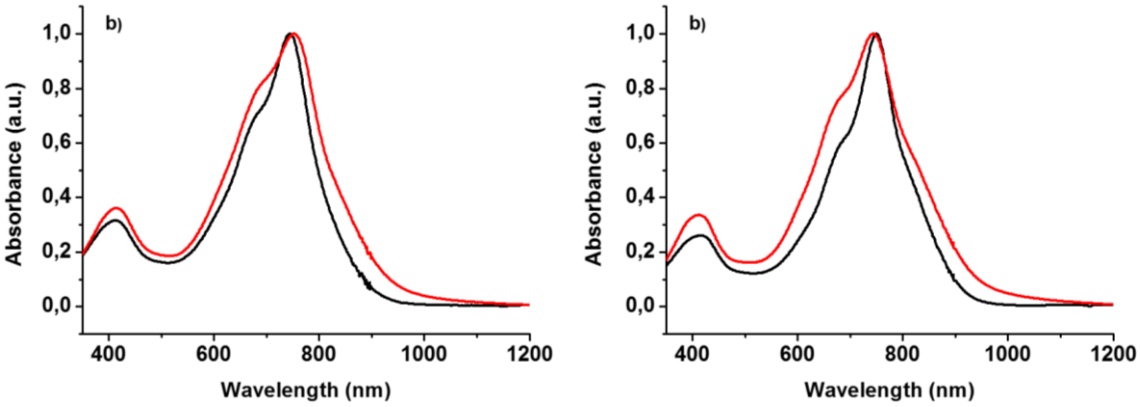


**Figure 8.1:** UV-Vis normalized spectra of **TegDPPBDT-HMW** (a) and **EHDPPBDT** (b) in $CHCl_3$ solution (black line) and in film (red line).

The UV-Vis absorption curves, for both polymers in thin films, exhibited a slight broadening of the absorption band and a red shift of the absorption onset, compared with the data acquired in solution. This is a clear indication of an increment of the structural order at the solid state.

**Table 8.2:** Optic properties of the synthesized polymers.

| Polymers | $\lambda_{max\ sol}$ (nm)[a] | $\lambda_{onset\ sol}$ (nm) [a] | $\lambda_{max\ film}$ (nm) [b] | $\lambda_{onset\ film}$ (nm) [b] | $E_g^{opt}$ (eV) [c] |
|---|---|---|---|---|---|
| TegDPPBDT-HMW | 745 | 869 | 752 | 913 | 1.35 |
| EHDPPBDT | 747 | 901 | 747 | 929 | 1.33 |

[a] Measured in dilute $CHCl_3$ solution. [b] Films deposited by spin-coating from $CHCl_3$ solution. [c] Optical band-gap evaluated as $E_g = 1240/\lambda_{onset\ film}$.

From the onset values, at the solid state for **TegDPPBDT-HMW** and **EHDPPBDT**, the optical bandgaps were calculated to be 1.35 and 1.33 eV, respectively.

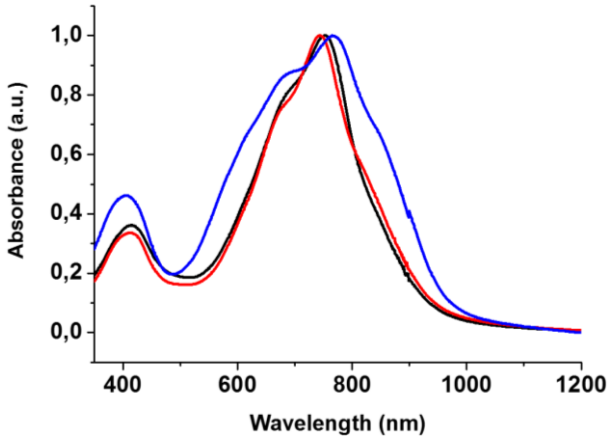


**Figure 8.2:** UV-Vis normalized spectra of **TegDPPBDT-HMW** (black line), **EHDPPBDT** (red line) and **TegDPPBDT** (blue line) as film.

Comparing UV-Vis spectra, at the solid state, of **TegDPPBDT-HMW** and **EHDPPBDT** with **TegDPPBDT**, a lower broadening in absorption profile and a blue-shift of the onset in **TegDPPBDT-HMW** and **EHDPPBDT** were observed, in spite their higher molecular weight. This suggests a lesser molecular aggregation when the polymeric chain is longer, probably due to

a decrease of the planar conformation and a reduction of the effective conjugation length, involving a worse molecular packing.[56,38]

This phenomenon caused also a slight increment of the optical energy gap from 1.28 eV for **TegDPPBDT** to 1.35 and 1.33 eV for **TegDPPBDT-HMW** and **EHDPPBDT**, respectively.

## 8.3 Determination of HOMO and LUMO levels

Electrochemical properties of the polymers were investigated through cyclic voltammetry, using a platinum working electrode, a platinum counter electrode and an $Ag/Ag^+$ reference electrode. Furthermore tetrabutylammonium hexafluorophosphate was utilized as supporting electrolyte and the ferrocene/ferrocenium ($Fc/Fc^+$) redox couple as external standard. The CV curves of the polymers are reported in figure 8.1.

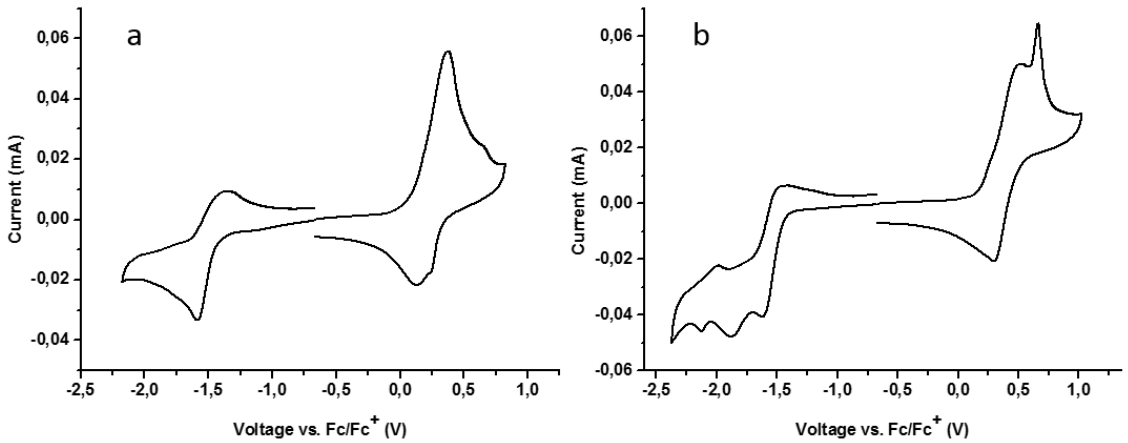


**Figure 8.4:** Cyclic voltammograms of **TegDPPBDT-HMW** (a), **EHDPPTBDT** (b) films on a Pt working electrode in 0.1 M $nBu_4NPF_6$/acetonitrile at room temperature.

The HOMO and LUMO energy levels were estimated according to the empirical equations:

$$\textbf{HOMO} = -(E^{ox}_{onset} + 5.1V) \quad \text{and} \quad \textbf{LUMO} = -(E^{red}_{onset} + 5.1\ V)$$

where the $E_{onset}$ is measured vs $Fc/Fc^+$ reference, and –5.1 eV is the position of the formal potential of the $Fc/Fc^+$ redox couple on the Fermi scale.[45] The electrochemical data are summarized in table 8.3.

**Table 8.3:** Electrochemical data of **DPP**-based polymers.

| Polymer | $E_{ox}$ (V) [a] | HOMO (eV) | $E_{red}$ (V)[a] | LUMO (eV) | $E_g^{el}$ (eV)[b] |
|---|---|---|---|---|---|
| TegDPPBDT-HMW | 0.09 | -5.19 | -1.45 | -3.65 | 1.54 |
| EHDPPBDT | 0.19 | -5.29 | -1.45 | -3.65 | 1.64 |

[a] Onset oxidation and reduction potentials vs $Fc/Fc^+$. [b] Electrochemical band-gap calculated from $E_g = -(E_{ox} - E_{red})$.

## 8.4 Tests in organic field-effect transistor

The polymers **TegDPPBDT-HMW** and **EHDPPBDT** were tested in a bottom-contact, top-gate field-effect transistor configuration, using the CYTOP or the Poly(methyl methacrylate) (PMMA), as dielectric layer. Gold source and drain contacts are used as the injecting/extracting electrodes, while aluminum is used as the top gate electrode (figure 8.5). The active layer was deposited from chloroform solution and thermally annealed at 150°C on hotplate under inert atmosphere for 15 minutes.

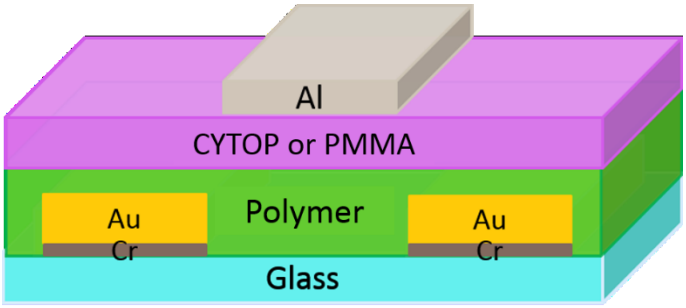


**Figure 8.5:** The architecture used for organic field-effect transistor.

Regrettably, investigations on devices processed using CYTOP or PMMA, presented poor performance data and in particular very low values of mobility, for which was not possible to register the output curves, for both the polymers.

This experimental evidence confirms, as previously mentioned, that molecular packing could negatively influenced by the high molecular weight of the polymers. Furthermore, it is known that opto-electronic performances can be improved by high molecular weight, but up to a certain range, while elevated molecular weight determined less significant enhancement.[57]

# Conclusions

During my PhD course I focused my attention on the DPP unit used as precursor for the synthesis of several small molecules and different polymers. To modulate the solubility of these compounds I introduced different chains on the N-atom of the lactam ring and in particular I used oligoether, alkyl chains or terz-Boc group.

DPP unit was used in the synthesis of new triazole-diketopyrrolopyrrole derivatives. The fine-tuning of their solubility results from the introduction of different side chains on the N atom of the lactam ring and on the triazole unit conjugated with the DPP central core.

Small molecules exhibit good solubility in common organic solvents and their solubility in alcohols increases as the number of oligoether chains increases. Remarkably, compound **5f**, possessing polar side chains both on DPP core and on triazole ring, is soluble also in water at room temperature. Optical and electrochemical properties of the compounds **5a–f** were investigated and all molecules show low energy gaps with maximum of absorption in the deep-red region.

Tests of small molecules in BHJ solar cells show that synthetized compounds may not be proficiently used in the fabrication of organic solar cells, probably because the conjugation of the backbone is not adequately extended.

To increase the extension of the conjugated backbone different polymers have been realized. For their synthesis I employed the DPP unit functionalized with triethylene glycol side chains and it was alternated to vinyl, ethylhexyloxy benzodithiophene or functionalized thiophene ring. **TegDPPV**, **TegDPPT**, **TegDPPBDT**, **TegDPPTegES** and **TegDPPK** have been

synthesized thought the Stille cross-coupling reaction, while to obtain the polymer **TegDPPK1** the direct hetero arylation polymerization has been involved. This reaction avoid the employment of stannilated derivatives making it a good candidate for industrial production on large scale.

All polymers were characterized through GPC chromatography, UV-Vis spectroscopy in solution and in film and CV.

All compounds, at the solid state, exhibit absorption peaks at wavelengths larger than 700 nm and low band-gaps. The spectra at the solid state show broader absorption band in the NIR region and shoulder peaks with respect to the corresponding spectra in solution. These effects are more pronounced for **TegDPPK1**, which exhibits a significant red-shift of the maximum absorption peak.

Films of **TegDPPK** and **TegDPPK1**, possessing thermally cleavable side chains, after thermal treatment at 300°C for 2 minutes exhibit resistance to common organic solvents attack.

Tests of the synthetized polymers, in BHJ solar cells, reveal that only **TegDPPBDT** can be profitably used as donor material, and at the same way it is the only material that exhibits interesting performance in OFETs, with hole mobilities around $1 \cdot 10^{-2}$ $cm^2 \cdot V^{-1} \cdot s^{-1}$.

In order to improve the performances of **TegDPPBDT** polymer in organic devices, a different synthetic procedure was used to increase the molecular weight obtaining **TegDPPBDT-HMW** polymer and to study the influence of the side chains on the DPP units **EHDPPBDT** polymer was also synthetized. GPC analyses reveal that both compounds exhibit higher molecular weight

than **TegDPPBDT**, suggesting that use of $Pd_2(dba)_3$ as catalyst improves polymerization reaction of DPP-based polymers.

UV-Vis data of **TegDPPBDT-HMW** and **EHDPPBDT** films show a blue shift of the absorption onset and a thinner band with respect to the film obtained from **TegDPPBDT**. These features suggest that high molecular weight induces a less planar conformation of the polymeric chain determining a worse molecular packing at the solid state. Instead the different alkyl or oligoether side chains, in this case, do not influence the packing.

**TegDPPBDT-HMW** and **EHDPPBDT** polymers were also characterized through CV, exhibiting low values of electrochemical band gaps.

Finally, tests in organic field-effect transistor exhibit low values of charge carrier mobility for the last two synthetized polymers, probably due to a worse molecular packing.

# Experimental section

# 9 Solvents and reagents

The reaction solvents were distilled in nitrogen stream immediately before their use. In particular, the THF and toluene were distilled from sodium-benzophenone and chloroform and methylene chloride with phosphorus pentoxide. The solvents for extraction and chromatography and the commercial reagents were used without further purification. The chromatography was conducted using silica gel Macherey-Nagel (60, Section particles 0.063-0.2 mm), while for the TLC analysis were used sheets of silica gel 60 F254 supported on aluminum (Alugram Sil G / UV254 Macherey-Nagel ).

## 9.1 Instruments

The spectra $^{1}$H-NMR and $^{13}$C-NMR were recorded on a Varian Inova 400 and 100.6 MHz respectively; using the peak of the proton of residue in $CDCl_3$ ($\delta$ = 7.24 ppm) as internal standard for $^{1}$H spectra, and the signals of the $CDCl_3$ ($\delta$ = 77 ppm) as internal standard for $^{13}$C spectra. The IR spectra were recorded on a Perkin-Elmer FT-IR Spectrum Bx. The UV-Vis absorption measurements were performed on a spectrometer Shimadzu UV-2401PC. TGA analysis were performed in air or under nitrogen using a Perkin–Elmer TGA-7 device. Cyclic voltammetry measurements were carried out with an Autolab potentiostat (model PGSTAT128N) by Metrohm using a conventional three-electrode configuration. Current density–voltage (J–V) characteristics of all solar-cell devices were measured using a Keithley 2420 instrument under an AM1.5 Class A ABET solar simulator with an intensity

of 1000 W/m$^2$. The EQE measurements were carried out using an IPCE (Incident Photon-to-current Conversion Efficiency) system (IPCELS200, Dyers) calibrated with an UV-enhanced Si detector (Thorlabs, 250–1100 nm). OFETs measurements were recorded trough an Agilent 4155C semiconductor parameter analyzer.

# 10 Synthesis of 3,6-Bis(5-bromothiophen-2-yl)-2,5-bis(2-ethylhexyl)pyrrolo-[3,4-c]pyrrole-1,4(2H,5H)-dione

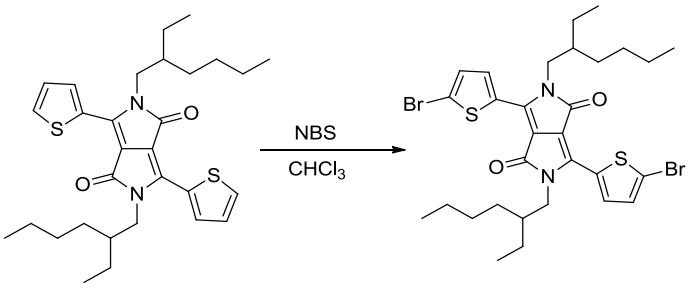


**1a** **2a**

**Scheme 10.1:** Synthesis of **2a**.

Monomer **2a** was synthesized according to a modified literature procedure.[58] A nitrogen-purged, three-necked, round-bottomed flask covered with aluminum foil and equipped with a magnetic stirrer was charged under nitrogen with a solution of 1.30 mmol of compound 2,5-bis(2-ethylhexyl)pyrrolo-[3,4-c]pyrrole-1,4(2H,5H)-dione (**1a**,) in dry chloroform (30ml). N-Bromosuccinimide (2.72 mmol) was added in one portion, and then the mixture was stirred at room temperature in the dark for 24 h. The mixture was poured into methanol (80 ml), and the resulting suspension was stirred at room temperature for 5 min. The solid was then collected by vacuum filtration and washed with several portions of methanol. After drying in vacuum, pure product **2a** was obtained as a dark purple solid (0.579 g, 65 %).

$^1$H NMR (400 MHz, $CDCl_3$): δ = 8.61 (d, J = 4.0 Hz, 2 H), 7.20 (d, J = 4.0 Hz, 2 H), 3.97–3.83 (m, 4 H), 1.86–1.74 (m, 2 H), 1.38–1.14 (m, 16 H), 0.90–0.80 (m, 12 H) ppm.

$^{13}C$ NMR (100.6 MHz, $CDCl_3$): δ = 161.3, 139.4, 135.4, 131.4, 131.1, 119.0, 107.9, 46.0, 39.1, 30.1, 28.3, 23.5, 23.0, 14.0, 10.4 (one coincident signal not observed) ppm.

IR (KBr): ῡ = 3085, 2957, 2926, 2859, 1655, 1556, 1449, 1412, 1399, 1100 $cm^{-1}$.

## 10.1 Synthesis of 2,5-bis(2-(2-(2-methoxyethoxy)ethoxy) ethyl)-3,6-di(thiophen-2-yl)pyrrolo[3,4-c]pyrrole-1,4 (2H,5H)-dione

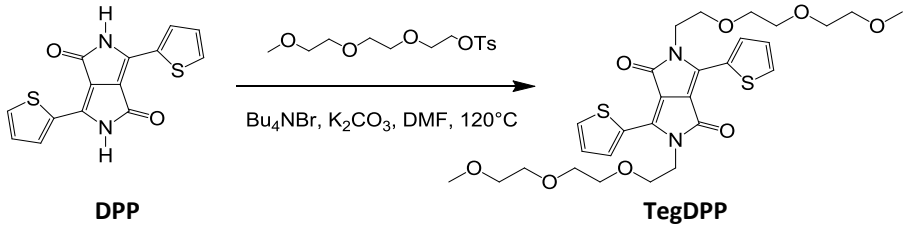


**DPP** **TegDPP**

**Scheme 10.2:** Synthesis of the **TegDPP**.

The alkylation of 3,6-di(thiophen-2-yl)pyrrolo[3,4-c]pyrrole-1,4(2H,5H)-dione (**DPP**) was carried out according to the literature procedure reported by Patil et al.[59] In a 3-neck flask of 50 ml, equipped with a bubble condenser and magnetic stirrer, were introduced, by operating in a current of nitrogen, the **DPP** (3.33 mmol), the $Bu_4NBr$ (0.33 mmol), and the $K_2CO_3$ (16.6 mmol). Then, a solution of tri(ethylene glycol) methyl ether tosylate (19.65 mmol) in DMF (25 mmol) was added.

The reaction mixture was heated at 120°C, for 48 hours. After cooling, it was added an aqueous solution of $NH_4Cl$ and extracted three times with methylene chloride. The organic extracts were washed several times with an aqueous solution of NaCl (10%), dried with anhydrous $Na_2SO_4$, filtered,

and concentrated under reduced pressure. The crude product was purified by column chromatography on silica gel using as eluent a mixture of DCM and acetone (8:2) yielded 1.290g of **TegDPP** (66%).

$^{1}$H-NMR (400 MHz, $CDCl_3$): δ= 8.69 (dd, $J_1$ = 1.2 Hz, $J_2$ = 3.9 Hz, 2H), 7.56 (dd, $J_1$ = 1.2 Hz, $J_2$ = 5.1 Hz, 2H), 7.17 (dd, $J_1$ = 3.9 Hz, $J_2$ = 5.1 Hz, 2H), 4.19 (t, J = 6.3 Hz, 4H), 3.71 (t, J = 6 Hz, 2H), 3.59–3.39 (m, 16H), 3.26 (s, 6H) ppm.

$^{13}$C-NMR (100.6 MHz, $CDCl_3$): δ= 161.6, 140.5, 135.0, 131.1, 129.9, 128.6, 108.0, 72.1, 70.9, 70.7, 69.1, 59.2, 42.0 ppm.

## 10.2 Synthesis of 3,6-Bis(5-bromothiophen-2-yl)-2,5-bis{2-[2-(2-methoxyethoxy)-ethoxy]ethyl}pyrrolo[3,4-c]pyrrole-1,4(2H,5H)-dione

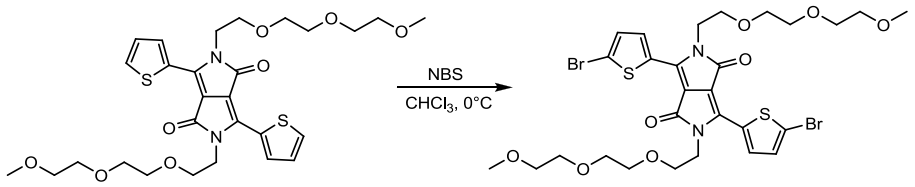


**TegDPP** **TegDPPBr$_2$**

**Scheme 10.3:** Synthesis of the **TegDPPBr$_2$**.

The bromination of the **TegDPP** was carried out following the literature procedure.[38,35] A solution of **TegDPP** (1.69 mmol), in anhydrous chloroform (30ml), was cooled to 0°C, and in the reaction flask, wrapped in aluminum foil, was added N-bromosuccinimide (3.38 mmol). The reaction was kept under stirring at 0°C and in the dark for 1h, then was stopped with a saturated aqueous solution of $NH_4Cl$ and extracted three times with DCM. The extracted organic phase, was extracted with an aqueous solution of

NaCl, dried over $Na_2SO_4$, filtered and concentrated under vacuum. The product was purified by washing with multiple aliquots of methanol. After drying under vacuum, 0.696 g of **TegDPPBr₂** (solid purple) were obtained corresponding to a yield of 55%.

$^1$H NMR (400 MHz, $CDCl_3$): δ = 8.44 (d, J = 4.0 Hz, 2 H), 7.14 (d, J = 4.0 Hz, 2 H), 4.11 (t, J = 5.8 Hz, 4 H), 3.71 (t, J = 5.8 Hz, 4 H), 3.61–3.56 (m, 4 H), 3.55–3.49 (m, 8 H), 3.46–3.41 (m, 4 H), 3.29 (s, 6 H) ppm.

$^{13}$C NMR (100.6 MHz, $CDCl_3$): δ = 161.1, 139.3, 134.8, 131.2, 131.0, 119.2, 107.8, 71.8, 70.7, 70.5, 70.4, 68.8, 58.9, 42.1 (one coincident signal not observed) ppm.

IR (KBr): ῡ = 3087, 2898, 2870, 1652, 1555, 1396, 1129, 1119 $cm^{-1}$.

## 10.3 Synthesis of di-tert-butyl 3,6-Bis(5-bromothiophen-2-yl)-1,4-dioxopyrrolo[3,4-c]pyrrole-2,5(1H,4H)-dicarboxylate

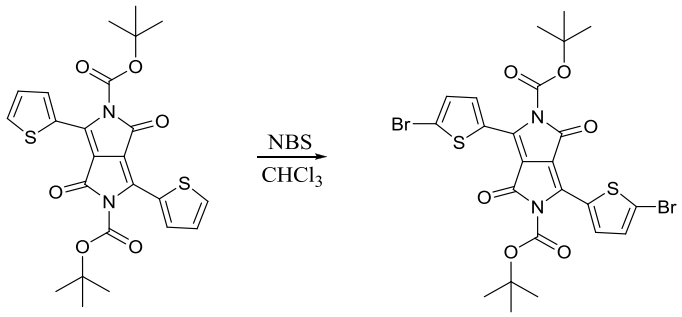


**1c** **2c**

**Scheme 10.4:** Synthesis of **2c**.

Compound **2c** was synthesized according to a modified literature procedure.[60] A round-bottomed flask covered with aluminum foil and equipped with a magnetic stirrer was charged with a solution of di-tert-

butyl-1,4-dioxopyrrolo[3,4-c]pyrrole-2,5(1H,4H)-dicarboxylate (**1c**; 1.00 mmol) in dry chloroform (30 ml). N-Bromosuccinimide (2.20 mmol) was then added in one portion at room temperature, and the mixture was stirred at the same temperature in the dark for 72 h. The mixture was poured into methanol (100 ml), and the resulting suspension was stirred at room temperature for 5 min. The solid was then collected by vacuum filtration and washed with several portions of hot methanol. After drying *in vacuum*, pure product **2c** was obtained as a purple solid (0.580 g, 88 %).

$^{1}$H NMR (400 MHz, CDCl3): δ = 8.04 (d, J = 4.0 Hz, 2 H), 7.12 (d, J = 4.0 Hz, 2 H), 1.59 (s, 18 H) ppm.

$^{13}$C NMR (100.6 MHz, CDCl3): δ = 158.6, 148.8, 136.7, 134.5, 131.0, 130.9, 120.9, 110.3, 86.3, 27.7 (one coincident signal not observed) ppm.

IR (KBr): ῡ= 2978, 2924, 1748, 1689, 1570, 1410, 1381, 1303, 1218, 1149, 1104 cm$^{-1}$.

## 10.4 Synthesis of 2,5-Bis(2-ethylhexyl)-3,6-bis{5-[(trimethylsilyl)ethynyl]thiophen-2-yl}pyrrolo[3,4-c] pyrrole-1,4(2H,5H)-dione

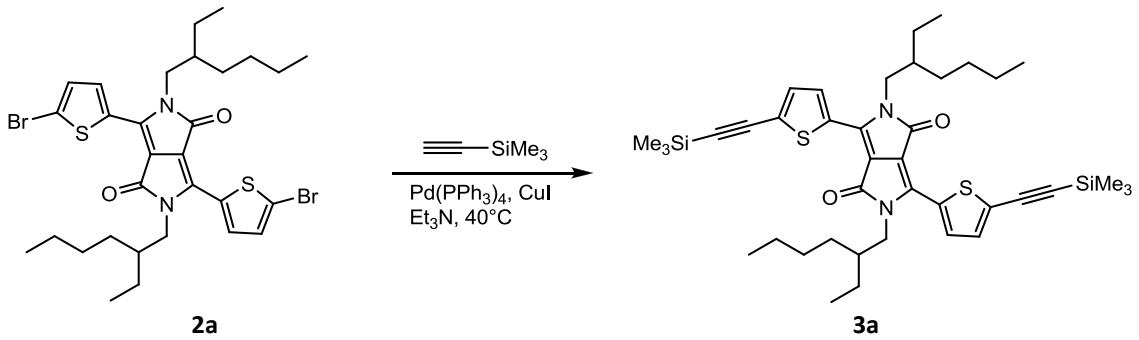


**2a** **3a**

**Scheme 10.5:** Synthesis of **3a**.

Compound **3a** was synthesized according to a modified literature procedure.[61] A nitrogen-purged, three-necked, round-bottomed flask equipped with a magnetic stirrer and a condenser was charged under nitrogen with 3,6-Bis(5-bromothiophen-2-yl)-2,5-bis(2-ethylhexyl)pyrrolo-[3,4-c]pyrrole-1,4(2H,5H)-dione (**2a**; 0.73 mmol), $Pd(PPh_3)_4$ (0.04 mmol) and CuI (0.08 mmol) and anhydrous THF (25 ml). Triethylamine (12 ml) and (trimethylsilyl) acetylene (3.75 mmol) were quickly added. The mixture was heated at 40°C for 1 h, and the progress of the reaction was monitored by TLC. The mixture was cooled to room temperature, then quenched with a saturated aqueous solution of $NH_4Cl$ (30 ml) and extracted with dichloromethane (3 × 60 ml). The organic extracts were washed with an aqueous solution of NaCl (3 × 30 ml), dried with $Na_2SO_4$, and concentrated under vacuum. The crude product was purified by washing with several aliquots of methanol, which led to pure **3a** as a dark purple solid (0.515 g, 98 %).

$^{1}$H NMR (400 MHz, $CDCl_3$): δ = 8.79 (d, J = 4.0 Hz, 2 H), 7.30 (d, J = 4.0 Hz, 2 H), 4.02–3.89 (m, 4 H), 1.88–1.78 (m, 2 H), 1.39–1.16 (m, 16 H), 0.90–0.82 (m, 12 H), 0.26 (s, 18 H) ppm.

$^{13}$C NMR (100.6 MHz, $CDCl_3$): δ = 161.5, 139.6, 135.2, 133.5, 130.5, 128.4, 108.9, 104.2, 96.7, 46.1, 39.1, 30.2, 28.4, 23.6, 23.0, 14.0, 10.5, –0.30 (one coincident signal not observed) ppm.

IR (KBr): ῡ = 2955, 2927, 2863, 2139, 1665, 1554, 853 $cm^{-1}$.

## 10.5 Synthesis of 2,5-Bis{2-[2-(2-methoxyethoxy) ethoxy]ethyl}-3,6-bis{5-[(trimethylsilyl)ethynyl] thiophen-2-yl}pyrrolo[3,4-c]pyrrole-1,4(2H,5H)-dione

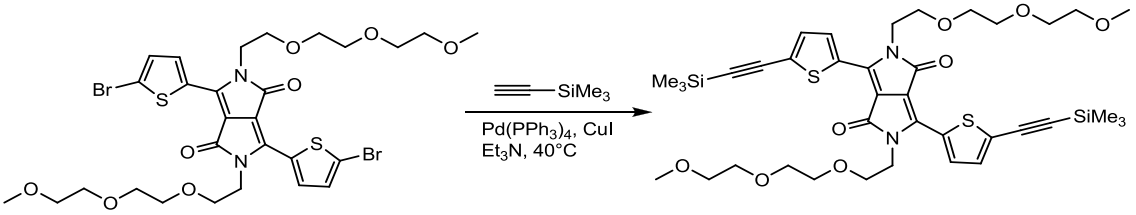


**TegDPPBr₂** **3b**

**Scheme 10.6:** Synthesis of **3b**.

A nitrogen-purged, three-necked, round bottomed flask equipped with a magnetic stirrer and a condenser was charged under nitrogen with **TegDPPBr₂** (0.71 mmol), $Pd(PPh_3)_4$ (0.04 mmol), and CuI (0.08 mmol) and anhydrous THF (25 ml). Triethylamine (15 ml) and (trimethylsilyl) acetylene (2.89 mmol) were quickly added. The mixture was heated at 40°C for 2 h, and the progress of the reaction was monitored by TLC. The mixture was cooled to room temperature, then quenched with a saturated aqueous solution of $NH_4Cl$ (30 ml), and extracted with dichloromethane (3 × 60 ml).

The combined organic extracts were washed with an aqueous solution of NaCl (3 × 30 ml), dried with $Na_2SO_4$ and concentrated under vacuum. The crude product was purified by column chromatography on silica gel ($CH_2Cl_2$/acetone, 9:1). A dark purple solid was isolated (0.401 g, 72 %).

$^1$H NMR (400 MHz, $CDCl_3$): δ = 8.65 (d, J = 4.0 Hz, 2 H), 7.26 (d, J = 4.0 Hz, 2 H), 4.19 (t, J = 6.0 Hz, 4 H), 3.73 (t, J = 6.0 Hz, 4 H), 3.62–3.57 (m, 4 H), 3.56–3.50 (m, 8 H), 3.46– 3.42 (m, 4 H), 3.30 (s, 6 H), 0.24 (s, 18 H) ppm.

$^{13}$C NMR (100.6 MHz, $CDCl_3$): δ = 161.2, 139.5, 134.7, 133.3, 130.3, 128.5, 108.7, 104.2, 96.6, 71.8, 70.7, 70.5, 70.5, 68.9, 58.9, 42.0, –0.4 (one coincident signal not observed) ppm.

IR (KBr): ῡ = 2869, 2804, 2136, 1660, 1555, 1442, 1398, 1138, 1093, 1055, 845 $cm^{-1}$.

## 10.6 Synthesis of di-tert-butyl 1,4-Dioxo-3,6-bis{5-[(trimethylsilyl)ethynyl]thiophen-2-yl}pyrrolo[3,4-c] pyrrole-2,5(1H,4H)-dicarboxylate

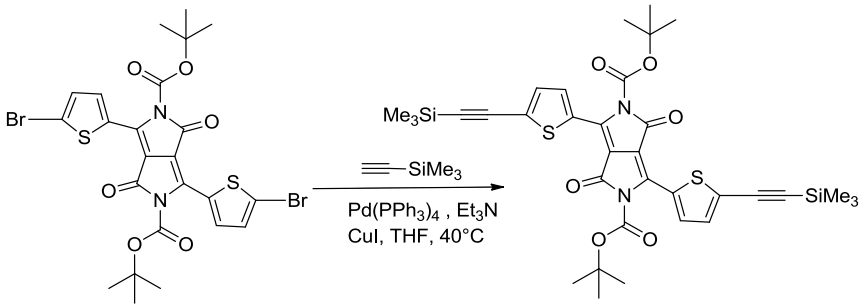


**2c** **3c**

**Scheme 10.7:** Synthesis of **3c**.

A nitrogen-purged, three-necked, round-bottomed flask equipped with a magnetic stirrer and a condenser was charged under nitrogen with di-tert-

butyl 3,6-Bis(5-bromothiophen-2-yl)-1,4-dioxopyrrolo[3,4-c]pyrrole-2,5(1H,4H)-dicarboxylate (**2c**; 0.38 mmol), $Pd(PPh_3)_4$ (0.02 mmol), CuI (0.04), and anhydrous THF (25 ml). Triethylamine (15 ml) and (trimethylsilyl)acetylene (1.52 mmol) were quickly added. The mixture was heated at 40 °C for 3 h, and the progress of the reaction was monitored by TLC. The mixture was cooled to room temperature, then quenched with a saturated aqueous solution of $NH_4Cl$ (30 ml), and extracted with dichloromethane (3 × 60 ml). The combined organic extracts were washed with an aqueous solution of NaCl (3 × 30 ml), dried with Na2SO4, and concentrated under vacuum. The crude product was purified by column chromatography on silica gel ($CH_2Cl_2$/hexane, 8:2). A dark purple solid was isolated (0.182 g, 70 %).

$^1$H NMR (400 MHz, $CDCl_3$): δ = 8.11 (d, J = 4.0 Hz, 2 H), 7.21 (d, J = 4.0 Hz, 2 H), 1.59 (s, 18 H), 0.24 (s, 18 H) ppm.

$^{13}$C NMR (100.6 MHz, $CDCl_3$): δ = 158.8, 148.7, 136.8, 133.8, 133.0, 130.1, 129.8, 111.0, 104.7, 96.6, 86.2, 27.7, –0.3 (one coincident signal not observed) ppm.

IR (KBr): ῡ= 2958, 2937, 2143, 1754, 1693, 1582, 1561, 1439, 1283, 1148, 1106, 843 $cm^{-1}$.

# 10.7 Synthesis of 2,5-bis(2-ethylhexyl)-3,6-bis(5-ethynylthiophen-2-yl)pyrrolo-[3,4-c]pyrrole-1,4 (2H,5H)-dione

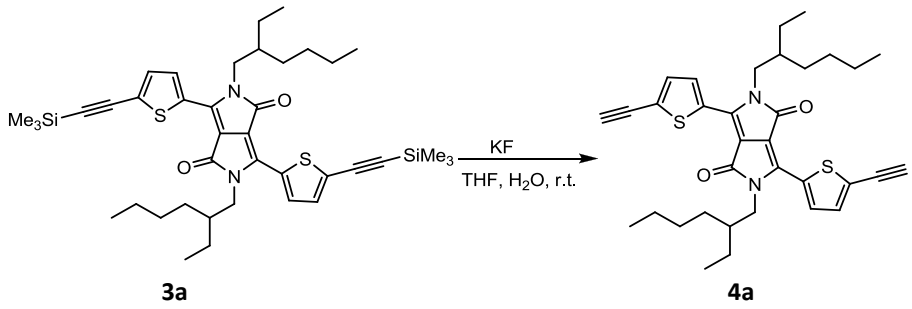


**3a** **4a**

**Scheme 10.8:** Synthesis of **4a**.

KF (6.21 mmol) was added at room temperature to a stirred suspension of compound **3a** (0.62 mmol) in nitrogen-purged THF (14 ml) and nitrogen-purged $H_2O$ (4 ml). The mixture was stirred at room temperature. Upon completion of the reaction (3 h), the mixture was quenched with a saturated aqueous solution of $NH_4Cl$ (30 ml) and then extracted with dichloromethane (3 × 60 ml). The combined organic extracts were washed with an aqueous solution of NaCl (3 × 30 ml), dried with $Na_2SO_4$, and concentrated under vacuum. The crude product was purified by washing with hexane, which led to pure compound **4a** as a dark purple solid (0.348 g, 98 %).

$^1$H NMR (400 MHz, $CDCl_3$): δ = 8.80 (d, J = 4.0 Hz, 2 H), 7.35 (d, J = 4.0 Hz, 2 H), 4.02–3.88 (m, 4 H), 3.57 (s, 2 H), 1.89–1.77 (m, 2 H), 1.39–1.15 (m, 16 H), 0.90–0.81 (m, 12 H) ppm.

$^{13}$C NMR (100.6 MHz, $CDCl_3$): δ = 161.4, 139.6, 135.2, 134.0, 130.7, 127.0, 108.9, 85.5, 76.3, 46.0, 39.1, 30.1, 28.3, 23.5, 23.0, 14.0, 10.4 (one coincident signal not observed) ppm.

IR (KBr): ῡ = 3259, 2958, 2928, 2856, 1660, 1559, 1452, 1403, 1095, 827 $cm^{-1}$.

## 10.8 Synthesis of 3,6-Bis(5-ethynylthiophen-2-yl)-2,5-bis{2-[2-(2-methoxyethoxy)ethoxy]ethyl}pyrrolo[3,4-c] pyrrole-1,4(2H,5H)-dione

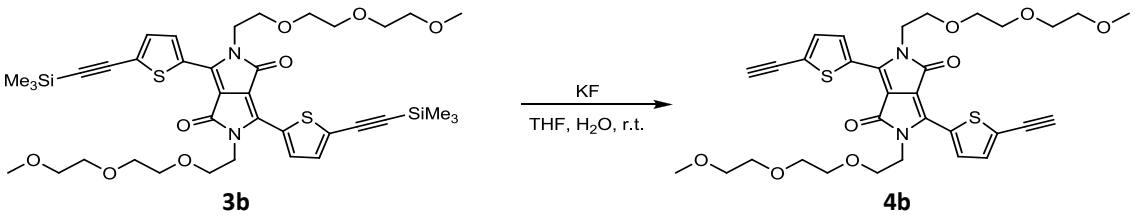


**3b** **4b**

**Scheme 10.9:** Synthesis of **4b**.

KF (4.84 mmol) was added at room temperature to a stirred suspension of compound **3b** (0.484 mmol) in nitrogen-purged THF (14 ml) and nitrogen-purged $H_2O$ (4 ml). The mixture was stirred at room temperature. Upon completion (3 h) of the reaction, the mixture was quenched with a saturated aqueous solution of $NH_4Cl$ (30 ml) and then extracted with dichloromethane (3 × 60 ml). The combined organic extracts were washed with an aqueous solution of NaCl (3 × 30 ml), dried with $Na_2SO_4$, and concentrated under vacuum, to give pure **4b** as a dark purple solid (0.295 g, 95 %).

$^{1}$H NMR (400 MHz, $CDCl_3$): δ = 8.65 (d, J = 4.0 Hz, 2 H), 7.32 (d, J = 4.0 Hz, 2 H), 4.20 (t, J = 6.0 Hz, 4 H), 3.74 (t, J = 6.0 Hz, 4 H), 3.63–3.58 (m, 4 H), 3.57–3.50 (m, 10 H), 3.47– 3.43 (m, 4 H), 3.31 (s, 6 H) ppm.

$^{13}$C NMR (100.6 MHz, $CDCl_3$): δ = 161.2, 139.6, 134.6, 133.9, 130.6, 127.2, 108.8, 85.5, 76.2, 71.8, 70.7, 70.5, 70.5, 68.9, 58.9, 42.1 (one coincident signal not observed) ppm.

IR (KBr): ῡ= 3239, 2910, 2871, 1655, 1553, 1404, 1134, 1119 $cm^{-1}$

## 10.9 Synthesis of di-tert-butyl 3,6-Bis(5-ethynylthiophen-2-yl)-1,4-dioxopyrrolo-[3,4-c]pyrrole-2,5(1H,4H)-dicarboxylate

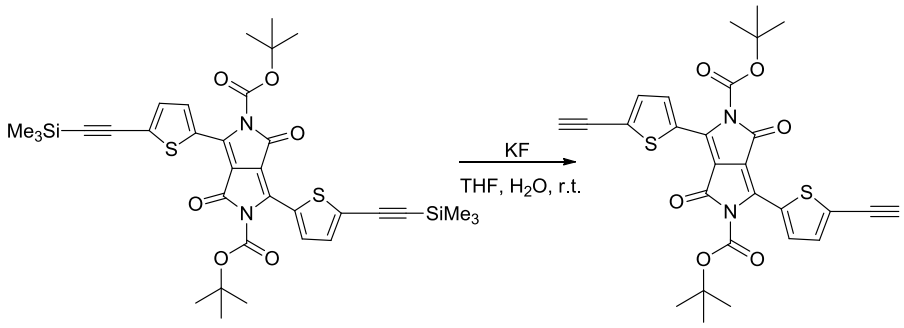


**3c** **4c**

**Scheme 10.10:** Synthesis of **4c**.

KF (1.21 mmol) was added at room temperature to a stirred suspension of compound **3c** ( 0.12 mmol) in nitrogen-purged THF (8 ml) and nitrogen-purged $H_2O$ (2ml). The mixture was stirred at room temperature. Upon completion of the reaction (1.5 h), the mixture was quenched with a saturated aqueous solution of $NH_4Cl$ (30 ml) and extracted with dichloromethane (3 × 50 ml). The combined organic extracts were washed with an aqueous solution of NaCl (3 × 30 ml), dried with $Na_2SO_4$, and

concentrated under vacuum, to give pure **4c** as a dark purple solid (0.065 g, 98 %).

$^{1}$H NMR (400 MHz, $CDCl_3$): δ = 8.16 (d, J = 4.0 Hz, 2 H), 7.28 (d, J = 4.0 Hz, 2 H), 3.56 (s, 2 H), 1.59 (s, 18 H) ppm.

$^{13}$C NMR (100.6 MHz, $CDCl_3$): δ = 158.7, 148.6, 136.9, 133.9, 133.5, 130.5, 128.4, 111.2, 86.3, 85.8, 76.2, 27.7 (one coincident signal not observed) ppm.

IR (KBr): ῡ= 3271, 2969, 2921, 1757, 1690, 1555, 1374, 1302, 1217, 1146, 1098 $cm^{-1}$.

## 10.10 Synthesis of 2,5-bis(2-ethylhexyl)-3,6-bis[5-(1-octyl-1H-1,2,3-triazol-4-yl)-thiophen-2-yl]pyrrolo[3,4-c]pyrrole-1,4(2H,5H)-dione

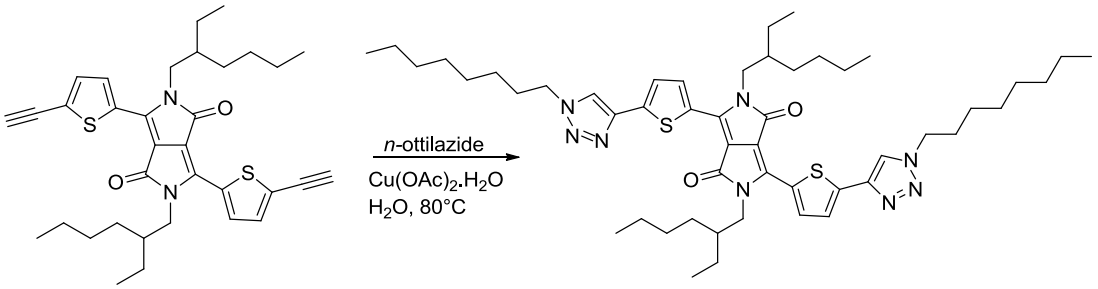


**4a** **5a**

**Scheme 10.11:** Synthesis of **5a**.

Compound **4a** (0.13 mmol) and n-octyl azide (0.39 mmol) were added at room temperature to a solution of $Cu(OAc)_2 \cdot H_2O$ (0.03 mmol) in $H_2O$ (10ml) in a round-bottomed flask equipped with a magnetic stirrer and a condenser. The mixture was heated at 80°C and vigorously stirred. Upon completion of the reaction (22 h), the mixture was cooled to room

temperature, then quenched with a saturated aqueous solution of $NH_4Cl$ (20 ml), and extracted with dichloromethane (3 × 40 ml). The combined organic extracts were washed with an aqueous solution of NaCl (3 × 30 ml), dried with $Na_2SO_4$, and concentrated under vacuum. The crude product was purified by column chromatography on silica gel ($CH_2Cl_2$/ethyl acetate, 9.5:0.5). A dark purple solid was isolated (75 mg, 67 %), which was then crystallized from dichloromethane/ hexane.

$^1$H NMR (400 MHz, $CDCl_3$): δ = 8.92 (d, J = 4.0 Hz, 2 H), 7.79 (s, 2 H), 7.44 (d, J = 4.0 Hz, 2 H), 4.38 (t, J = 7.2 Hz, 4 H), 4.09–3.98 (m, 4 H), 1.98–1.87 (m, 6 H), 1.42–1.15 (m, 36 H), 0.78–0.90 (m, 18 H) ppm.

$^{13}$C NMR (100.6 MHz, $CDCl_3$): δ = 161.6, 141.8, 139.9, 138.4, 136.3, 128.9, 125.0, 119.9, 108.3, 50.6, 46.0, 39.1, 31.7, 30.2, 30.1, 29.0, 28.9, 28.3, 26.4, 23.6, 23.0, 22.6, 14.0, 14.0, 10.5 (one coincident signal not observed) ppm.

IR (KBr): ῡ = 3117, 2958, 2923, 2954, 1647, 1553, 1430, 1241, 1077, 1058, 817 $cm^{-1}$.

## 10.11 Synthesis of 2,5-Bis{2-[2-(2-methoxyethoxy) ethoxy]ethyl}-3,6-bis[5-(1-octyl-1H-1,2,3-triazol-4-yl) thiophen-2-yl]pyrrolo[3,4-c]pyrrole-1,4(2H,5H)-dione

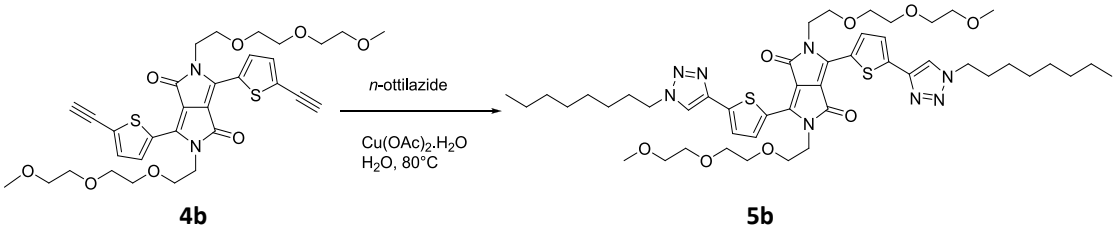


**4b** **5b**

**Scheme 10.12:** Synthesis of **5b**.

Compound **4b** (0.156 mmol) and n-octyl azide (0.47 mmol) were added at room temperature to a solution of $Cu(OAc)_2 \cdot H_2O$ (0.03 mmol) in $H_2O$ (14 ml) in a round-bottomed flask equipped with a magnetic stirrer and a condenser. The mixture was heated at 80 °C and vigorously stirred. Upon completion of the reaction (16 h, TLC analysis), the mixture was cooled to room temperature, then quenched with a saturated aqueous solution of $NH_4Cl$ (30 ml), and extracted with dichloromethane (3 × 50 ml). The combined organic extracts was washed with an aqueous solution of NaCl (3 × 30 ml), dried with $Na_2SO_4$, and concentrated under vacuum. The crude product was purified by column chromatography on silica gel ($CH_2Cl_2$/acetone, 7:3). A dark purple solid was isolated (129 mg, 87 %), which was then crystallized from dichloromethane/hexane.

$^1$H NMR (400 MHz, $CDCl_3$): δ = 8.82 (d, J = 4.0 Hz, 2 H), 7.79 (s, 2 H), 7.45 (d, J = 4.0 Hz, 2 H), 4.36 (t, J = 7.2 Hz, 4 H), 4.29 (t, J = 6.0 Hz, 4 H), 3.78 (t, J = 6.2 Hz, 4 H), 3.64–3.60 (m, 4 H), 3.58–3.51 (m, 8 H), 3.45–3.40 (m, 4 H), 3.28 (s, 6 H), 1.98–1.85 (m, 4 H), 1.38–1.18 (m, 20 H), 0.84 (t, J = 7.0 Hz, 6 H) ppm.

$^{13}$C NMR (100.6 MHz, $CDCl_3$): δ = 161.3, 141.6, 139.7, 138.5, 135.9, 128.7, 125.0, 120.0, 108.1, 71.8, 70.7, 70.5, 69.0, 58.9, 50.6, 41.9, 31.6, 30.2, 29.0, 28.9, 26.4, 22.5, 14.0 (two coincident signals not observed) ppm.

IR (KBr): ῡ= 3119, 2923, 2854, 1656, 1553, 1431, 1242, 1108, 1067 $cm^{-1}$.

## 10.12 Synthesis of di-tert-butyl 3,6-Bis[5-(1-hexyl-1H-1,2,3-triazol-4-yl)thiophen-2-yl]-1,4-dioxopyrrolo[3,4-c] pyrrole-2,5(1H,4H)-dicarboxylate

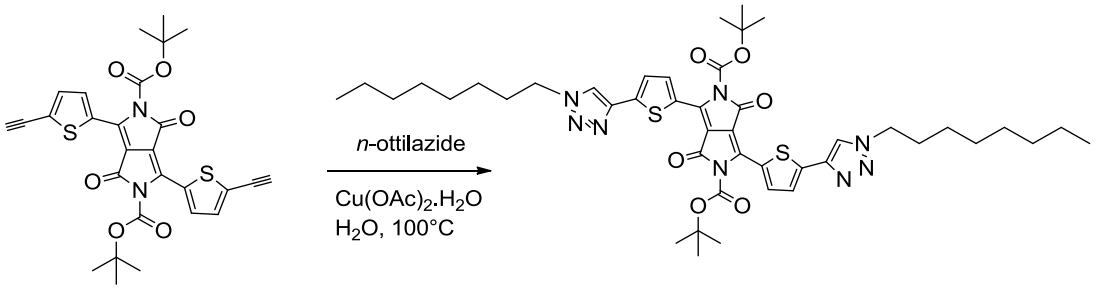


**4c** **5c**

**Scheme 10.13:** Synthesis of **5c**.

Compound **4c** (0.12 mmol) and n-octyl azide (0.36 mmol) were added at room temperature to a solution of $Cu(OAc)_2{\cdot}H_2O$ 6 mg, (0.03 mmol) in $H_2O$ (5 ml) in a round-bottomed flask equipped with a magnetic stirrer and a condenser. The mixture was heated at 100 °C and vigorously stirred. After 24 h, n-octyl azide (0.36 mmol) and $Cu(OAc)_2{\cdot}H_2O$ (0.03 mmol) were added, and then the mixture was heated at 100 °C for additional 24 h. The progress of the reaction was monitored by TLC. The mixture was cooled to room temperature, then quenched with a saturated aqueous solution of $NH_4Cl$ (20 ml), and extracted with dichloromethane (3 × 40 ml). The combined organic extracts was washed with an aqueous solution of NaCl (3 × 30 ml), dried with $Na_2SO_4$, and concentrated under vacuum. The crude product was purified by column chromatography on silica gel (hexane/ethyl acetate/dichloromethane, 6:4:4). A purple solid was isolated (54 mg, 53 %), which was then crystallized from dichloromethane/hexane.

$^{1}$H NMR (400 MHz, $CDCl_3$): δ = 8.28 (d, J = 4.0 Hz, 2 H), 7.76 (s, 2 H), 7.44 (d, J = 4.0 Hz, 2 H), 4.38 (t, J = 7.2 Hz, 4 H), 1.98–1.88 (m, 4 H), 1.61 (s, 18 H), 1.38–1.20 (m, 20 H), 0.86 (t, J = 6.6 Hz, 6 H) ppm.

$^{13}$C NMR (100.6 MHz, $CDCl_3$): δ = 159.1, 148.8, 141.7, 139.7, 137.3, 135.0, 128.7, 124.8, 120.1, 110.4, 86.1, 50.7, 31.7, 30.3, 29.0, 28.9, 27.8, 26.5, 22.6, 14.0 (one coincident signal not observed) ppm.

IR (KBr): ῡ = 3107, 2925, 2855, 1756, 1695, 1572, 1433, 1294, 1253, 1148, 1093, 1057 $cm^{-1}$.

## 10.13 Synthesis of 3,6-Bis[5-(1-hexadecyl-1H-1,2,3-triazol-4-yl)thiophen-2-yl]-2,5-bis{2-[2-(2-methoxyethoxy)ethoxy]ethyl}pyrrolo[3,4-c]pyrrole-1,4(2H,5H)-dione

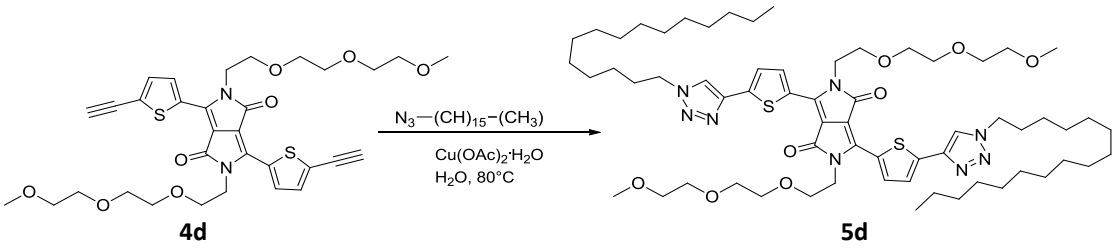


**Scheme 10.14:** Synthesis of **5d**.

Compound **4b** (0.0697 mmol) and n-hexadecyl azide (0.29 mmol) were added at room temperature to a solution of $Cu(OAc)_2{\cdot}H_2O$ (0.02 mmol) in $H_2O$ (5 ml) in a round-bottomed flask equipped with a magnetic stirrer and a condenser. The mixture was heated at 80 °C and vigorously stirred. Upon completion of the reaction (16 h; TLC analysis), the mixture was cooled to room temperature, then quenched with a saturated aqueous solution of

$NH_4Cl$ (30 ml), and extracted with dichloromethane (3 × 50 ml). The combined organic extracts were washed with an aqueous solution of NaCl (3 × 30 ml), dried with $Na_2SO_4$, and concentrated under vacuum. The crude product was purified by column chromatography on silica gel ($CH_2Cl_2$/acetone, 8:2). A dark purple solid was isolated (83 mg, 73 %), which was then washed with methanol.

$^1$H NMR (400 MHz, $CDCl_3$): δ = 8.82 (d, J = 4 Hz, 2 H), 7.79 (s, 2 H), 7.46 (d, J = 4 Hz, 2 H), 4.36 (t, J = 7.4 Hz, 4 H), 4.29 (t, J = 6.0 Hz, 4 H), 3.78 (t, J = 6.2 Hz, 4 H), 3.65–3.60 (m, 4 H), 3.59–3.51 (m, 8 H), 3.45–3.41 (m, 4 H), 3.28 (s, 6 H), 1.97–1.87 (m, 4 H), 1.38–1.18 (m, 52 H), 0.84 (t, J = 6.8 Hz, 6 H) ppm.

$^{13}$C NMR (100.6 MHz, $CDCl_3$): δ = 161.3, 141.7, 139.7, 138.5, 135.9, 128.7, 125.0, 120.0, 108.1, 71.8, 70.7, 70.5, 70.0, 58.9, 50.6, 41.9, 31.9, 30.2, 29.6, 29.6, 29.5, 29.5, 29.3, 29.3, 29.0, 26.4, 22.6, 14.1 (five coincident signals not observed) ppm.

IR (KBr): ῡ = 3112, 2915, 2850, 1656, 1555, 1432, 1247, 1117, 1068 $cm^{-1}$.

## 10.14 Synthesis of 2,5-Bis(2-ethylhexyl)-3,6-bis{5-[1-(2-{2-[2-(2-hydroxyethoxy)-ethoxy]ethoxy}ethyl)-1H-1,2,3-triazol-4-yl]thiophen-2-yl}pyrrolo[3,4-c]pyrrole-1,4(2H,5H)-dione

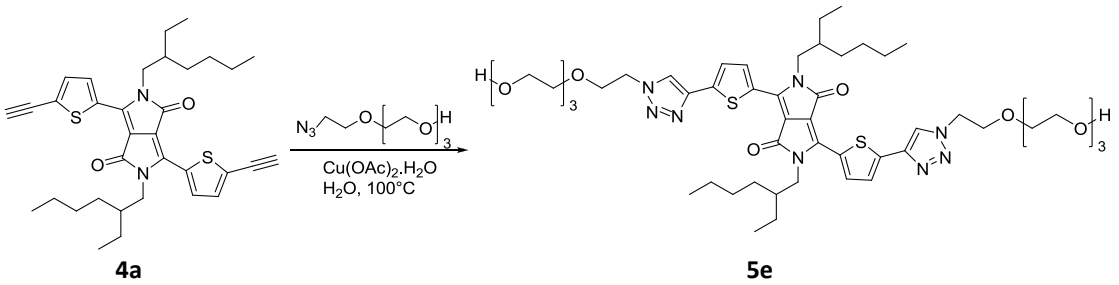


**4a** **5e**

**Scheme 10.15:** Synthesis of **5e**.

Compound **4a** (0.14 mmol) and 2-{2-[2-(2-azidoethoxy) ethoxy]ethoxy}-ethanol (0.46 mmol) were added at room temperature to a solution of $Cu(OAc)_2{\cdot}H_2O$ (0.04 mmol) in $H_2O$ (15 ml) in a round-bottomed flask equipped with a magnetic stirrer and a condenser. The mixture was heated at 100 °C and vigorously stirred. Upon completion of the reaction (20 h; TLC analysis), the mixture was cooled to room temperature, then quenched with a saturated aqueous solution of $NH_4Cl$ (30 ml), and extracted with dichloromethane (3 × 50 ml). The combined organic extracts were washed with an aqueous solution of NaCl (3 × 30 ml), dried with $Na_2SO_4$, and concentrated under vacuum. The crude product was purified by column chromatography on silica gel ($CH_2Cl_2$/ethyl acetate/methanol, 5:5:1 to 5:5:3). After washing with hexane, a dark purple solid was isolated (99 mg, 70 %), which was then crystallized from dichloromethane/hexane.

$^1$H NMR (400 MHz, $CDCl_3$): δ = 8.92 (d, J = 4.0 Hz, 2 H), 8.11 (s, 2 H), 7.46 (d, J = 4.0 Hz, 2 H), 4.58 (t, J = 4.8 Hz, 4 H), 4.09–3.98 (m, 4 H), 3.88 (t, J = 4.8

Hz, 4 H), 3.69 (t, J = 4.6 Hz, 4 H), 3.66–3.55 (m, 20 H), 2.70 (br. s, 2 H), 1.96–1.85 (m, 2 H), 1.43–1.15 (m, 16 H), 0.86 (t, J = 7.4 Hz, 6 H), 0.81 (t, J = 6.8 Hz, 6 H) ppm.

$^{13}$C NMR (100.6 MHz, $CDCl_3$): δ = 161.7, 141.8, 140.1, 138.7, 136.4, 128.8, 125.0, 121.8, 108.3, 72.4, 70.5, 70.5, 70.3, 70.2, 69.4, 61.6, 50.5, 46.1, 39.1, 30.1, 28.3, 23.6, 23.0, 14.0, 10.5 (one coincident signal not observed) ppm.

IR (KBr): ῡ = 3443, 3120, 2947, 2925, 2867, 1641, 1540, 1432, 1245, 1088, 1059 $cm^{-1}$.

## 10.15 Synthesis of 3,6-Bis{5-[1-(2-{2-[2-(2-hydroxyethoxy)ethoxy]ethoxy}ethyl)-1H-1,2,3-triazol-4-yl]thiophen-2-yl}-2,5-bis{2-[2-(2-methoxyethoxy) ethoxy]ethyl}pyrrolo[3,4-c]pyrrole-1,4(2H,5H)-dione

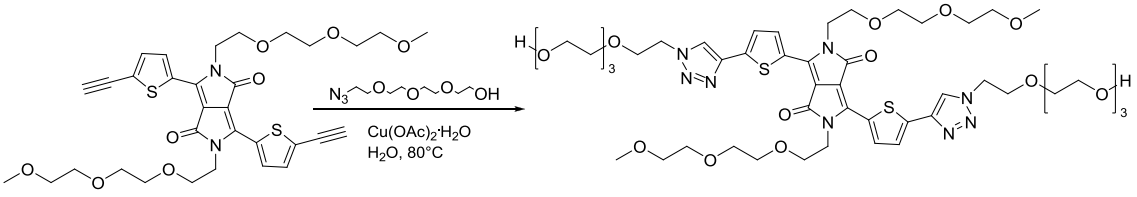


**4b** **5f**

**Scheme 10.16:** Synthesis of **5f**.

Compound **4b** (0.08 mmol) and 2-{2-[2-(2-azidoethoxy) ethoxy]ethoxy}ethanol (0.24 mmol) were added to a solution of $Cu(OAc)_2{\cdot}H_2O$ ( 0.02 mmol) in $H_2O$ (7 ml), at room temperature, in a round-bottomed flask equipped with a magnetic stirrer and a condenser. The mixture was heated at 80°C and vigorously stirred. Upon completion of the reaction (22 h; TLC analysis), the mixture was cooled to room temperature,

then quenched with $H_2O$ (30 ml), and extracted with a mixture of dichloromethane and acetone (1:1; 4 × 50 ml). The combined organic extracts were washed with an aqueous solution of 0.1 N EDTA (2 × 30 ml) and $H_2O$ (1 × 30 ml), dried with $Na_2SO_4$, and concentrated under vacuum. The crude product was purified by crystallization from $CH_2Cl_2$/hexane. A dark purple solid was isolated (68 mg, 79 %).

$^1$H NMR (400 MHz, $CDCl_3$): δ = 8.83 (d, J = 4.0 Hz, 2 H), 8.13 (s, 2 H), 7.49 (d, J = 4.0 Hz, 2 H), 4.59 (t, J = 4.8 Hz, 4 H), 4.31 (t, J = 6.2 Hz, 4 H), 3.89 (t, J = 4.8 Hz, 4 H), 3.78 (t, J = 6.2 Hz, 4 H), 3.72–3.68 (m, 4 H), 3.67–3.52 (m, 32 H), 3.45–3.41 (m, 4 H), 3.29 (s, 6 H), 2.31 (br. s, 2 H) ppm.

$^{13}$C NMR (100.6 MHz, CDCl3): δ = 161.4, 141.7, 139.9, 138.8, 136.1, 128.6, 125.1, 121.9, 108.1, 72.4, 71.8, 70.7, 70.5, 70.5, 70.3, 70.2, 69.3, 69.0, 61.6, 58.9, 50.5, 41.9 (three coincident signals not observed) ppm.

IR (KBr): ῡ= 3398, 2869, 1669, 1652, 1547, 1426, 1244, 1103, 1089, 1066 $cm^{-1}$.

# 11 Fabrication of 5a in BHJ solar cells

The devices were fabricated on ITO coated glass substrates, patterned with wet-etching in hydrobromic acid followed by cleaning in ultrasonic bath with acetone and 2 propanol each step for 10 min. Next the substrates were transferred inside the glove box. At first, PEDOT:PSS layer was deposited by spin coating and then dried on a hot plat at 150°C for 10 min. The active layer (**5a**/$PC_{60}BM$), dissolved in chlororm, was spin coated at 500 or 1000 rpm and then annealed on hot plat at 130°C for 10 min. After the substrates were transferred inside the metal evaporator and Ca (5nm) and Al (100nm) were thermally evaporated through the shadow mask. Six devices with 0.1$cm^2$ area were fabricated on each substrate.

# 12 Synthesis of the copolymer TegDPPV

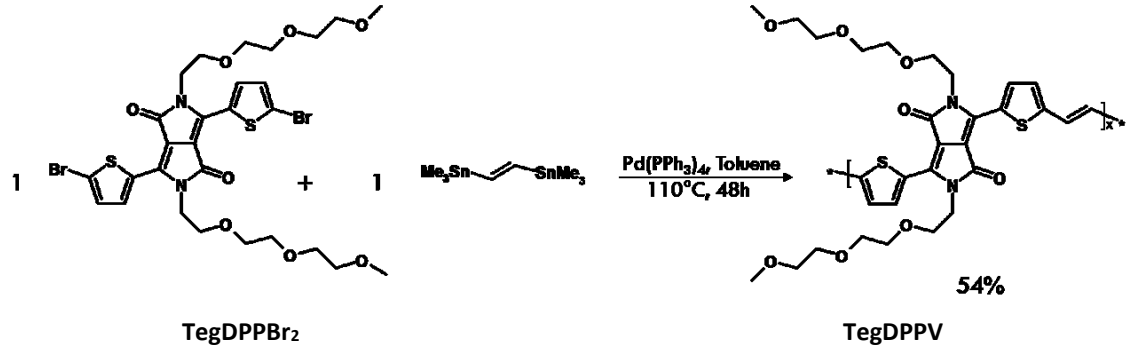


**Scheme 12.1:** Synthesis of **TegDPPV**.

In a 3-neck flask of 25 ml, equipped with a bubble condenser, and magnetic stirrer, were introduced, operating in nitrogen stream, the **TegDPPBr$_2$** (0.267 mmol), the trans-1,2-bis(trimethylstannyl)ethene (0.267 mmol) and the Pd ($PPh_3$)$_4$ (0.008 mmol) in dry toluene (10 ml). The mixture was reacted for 48h, then the iodobenzene (1.33 mmol) was added, in nitrogen stream, and the mixture was reacted, always at 110 °C for 4h and finally it was added the tributylstannyl thiophene (1.33 mmol) in stream of nitrogen and allowed to react for other 4h. The whole mixture was cooled to room temperature and poured in methanol, and the solid was recovered by filtration. The polymer was purified by Soxhlet extraction using methanol, acetone and then hexane. The polymer was then extracted with chloroform and the solvent was reduced to about 10−15 ml. The mixture was poured into methanol and the polymer was recovered by filtration. Polymer **TegDPPV** was obtained as a dark blue solid (0.094 g, 54 %).

$^1$H NMR (400 MHz, $C_2D_2Cl_4$, 90 °C): δ = 8.78–8.67 (m, 2 H), 7.29–7.14 (m, 4 H), 4.30–4.10 (m, 4 H), 3.82–3.70 (m, 4 H), 3.68–3.38 (m, 16 H), 3.30–3.22 (m, 6 H) ppm.

IR (KBr): ῡ = 2914, 2015, 1657, 1543, 1434, 1402, 1092, 1055 $cm^{-1}$.

## 12.1 Synthesis of the copolymer TegDPPT

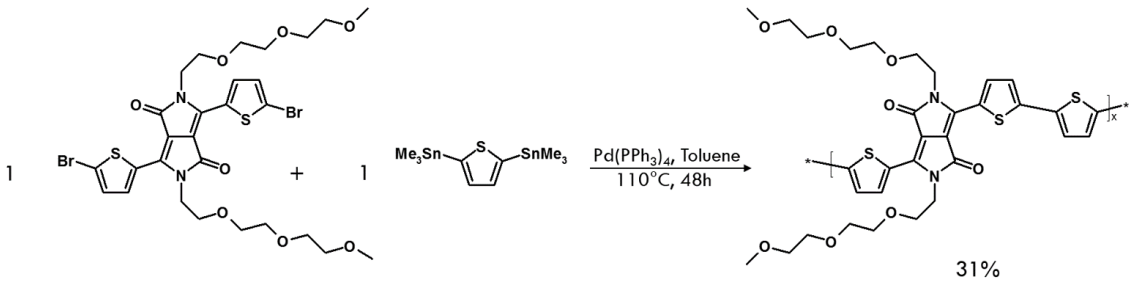


**TegDPPBr₂** **TegDPPT**

**Scheme 12.2:** Synthesis of **TegDPPT**.

In a 3-neck flask of 25 ml, equipped with a bubble condenser, and magnetic stirrer, were introduced, operating in nitrogen stream, the **TegDPPBr₂** (0.267 mmol), the 2,5-bis(trimethylstannyl)thiophene (0.267 mmol) and the Pd $(PPh_3)_4$ (0.008 mmol) in dry toluene (10ml). The mixture was reacted for 48h, then the iodobenzene (1.33 mmol) was added, in nitrogen stream, and the mixture was reacted, always at 110 °C for 4h and finally it was added the tributylstannyl thiophene (1.33 mmol) in stream of nitrogen and allowed to react for other 4h. The whole mixture was cooled to room temperature and poured in methanol, and the solid was recovered by filtration. The polymer was purified by Soxhlet extraction using methanol, acetone and then hexane. The polymer was then extracted with chloroform and the solvent was reduced to about 10−15 ml. The mixture was poured into methanol and the polymer was recovered by filtration. Polymer **TegDPPT** was obtained as a dark solid (0.055 g, 31 %).

$^1$H NMR (400 MHz, $C_2D_2Cl_4$, 90 °C): δ = 8.80–8.60 (m, 2 H), 7.35–7.10 (m, 6 H), 4.29–4.16 (m, 4 H), 3.84–3.71 (m, 4 H), 3.70–3.38 (m, 16 H), 3.29–3.24 (m, 6 H) ppm.

IR (KBr): ῡ = 2962, 2909, 2845, 1657, 1540, 1530, 1422, 1260, 1095, 1055, 1020, 800 $cm^{-1}$.

## 12.2 Synthesis of the copolymer TegDPPBDT

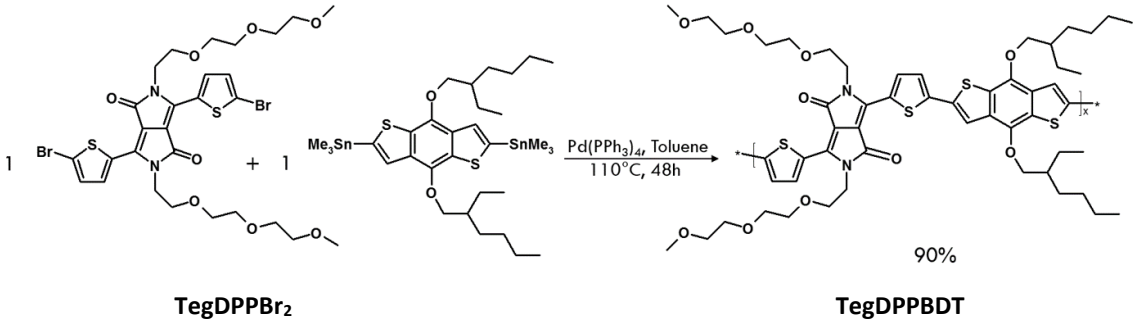


**TegDPPBr$_2$** **TegDPPBDT**

**Scheme 12.3:** Synthesis of **TegDPPBDT**.

In a 3-neck flask of 25 ml, equipped with a bubble condenser, and magnetic stirrer, were introduced, operating in nitrogen stream, the **TegDPPBr$_2$** (0.267 mmol), the 2,6-bis(trimethylstannyl)-4,8-bis(2-ethylhexyloxy)benzo[1,2-b:4,5-b']dithiophene (0.267 mmol) and the Pd $(PPh_3)_4$ (0.008 mmol) in dry toluene (10ml). The mixture was reacted for 48h, then the iodobenzene (1.33 mmol) was added, in nitrogen stream, and the mixture was reacted, always at 110 °C for 4h and finally it was added the tributylstannyl thiophene (1.33 mmol) in stream of nitrogen and allowed to react for other 4h. The whole mixture was cooled to room temperature and poured in methanol, and the solid was recovered by filtration. The polymer was purified by Soxhlet extraction using methanol,

acetone and then hexane. The polymer was then extracted with chloroform and the solvent was reduced to about 10−15 ml. The mixture was poured into methanol and the polymer was recovered by filtration. Polymer **TegDPPBDT** was obtained as a dark solid (0.240 g, 90 %).

$^1$H NMR (400 MHz, $C_2D_2Cl_4$, 90 °C): δ = 9.25–8.60 (m, 2 H), 7.55–6.50 (m, 4 H), 4.24–3.00 (m, 34 H), 1.70–0.85 (m, 30 H) ppm.

IR (KBr): ῡ = 2914, 2856, 1657, 1543, 1422, 1353, 1099, 1055, 1033cm$^{-1}$.

## 12.3 Synthesis of 2-(2-(2-methoxyethoxy)ethoxy)ethyl 2,5-dibromothiophen-3-carboxylate

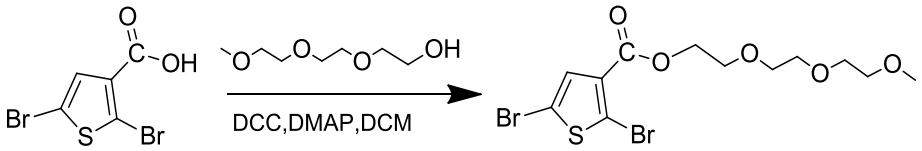


**Scheme 12.4:** Synthesis of the monomer **5**.

In a 3-neck flask, equipped with magnetic stirrer, were introduced, by operating in a current of nitrogen, 1.05 mmol of the acid 2,5-dibromothiophene-3-carboxylic acid (dried under vacuum for 5h at 50 °C), the solution of 2-(2- (2-methoxyethoxy)ethoxy)ethanol (0.81 mmol) in anhydrous DCM (6 ml) and the 4-dimethylaminopyridine (1.21 mmol). The mixture was reacted at room temperature for 1h, after cooling to 0 °C, the *N,N'* dicyclohexylcarbodiimide (DCC; 1.05 mmol) was introduced and it was reacted overnight at room temperature. The solvent was removed by evaporation under vacuum and the crude product purified by column chromatography on silica gel using as eluent a mixture of hexane and ethyl

acetate in the ratio 1:1. Were obtained 0.328 g of product corresponding to a yield of 93%.

$^{1}$H NMR (400 MHz, $CDCl_3$): δ = 7.35 (s, 1 H), 4.43–4.38 (m, 2 H), 3.80–3.76 (m, 2 H), 3.70–3.60 (m, 6 H), 3.54–3.51 (m, 2 H), 3.36 (s, 3 H) ppm.

$^{13}$C NMR (100.6 MHz, $CDCl_3$): δ = 160.6, 131.7, 131.5, 119.4, 111.3, 71.9, 70.6, 70.6, 70.5, 68.9, 64.2, 59.0 ppm.

IR (KBr): ῡ = 2914, 2873, 1725, 1425, 1223, 1135, 1109, 769 $cm^{-1}$.

## 12.4 Synthesis of the polymer TegDPPTegES

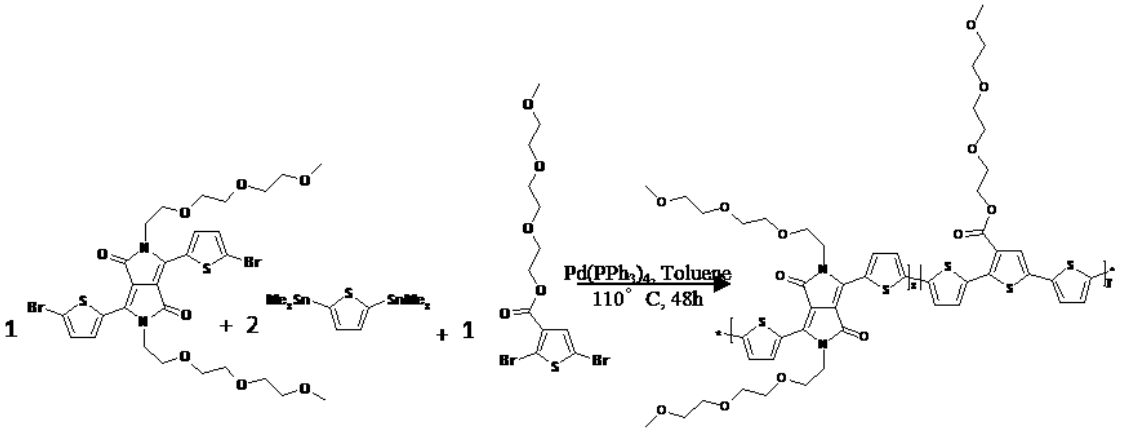


**TegDPPBr₂** **5** **TegDPPTegES**

**Scheme 12.5:** Synthesis of **TegDPPTegES**.

In a 3-neck flask, equipped with a bubble condenser, and magnetic stirrer, were introduced, operating in nitrogen stream, the **TegDPPBr₂** (0.240 mmol) the monomer **5** (0.240 mmol), the 2,5-bis (trimethylstannyl) thiophene (0.480 mmol) and the Pd $(PPh_3)_4$ (0.014 mmol) in dry toluene (10 ml). The mixture was reacted for 48h, then the iodobenzene (1.33 mmol) was added, in nitrogen stream, and the mixture was reacted, always at 110 °C for 4h and finally it was added the tributylstannyl thiophene (1.33 mmol)

in stream of nitrogen and allowed to react for other 4h. The whole mixture was cooled to room temperature and poured in methanol, and the solid was recovered by filtration. The polymer was purified by Soxhlet extraction using methanol, acetone and then hexane. The polymer was then extracted with chloroform and the solvent was reduced to about 10−15 ml. The mixture was poured into methanol and the polymer was recovered by filtration. Were obtained 0.328 g of product corresponding to a yield of 93%.

$^1$H NMR (400 MHz, $C_2D_2Cl_4$, 90 °C): δ = 8.84–8.63 (m, 2 H), 7.64–6.75 (m, 7 H), 4.48–4.13 (m, 6 H), 3.88–3.20 (m, 39 H) ppm.

IR (KBr): ῡ = 2914, 2856, 1700, 1655, 1535, 1422, 1222, 1196, 1095, 1055, 1020cm$^{-1}$.

## 12.5 Synthesis of 4-(2,3-bis(tert-butyldimethylsilyloxy) propoxy)-2-methylbutan-2-yl 2,5-dibromo-thiophene-3-carboxylate

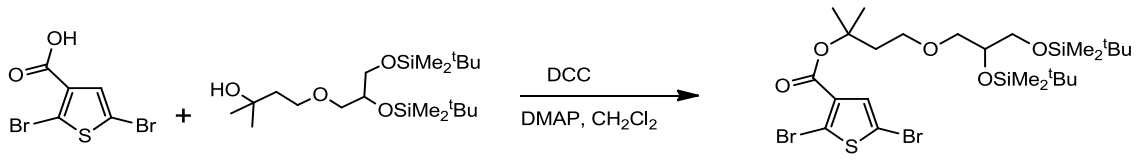


**Scheme 12.6:** Synthesis of monomer **6**.

In a 3-neck flask, equipped with magnetic stirrer, were introduced, by operating in a current of nitrogen, 0.524 mmol of the acid 2,5-dibromothiophene-3-carboxylic acid (dried under vacuum for 5h at 50 °C), the solution of 4-(2,3-bis (tert-butyldimethylsilyloxy)propoxy)- 2-

methylbutan-2-ol (0.403 mmol) in anhydrous DCM (3 ml) and the 4-dimethylaminopyridine (0.604 mmol). The mixture was reacted at room temperature for 1h. After cooling to 0 °C, the DCC (0.504 mmol) was introduced and it was reacted overnight at room temperature. The solvent was removed by evaporation under vacuum and the crude product purified by column chromatography on silica gel using as eluent a mixture of hexane and ethyl acetate in the ratio 10:0.5. Were obtained 0.217 g of product corresponding to a yield of 80%.

$^{1}$H NMR (400 MHz, $CDCl_3$): δ = 7.25 (s, 1 H), 3.75 (quint-like, J = 5.4 Hz, 1 H), 3.60–3.46 (m, 4 H), 3.45–3.40 (m, 1 H), 3.36–3.30 (m, 1 H), 2.14 (t, J = 6.6 Hz, 2 H), 1.57 (s, 6 H), 0.86 (s, 9 H), 0.85 (s, 9 H), 0.04 (s, 6 H), 0.02 (s, 6 H) ppm.

$^{13}$C NMR (100.6 MHz, $CDCl_3$): δ = 159.8, 133.2, 131.9, 118.1, 111.0, 83.72, 72.9, 72.7, 67.4, 65.0, 40.3, 26.6, 26.5, 25.9, 25.8, 18.3, 18.2, –4.6, –4.7, –5.4, –5.4 ppm.

IR (KBr): ῡ = 2945, 2928, 2887, 2856, 1711, 1468, 1424, 1386, 1364, 1249, 1136, 1112, 1007, 835, 776 $cm^{-1}$.

## 12.6 Synthesis of the polymer TegDPPK

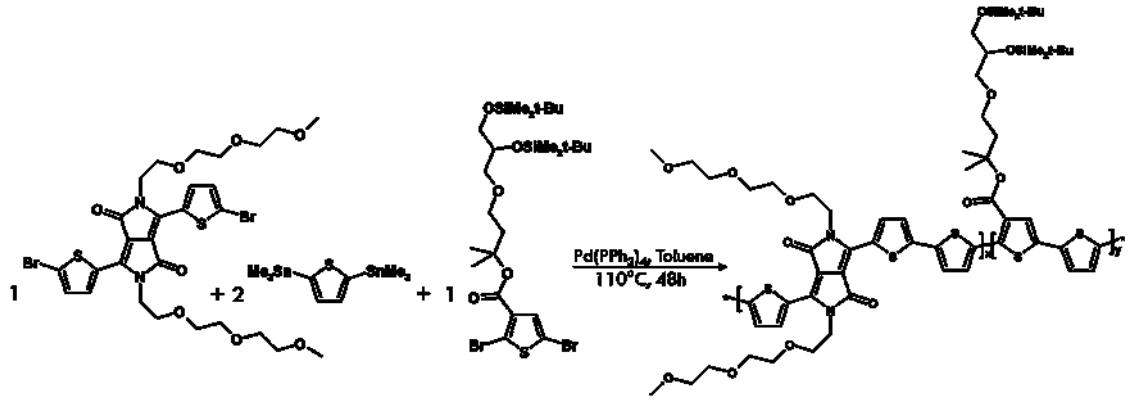


**TegDPPBr$_2$** **6** **TegDPPK**

**Scheme 12.7:** Synthesis of **TegDPPK**.

In a 3-neck flask of 25 ml, equipped with a bubble condenser, and magnetic stirrer, were introduced, operating in nitrogen stream, the **TegDPPBr$_2$** (0.266 mmol), the monomer **6** (0.266 mmol), the 2,5-bis (trimethylstannyl) thiophene (0.533 mmol) and the Pd ($PPh_3$)$_4$ (0.016 mmol) in dry toluene (11 ml). The mixture was reacted for 48h, then the iodobenzene (1.33 mmol) was added, in a nitrogen stream, and the mixture was reacted, always at 110 °C, for 4h and finally it was added the tributylstannyl thiophene (1.33 mmol) in stream of nitrogen and allowed to react for other 4h. The whole mixture was cooled to room temperature, poured in methanol, and the solid was recovered by filtration. The polymer was purified by Soxhlet extraction using methanol, acetone and hexane. The polymer was then extracted with chloroform and the solvent was reduced to about 10−15 ml. The mixture was poured into methanol and the polymer was recovered by filtration. Were obtained 0.142 g of product corresponding to a yield of 53%.

$^1$H NMR (400 MHz, $C_2D_2Cl_4$, 90 °C): δ = 8.80–8.64 (m, 2 H), 7.50–7.04 (m, 10 H), 4.30–4.20 (m 4 H), 3.84–3.24 (m, 40 H), 2.20–2.10 (m, 4 H), 1.54 (br. s, 12 H), 0.84 (br. s, 36 H), 0.02 (br. s, 12 H), –0.01 (br. s, 12 H) ppm.

IR (KBr): ῡ = 2924, 2854, 1702, 1663, 1540, 1427, 1251, 1227, 1107, 1061, 835, 777cm$^{-1}$.

## 12.7 Deprotection of the hydroxyl groups in the TegDPPK

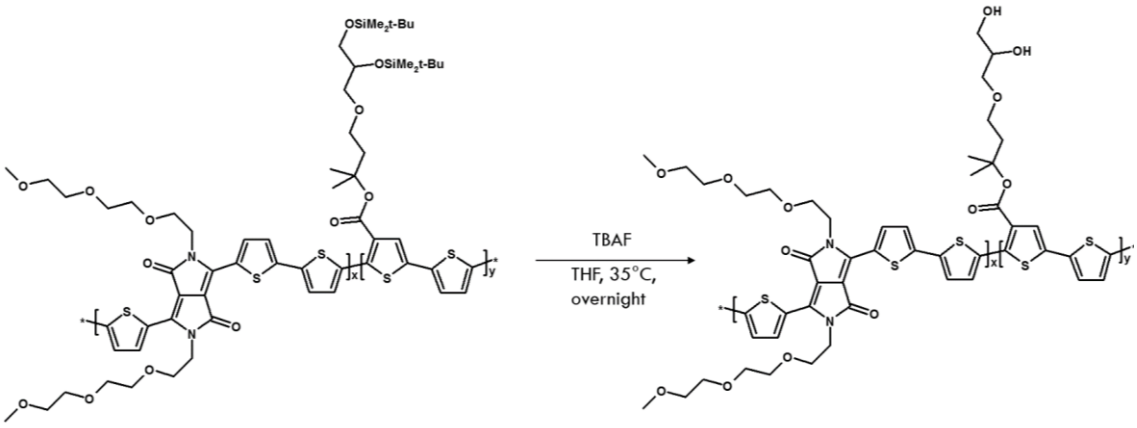


**Scheme 12.8:** Deprotection of **TegDPPK**.

The **TegDPPK** (0.0390 mmol) was dissolved in THF (3 ml) followed by addition of TBAF (1M in THF; 0.16 ml). The mixture was heated to 35 °C and reacted overnight. Methanol was then added and the mixture stirred for additional 24h. The compound was precipitated by drop wise addition of AcOEt, and then recovered by filtration. The precipitate was washed with isopropanol and dried under vacuum. Were obtained 0.021 g of product corresponding to a yield of 55%.

IR (KBr): ῡ = 3432, 2914, 2851, 1692, 1647, 1530, 1418, 1381, 1214, 1196, 1092, 1055, 790cm$^{-1}$.

## 12.8 Synthesis of the polymer TegDPPK1

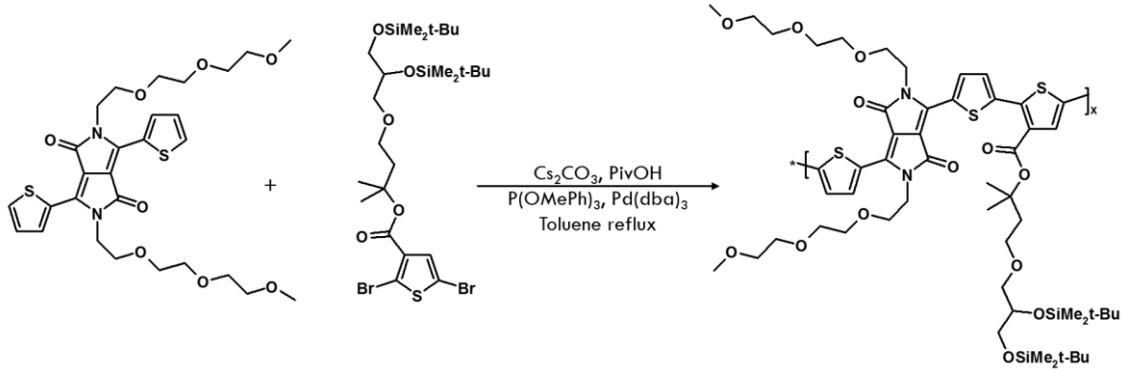


**TegDPP** **6** **TegDPPK1**

**Scheme 12.9:** Synthesis of **TegDPPK1**.

Polymer **TegDPPK1** was synthesized according to literature procedure. **TegDPPBr$_2$** (0.266 mmol), 4-(2,3-bis (tert-butyldimethylsilyloxy) propoxy)-2-methylbut-2-yl 2,5-dibromothiophen-3-carboxylate (0.266 mmol), $Cs_2CO_3$ (0.016 mmol), pivalic acid (PivOH, 0.101 mmol) and tris(o-methoxyphenyl)phosphine ($P(OMePh)_3$; 0.034 mmol) were introduced in a flask, after it was evacuated and back filled with nitrogen three times and 8 ml of dry toluene and the tris(dibenzylideneacetone) dipalladium(0) ($Pd_2(dba)_3$; 0.017 mmol) were added. The mixture was heated to 110 °C and reacted for 48 h. The whole mixture was cooled to room temperature, poured in methanol and the solid was recovered by filtration. The polymer was purified by Soxhlet extraction using methanol, acetone, hexane and then chloroform. The majority of the polymer was extracted with hexane and was obtained 0.185 g of product corresponding to a yield of 49%.

$^1$H NMR (400 MHz, $C_2D_2Cl_4$, 90 °C): δ = 8.80–8.65 (m, 2 H), 7.64–7.54 (m, 2 H), 7.38–7.30 (m, 1 H), 4.32–4.18 (m, 4 H), 3.84–3.70 (m, 4 H), 3.68–3.20

(m, 29 H), 2.20–2.10 (m, 2 H), 1.56 (br. s, 6 H), 0.84 (br. s, 18 H), 0.03 (br. s, 6 H), 0.00 (br. s, 6 H) ppm.

IR (KBr): ῡ = 2925, 2855, 1792, 1666, 1544, 1434, 1257, 1206, 1103, 1023, 832, 805, 774cm$^{-1}$.

## 12.9 Deprotection of the hydroxyl groups in the TegDPPK1

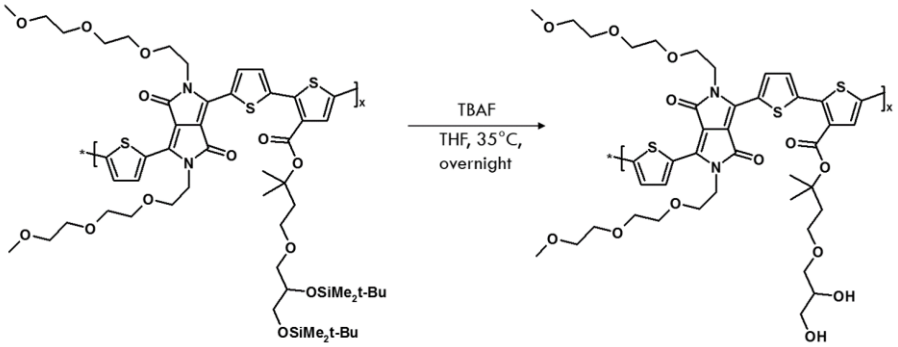


**Scheme 12.10:** Deprotection of **TegDPPK1**.

The **TegDPPTK** (0.0390 mmol) was dissolved in THF (3 ml) followed by addition of TBAF (1M in THF; 0.16 ml). The mixture was heated to 35 °C and left standing over night. Methanol was then added and the mixture stirred for addition 24h. The compound was precipitated by drop wise addition of AcOEt, and then recovered by filtration. The precipitate was washed with isopropanol and dried under vacuum. Were obtained 0.017 g of product corresponding to a yield of 42%. The product was characterized by means FT-IR (Appendix spectra).

IR (KBr): ῡ = 3394, 2914, 2869, 1700, 1662, 1540, 1430, 1108, 1060, 731 cm$^{-1}$.

# 13 Fabrication of TegDPPBDT in BHJ solar cells

Inverted solar cell devices were fabricated on ITO coated glass substrate (Kintec, 8 Ω/cm$^2$) patterned with wet etching in hydrobromic acid and cleaned in an ultrasonic bath using acetone and 2-propanol for 10 min each, one after the other. At first, ZnO nanoparticles were deposited on the ITO substrate by spin coating at 2500 rpm for 45 s and then annealed at 140°C in air for 40 min. Next, the active layer (1:2) of **TegDPPBDT** and $PC_{70}BM$ dissolved in ortho-dichlorobenzene solvent with 3 % 1,8-diiodooctane (DIO) additive was spin-coated at 1000 rpm for 60 s and annealed at 290 °C under inert atmosphere for 2 min. Finally, all devices were transferred inside the metal evaporator where a 5 nm thick $MoO_3$ layer and silver contact with 100 nm thickness were deposited through the shadow mask at below 10–6 mbar pressure. Thus, we obtained a total of 4 devices with 0.1 cm$^2$ area for each cell.

## 13.1 Fabrication of TegDPPBDT in OFETs

Top gate devices were fabricated on Corning glass substrate cleaned in an ultrasonic bath using soap solution, water, acetone and 2-propanol at 50 °C for 20 min each, one after the other. At first, on the substrate, source/drain electrodes were thermal evaporated (3 nm thick Cr and 30 nm thick Au), above semiconductor layer was spin-coated from chloroform solution, at 1000 rpm for 60 s and annealed at 150 °C for 15 min under inert atmosphere. On top of the semiconductor layer a CYTOP solution was spin

coated at 6000 rpm for 90 s and annealed at 110 °C for 5 h under inert atmosphere. Finally, the gate electrode in Al (40 nm thick) was evaporated thermally upon the dielectric layer and the devices were annealed at 120 °C overnight under vacuum.

# 14 Synthesis of the polymer TegDPPBDT-HMW

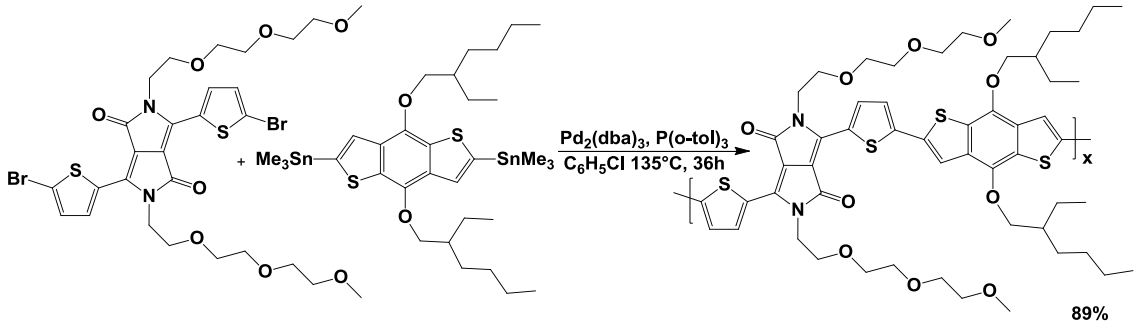


**1** **4** **TegDPPBDT-HMW**

**Scheme 14.1:** Synthesis of **TegDPPBDT-HMW**.

In a vial of 10 ml were introduced, operating in glove box, the **TegDPPBr$_2$** (0.140 mmol), the 2,6-bis(trimethylstannyl)-4,8-bis(2-ethylhexyloxy)benzo[1,2-b:4,5-b']dithiophene (0.140 mmol), the $Pd_2(dba)_3$ (0.0046 mmol) and the $P(o\text{-}tol)_3$ (0.028 mmol) in dry chloroform (5 ml). The mixture was reacted for 36h, then the bromobenzene (0.140 mmol) was added, in nitrogen stream, and the mixture was reacted, always at 135 °C for additional 2h. The whole mixture was cooled to room temperature, precipitated in methanol, and the solid was recovered by filtration. The polymer was purified by Soxhlet extraction using methanol, acetone and hexane. The polymer was then extracted with chloroform and the solvent was reduced to about 10−15 ml. The mixture was poured into methanol and the polymer was recovered by filtration. Polymer **TegDPPBDT-HMW** was obtained as a dark green solid (0.129 g, 89 %).

## 14.1 Synthesis of the polymer EHDPPBDT

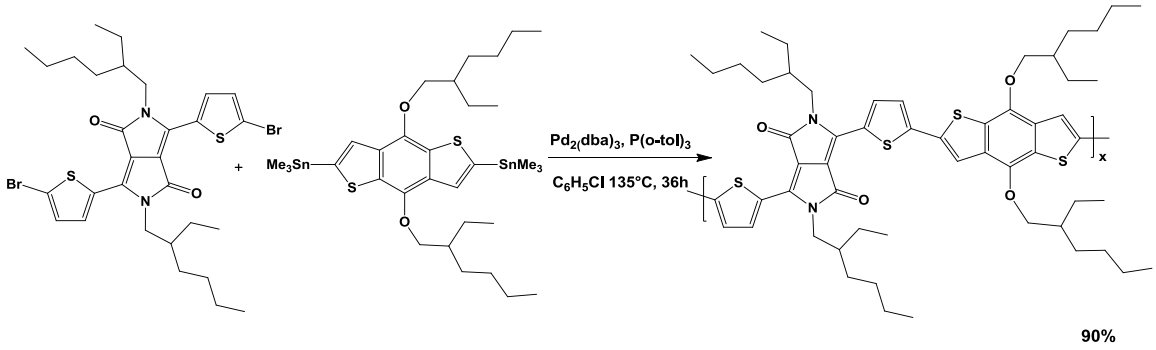


**EHDPP** **4** **EHDPPBDT**

**Scheme 14.2:** Synthesis of **EHPPBDT**.

In a vial of 10 ml were introduced, operating in glove box, the **EHDPP** (0.140 mmol), the 2,6-bis(trimethylstannyl)-4,8-bis(2-ethylhexyloxy)benzo[1,2-b:4,5-b']dithiophene (0.140 mmol), the $Pd_2(dba)_3$ (0.0046 mmol) and the $P(o\text{-}tol)_3$ (0.028 mmol) in dry chloroform (5 ml). The mixture was reacted for 36h, then the bromobenzene (0.140 mmol) was added, in nitrogen stream, and the mixture was reacted, always at 135 °C for additional 2h. The whole mixture was cooled to room temperature, precipitated in methanol, and the solid was recovered by filtration. The polymer was purified by Soxhlet extraction using methanol, acetone and hexane. The polymer was then extracted with chloroform and the solvent was reduced to about 10−15 ml. The mixture was poured into methanol and the polymer was recovered by filtration. Polymer **EHPPBDT** was obtained as a dark green solid (0.123 g, 90 %).

# Appendix spectra

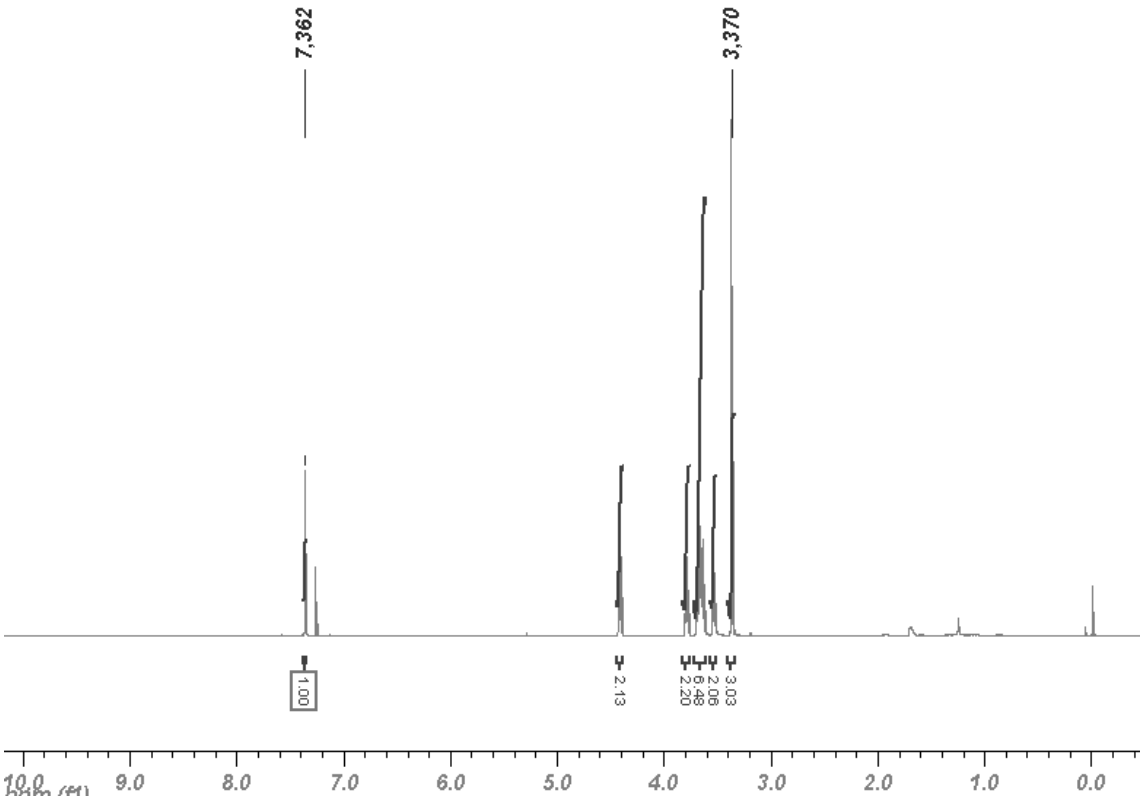


**Figure A1**. $^{1}H$ NMR spectrum of compound monomer **5** (400 MHz, $CDCl_3$).

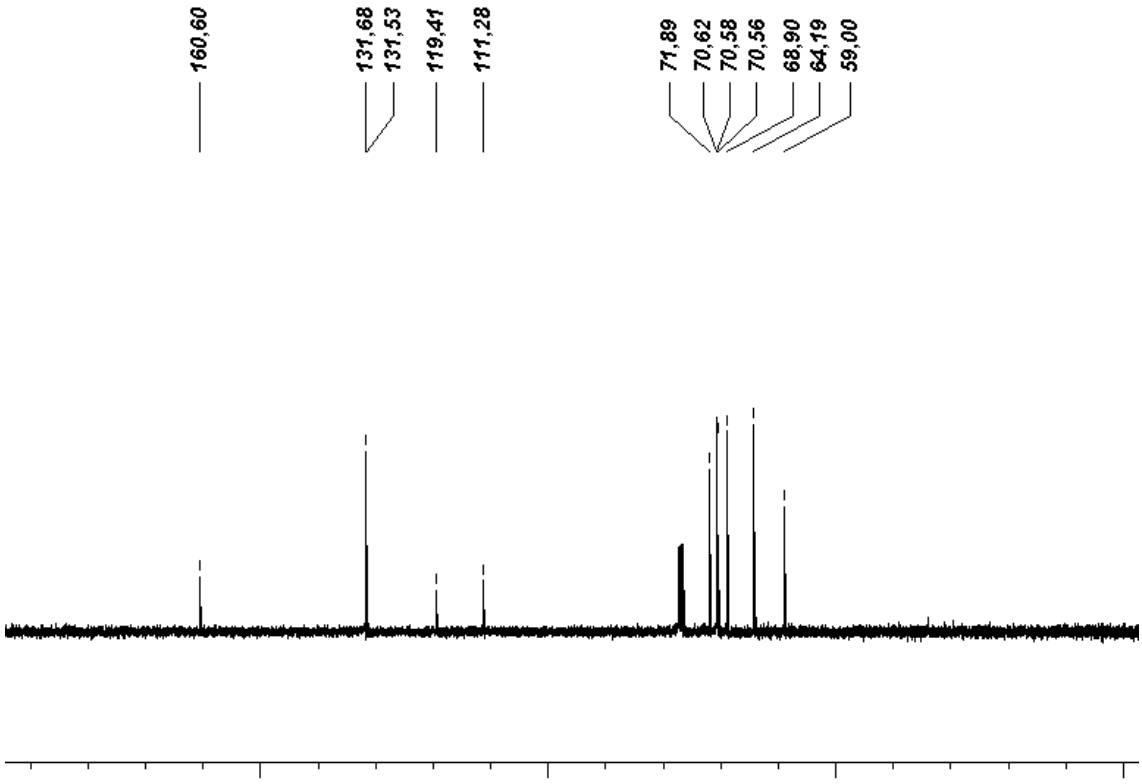


**Figure A2**. $^{13}C$ NMR spectrum of compound monomer **5** (100.6 MHz, $CDCl_3$).

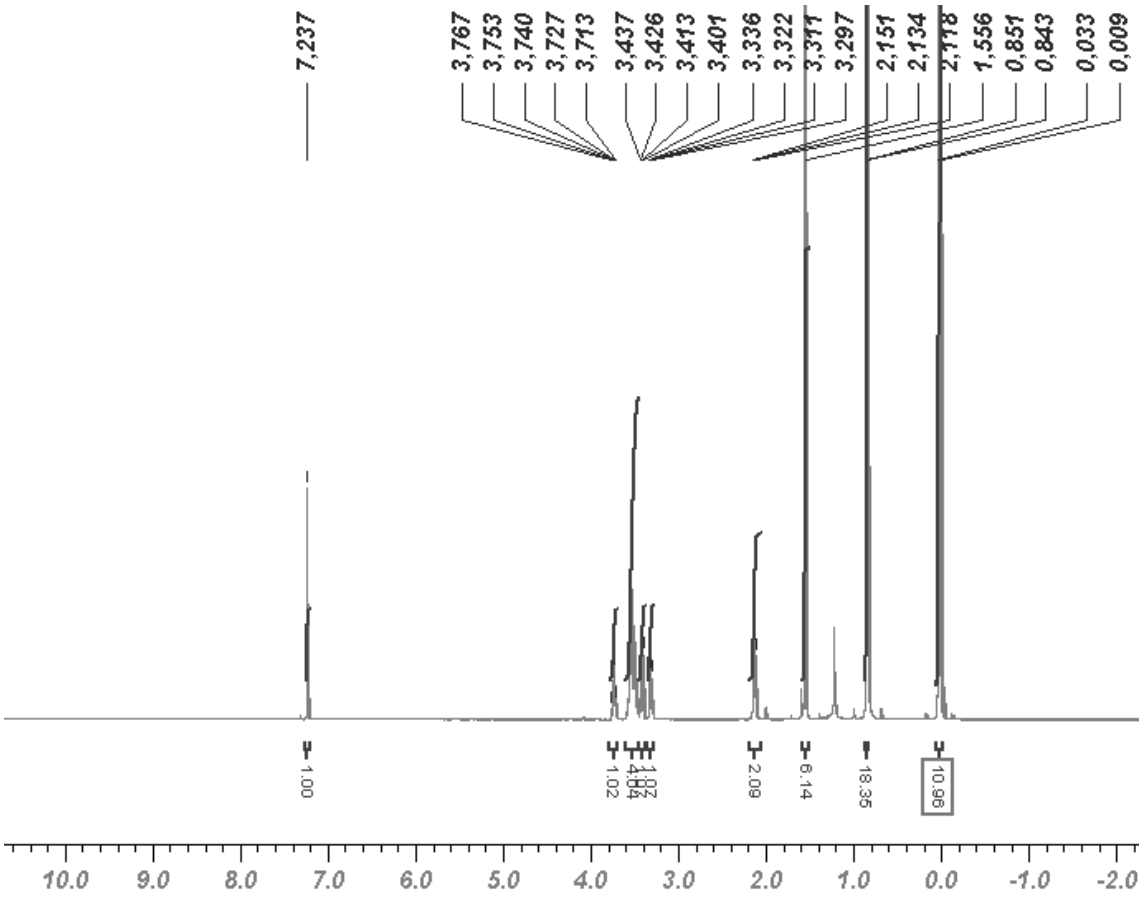


**Figure A3**. $^{1}$H NMR spectrum of compound monomer **6** (400 MHz, $CDCl_3$).

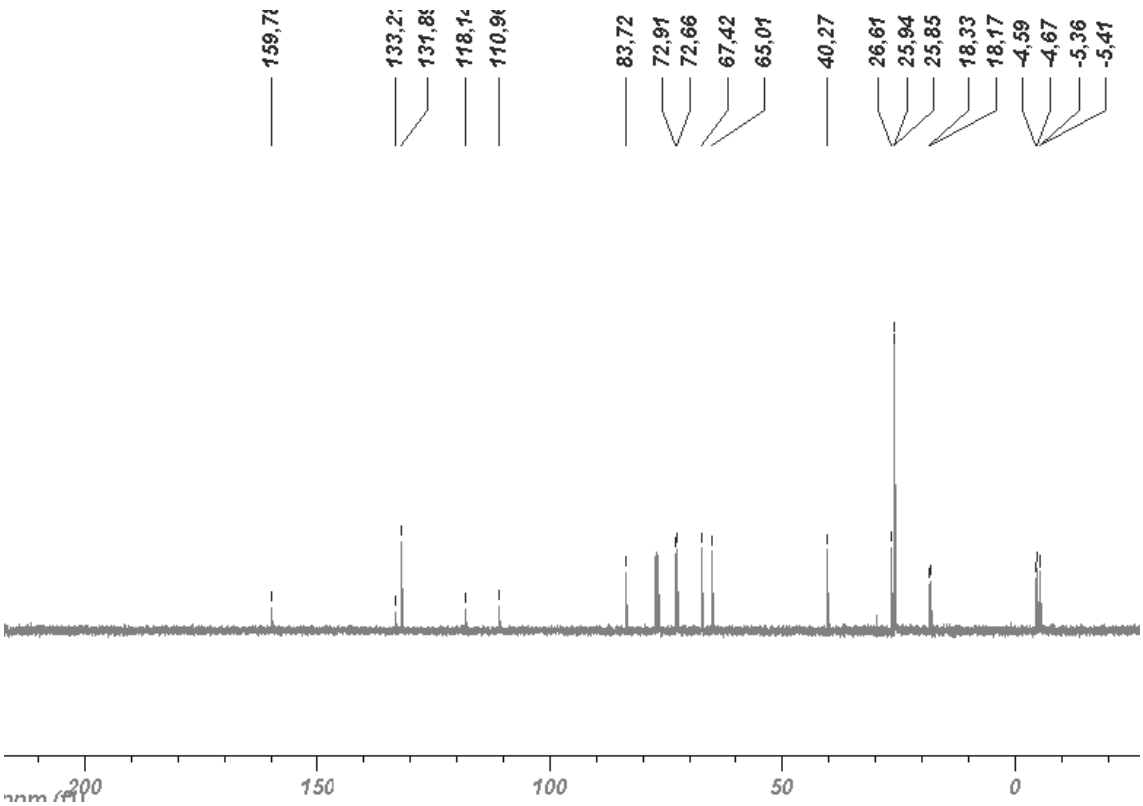


**Figure A4**. $^{13}$C NMR spectrum of compound monomer **6** (100.6 MHz, $CDCl_3$).

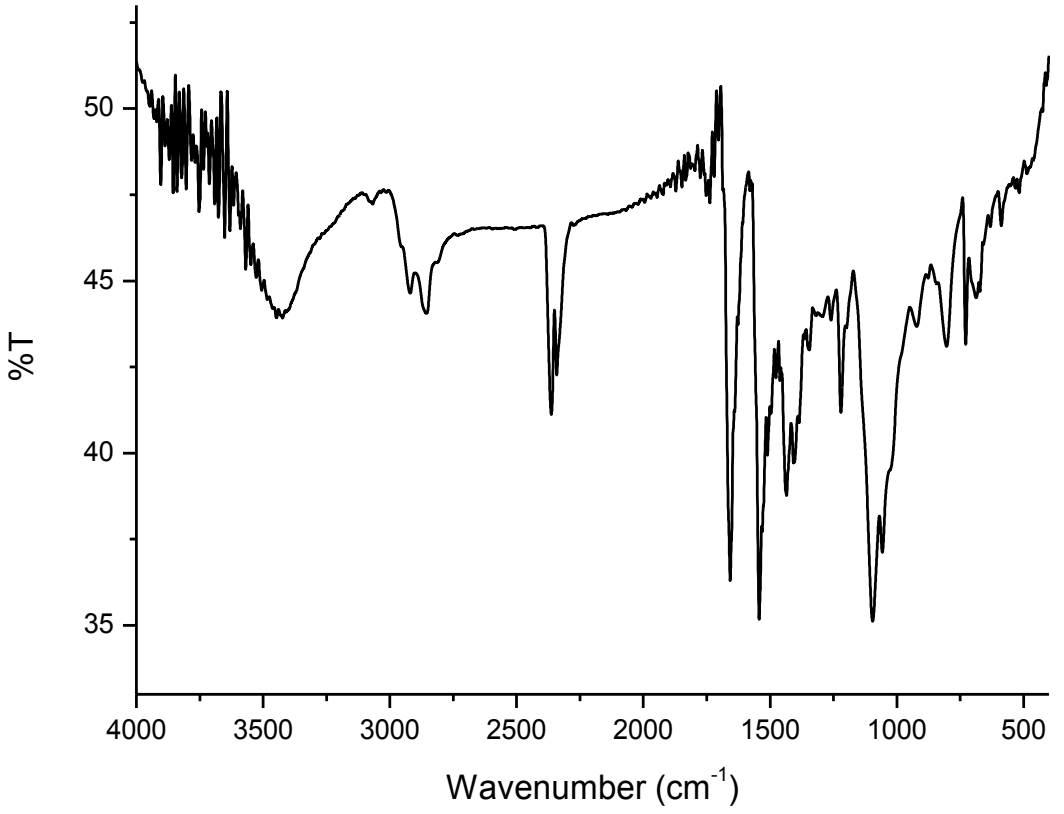


**Figure A5**. FT-IR spectrum of polymer **TegDPPV** (KBr).

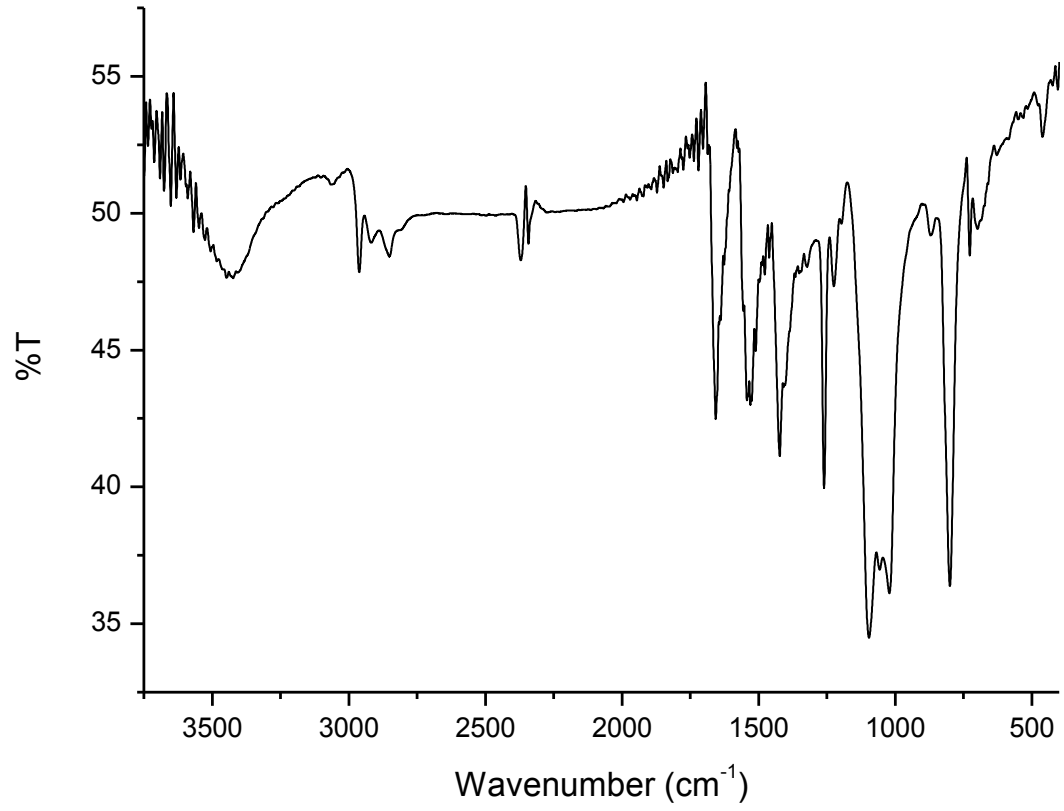


**Figure A6**. FT-IR spectrum of polymer **TegDPPT** (KBr).

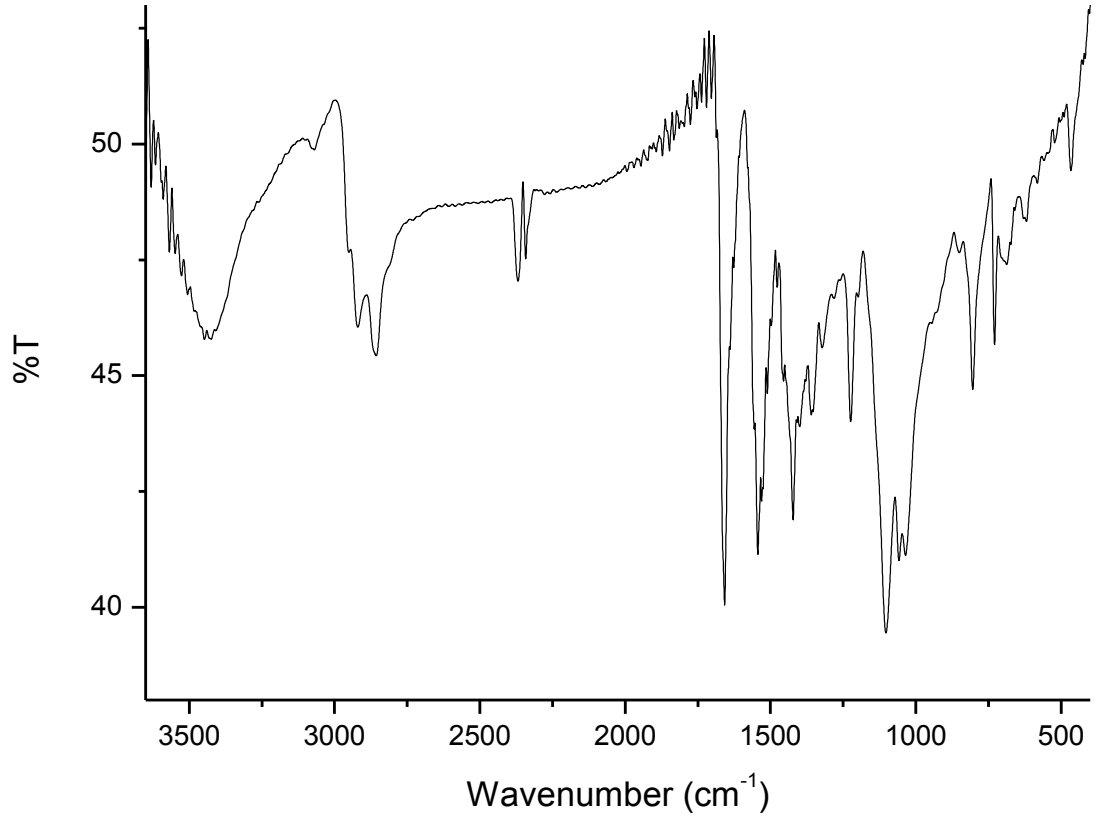


**Figure A7**. FT-IR spectrum of polymer **TegDPPBDT** (KBr).

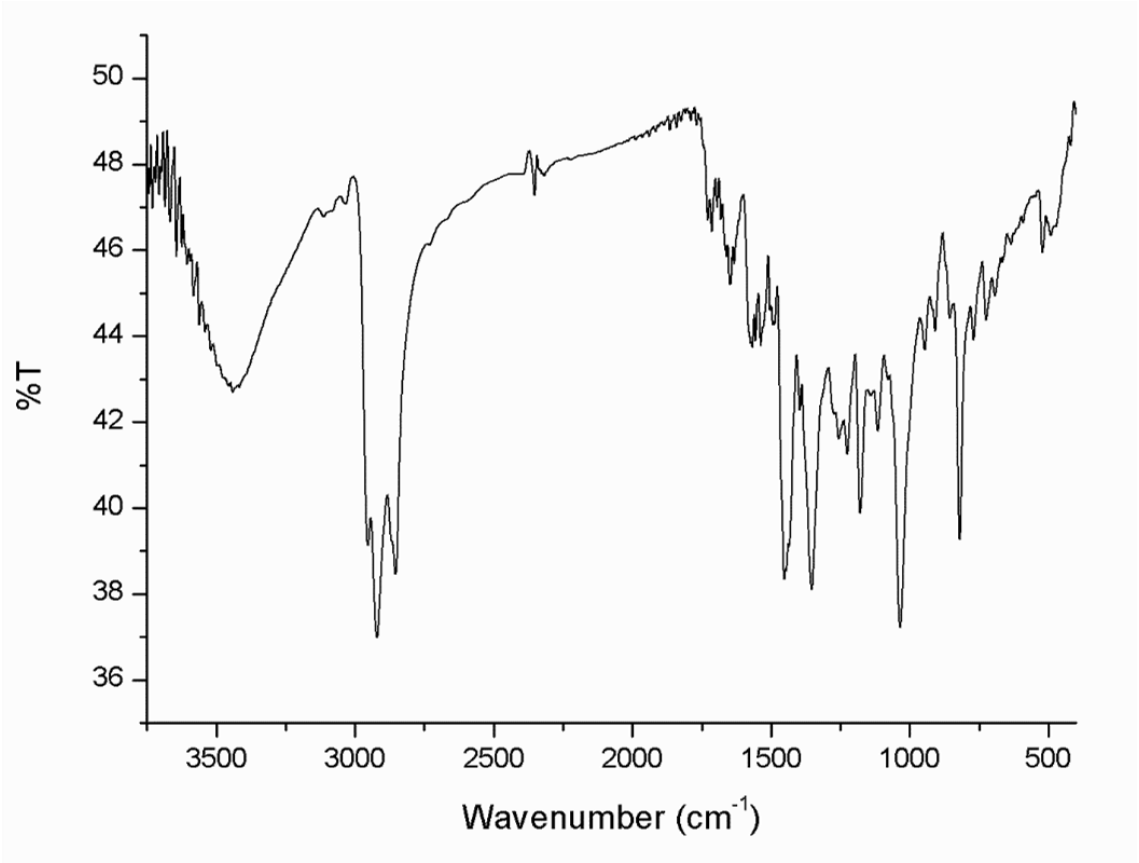


**Figure A8**. FT-IR spectrum of polymer **TegDPPTegES** (KBr).

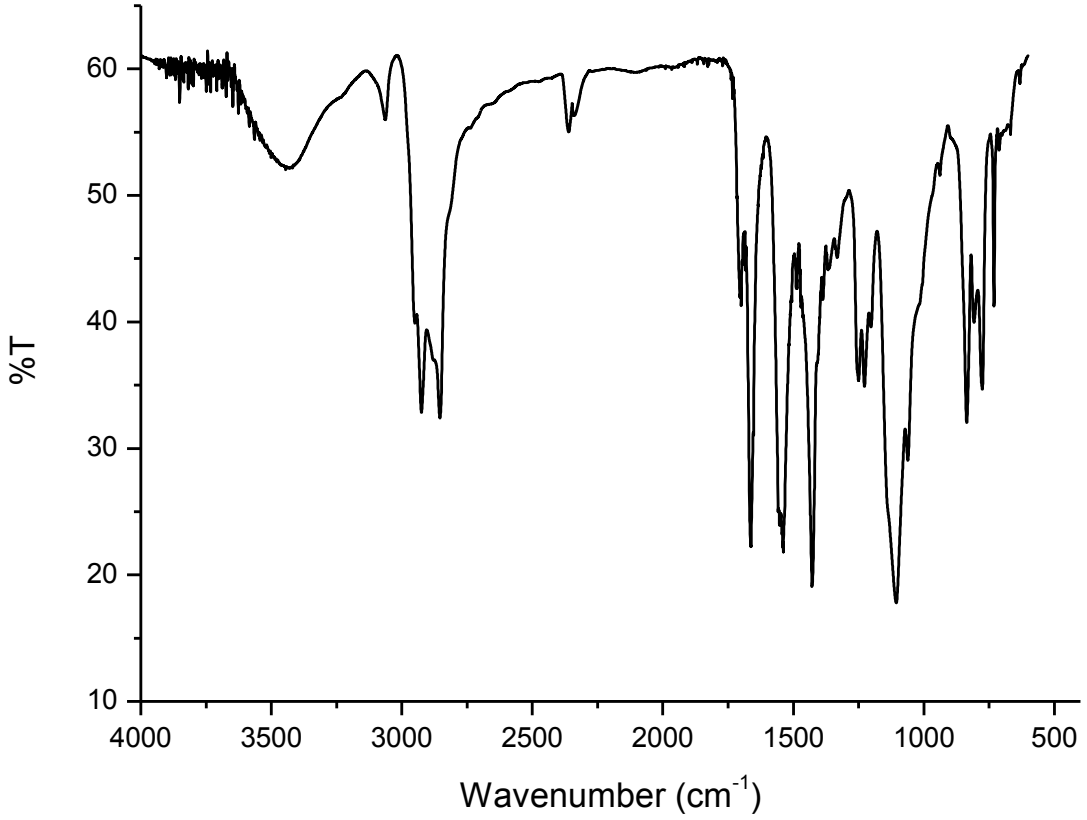


**Figure A9**. FT-IR spectrum of polymer **TegDPPK** (KBr).

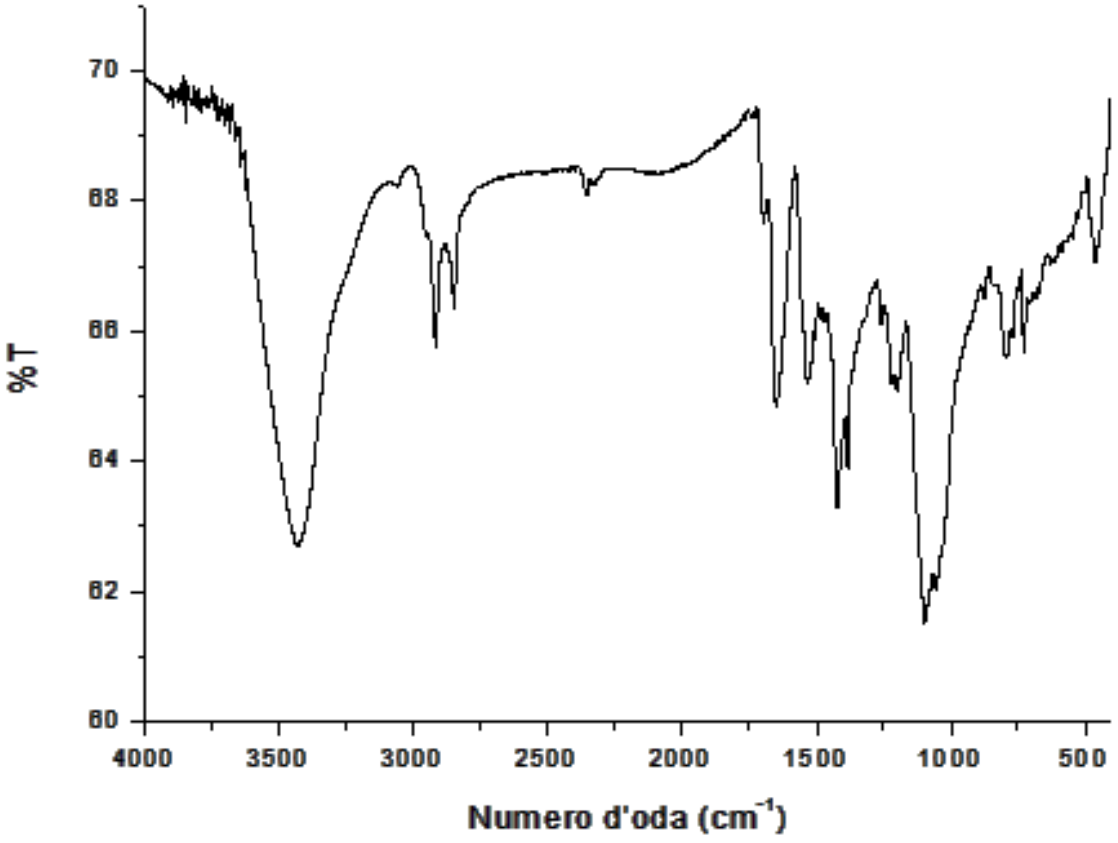


**Figure A10**. FT-IR spectrum of polymer **TegDPPKdep** (KBr).

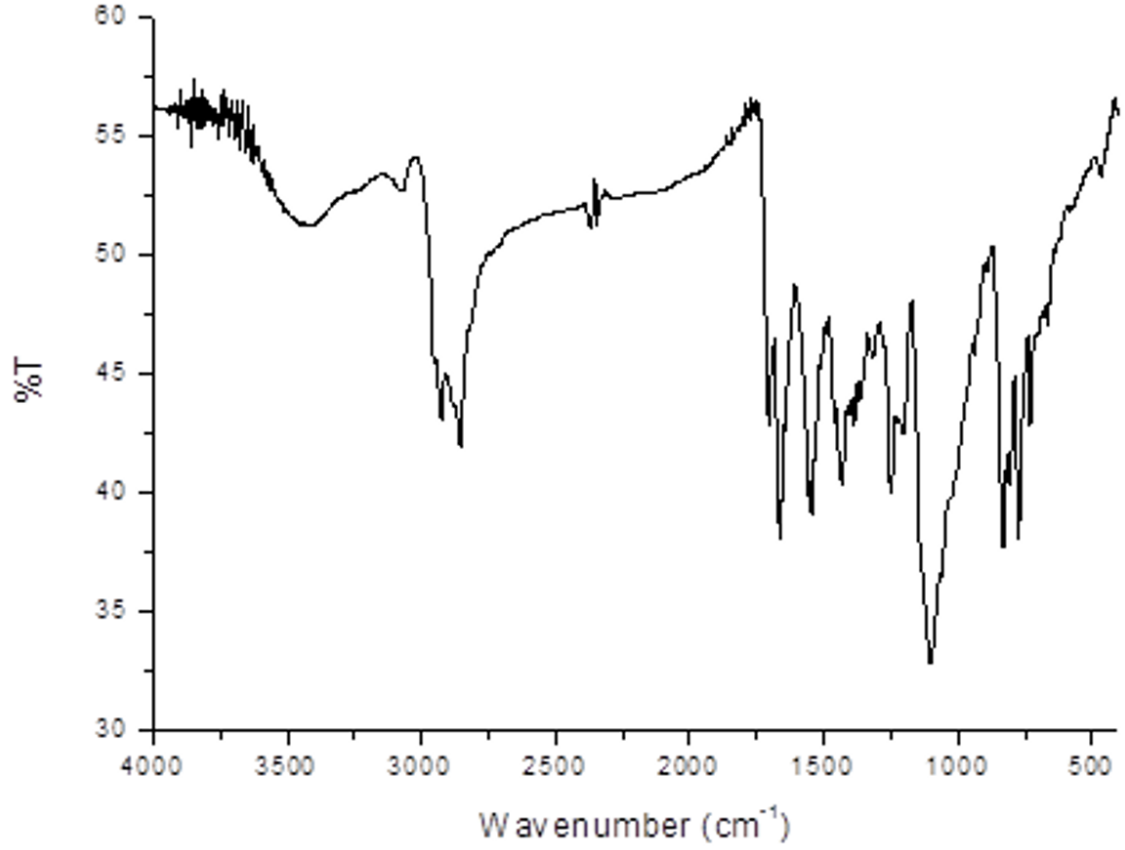


**Figure A11**. FT-IR spectrum of polymer **TegDPPK1** (KBr).

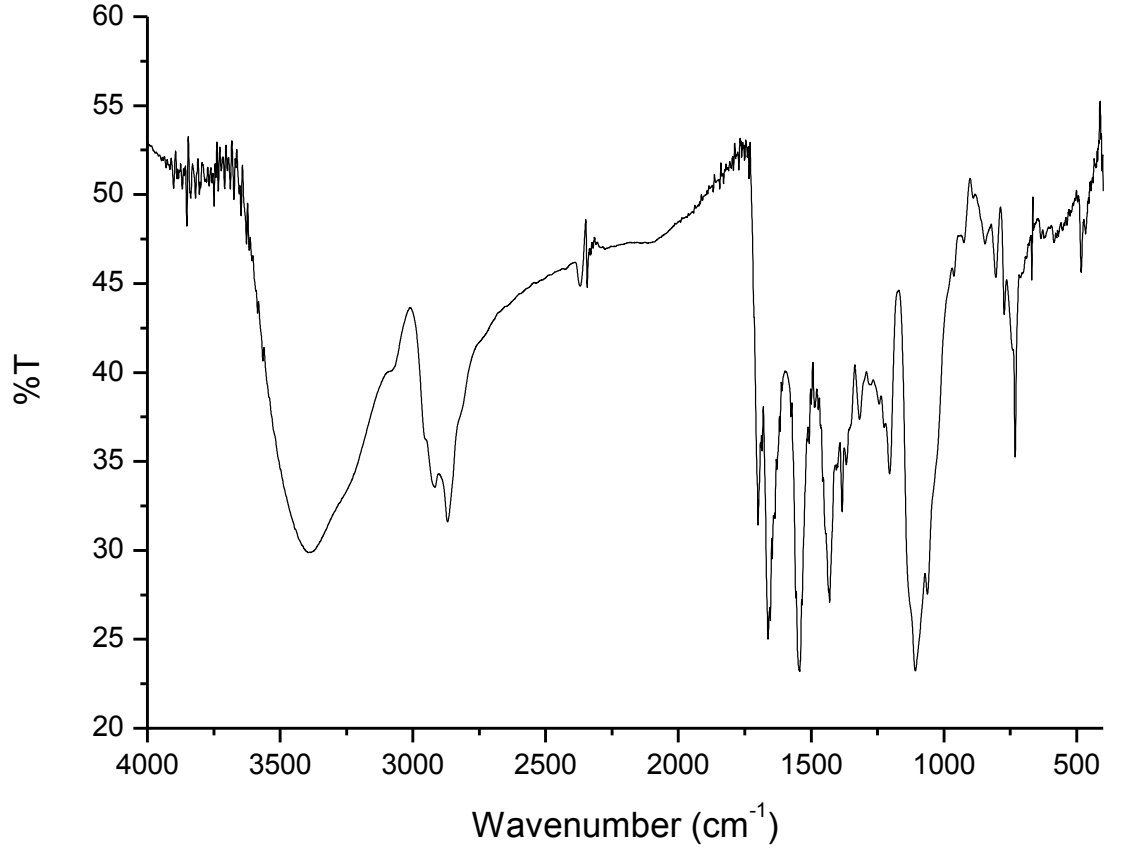


**Figure A12**. FT-IR spectrum of polymer **TegDPPK1dep** (KBr).

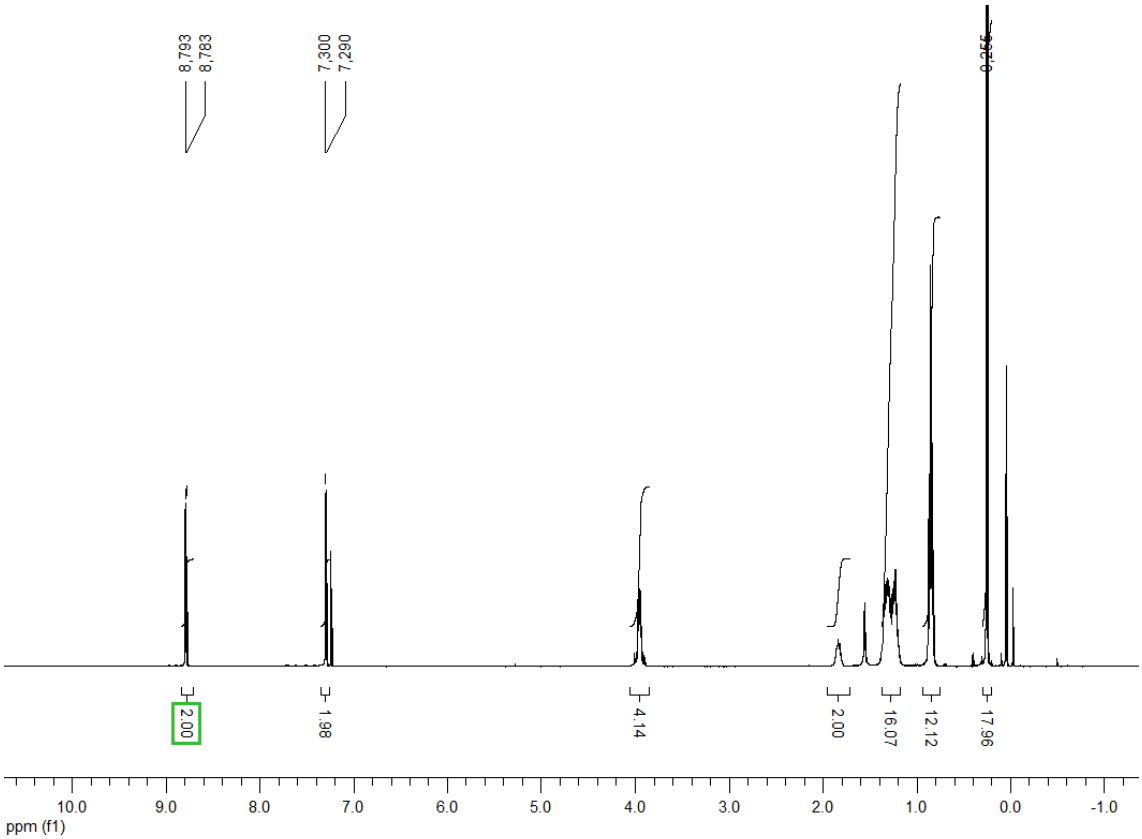


**Figure A13**. $^{1}$H NMR spectrum of compound **3a** (400 MHz, $CDCl_3$).

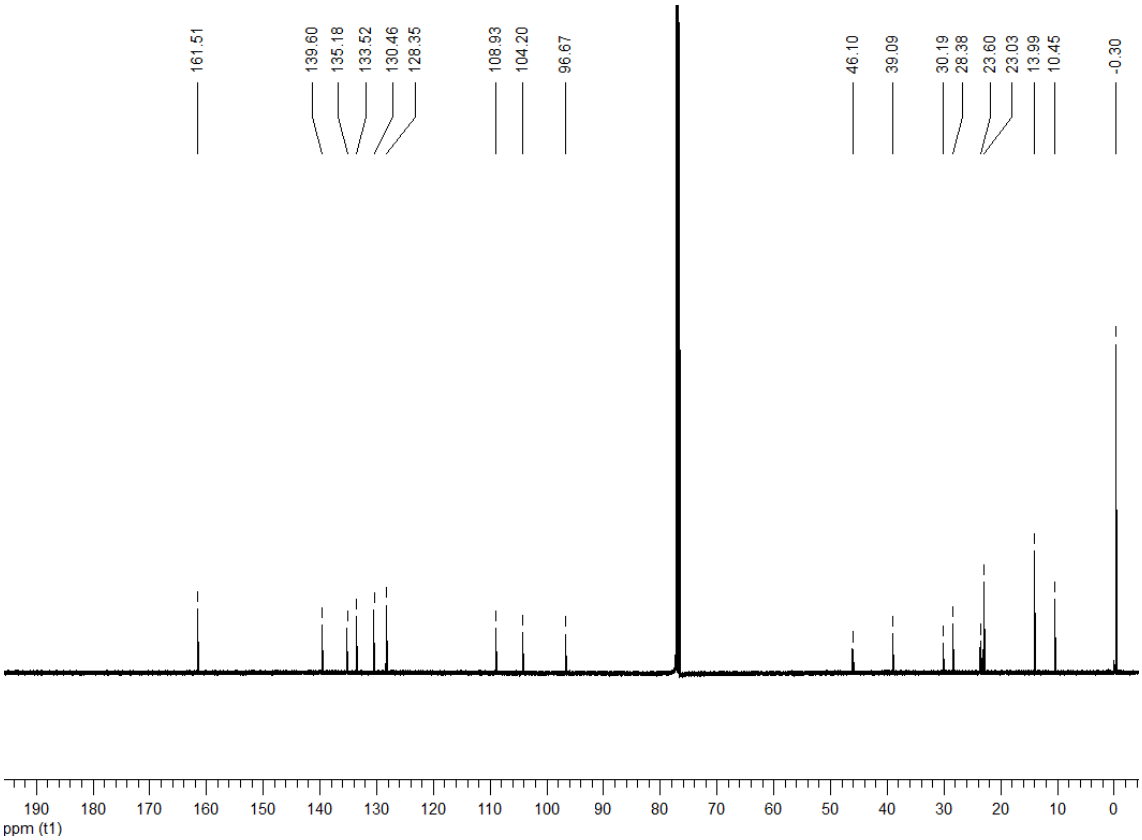


**Figure A14**. $^{13}$C NMR spectrum of compound **3a** (100.6 MHz, $CDCl_3$).

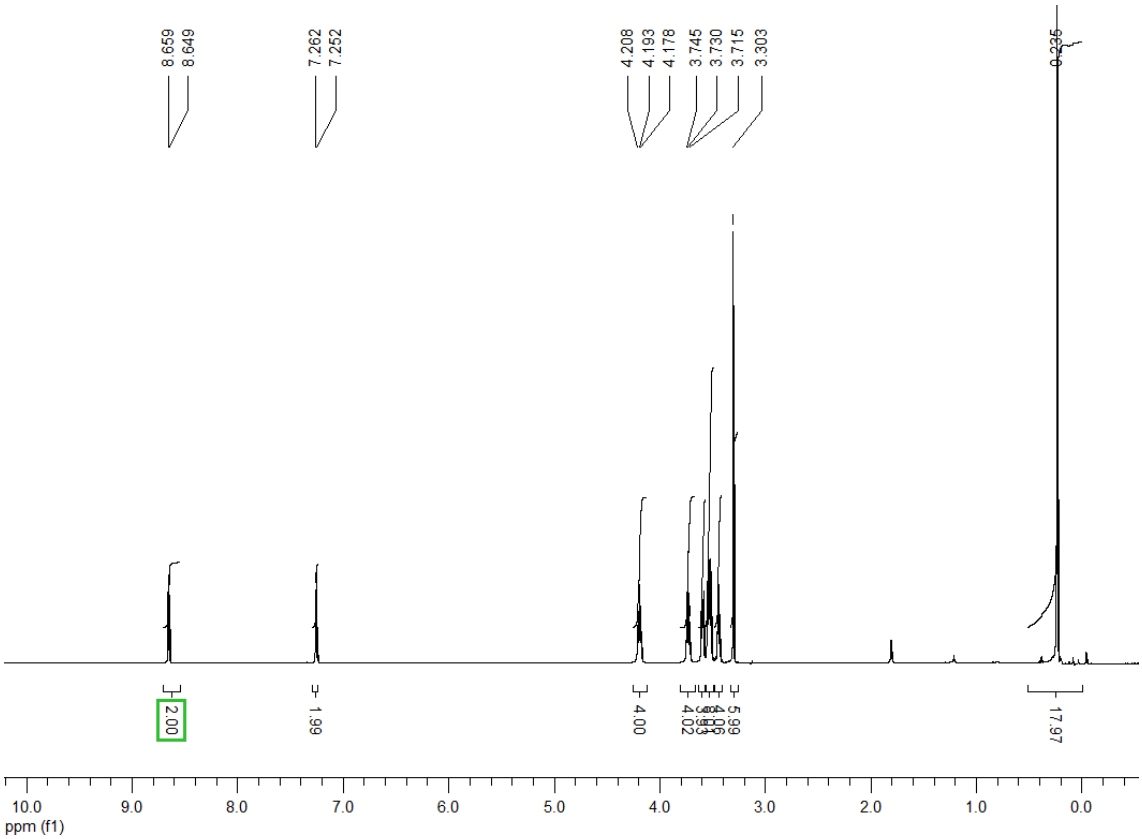


**Figure A15**. $^{1}$H NMR spectrum of compound **3b** (400 MHz, $CDCl_3$).

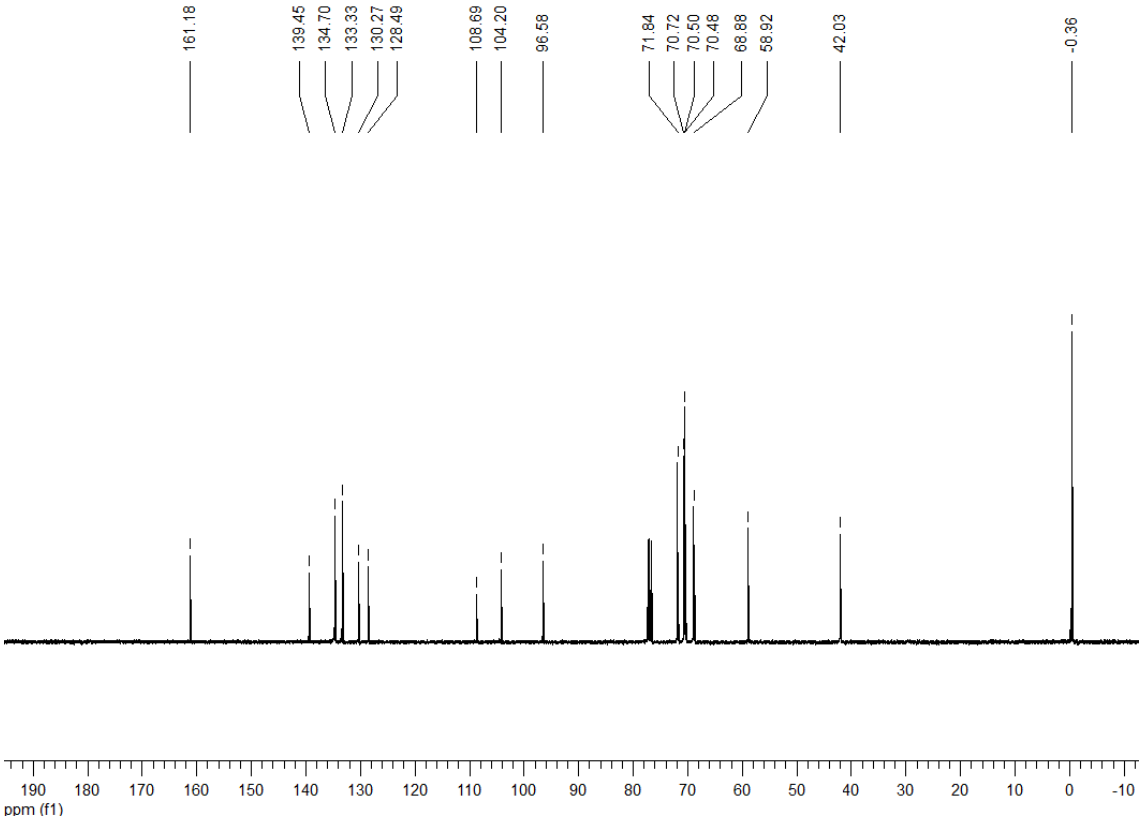


**Figure A16.** $^{13}$C NMR spectrum of compound **3b** (100.6 MHz, $CDCl_3$).

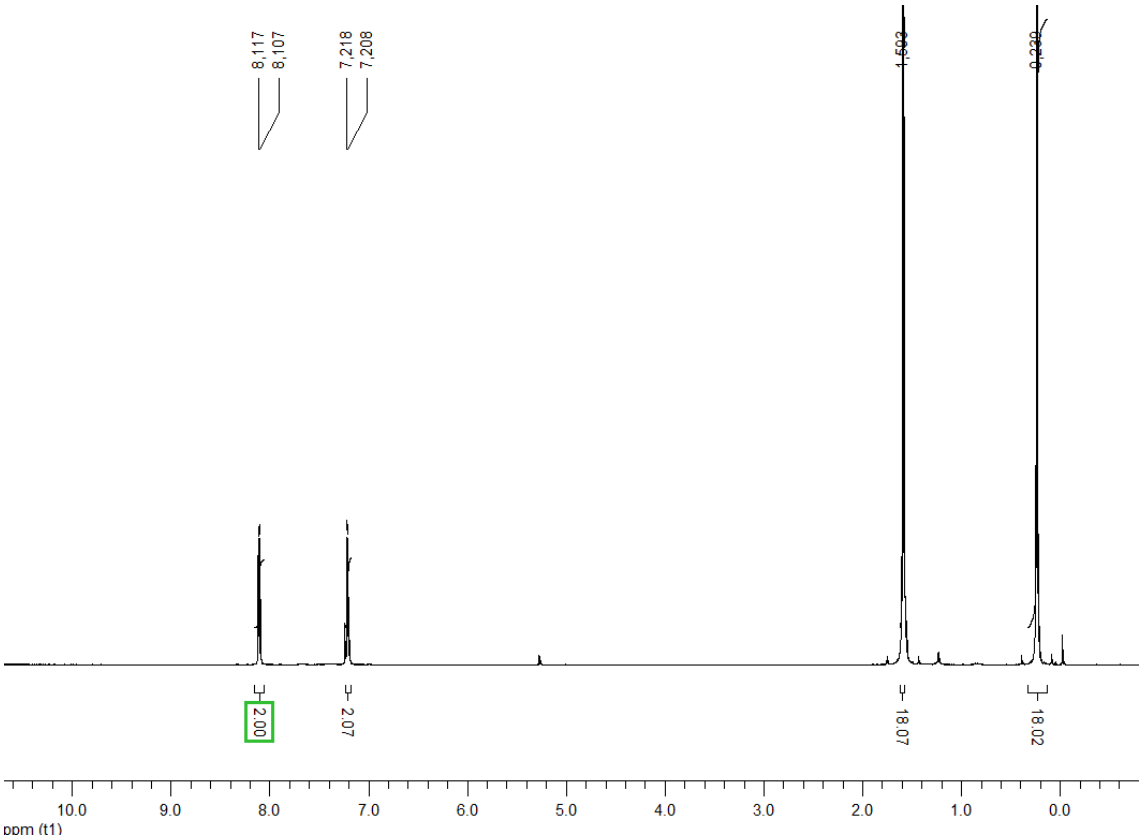


**Figure A17**. [1] H NMR spectrum of compound **3c** (400 MHz, $CDCl_3$).

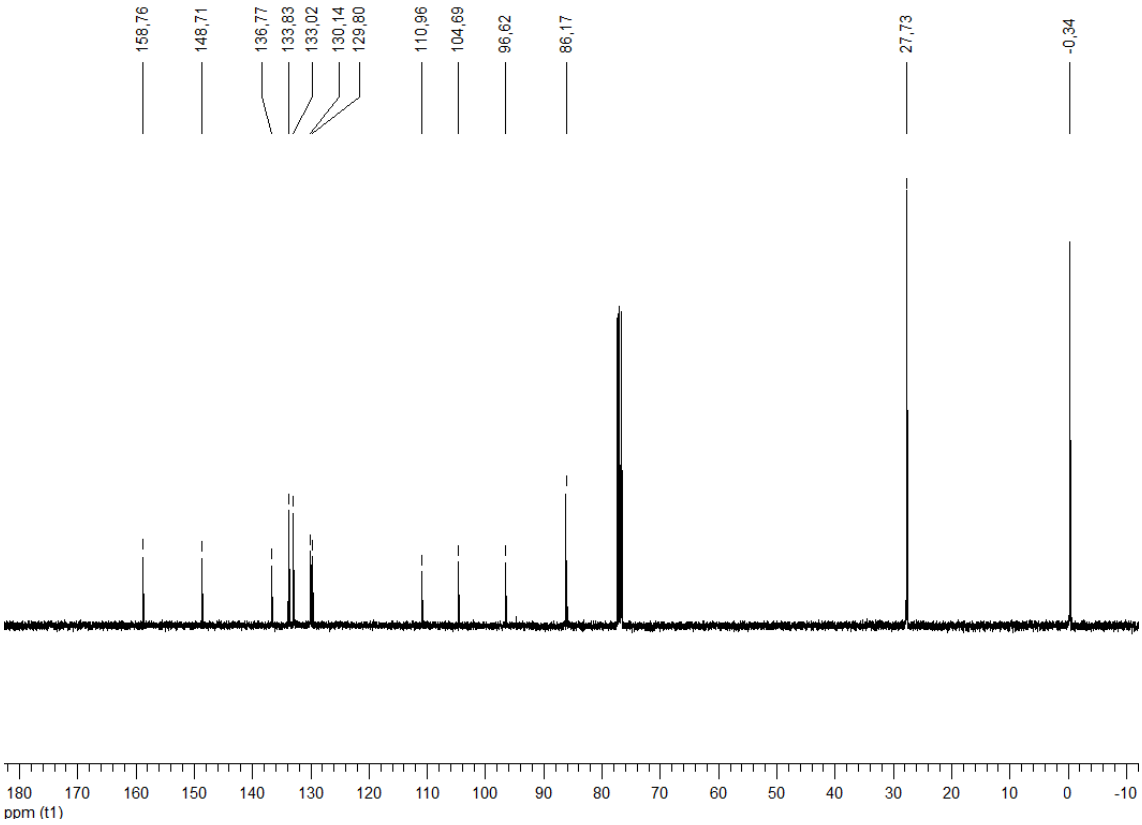


**Figure A18**. [13]C NMR spectrum of compound **3c** (100.6 MHz, $CDCl_3$).

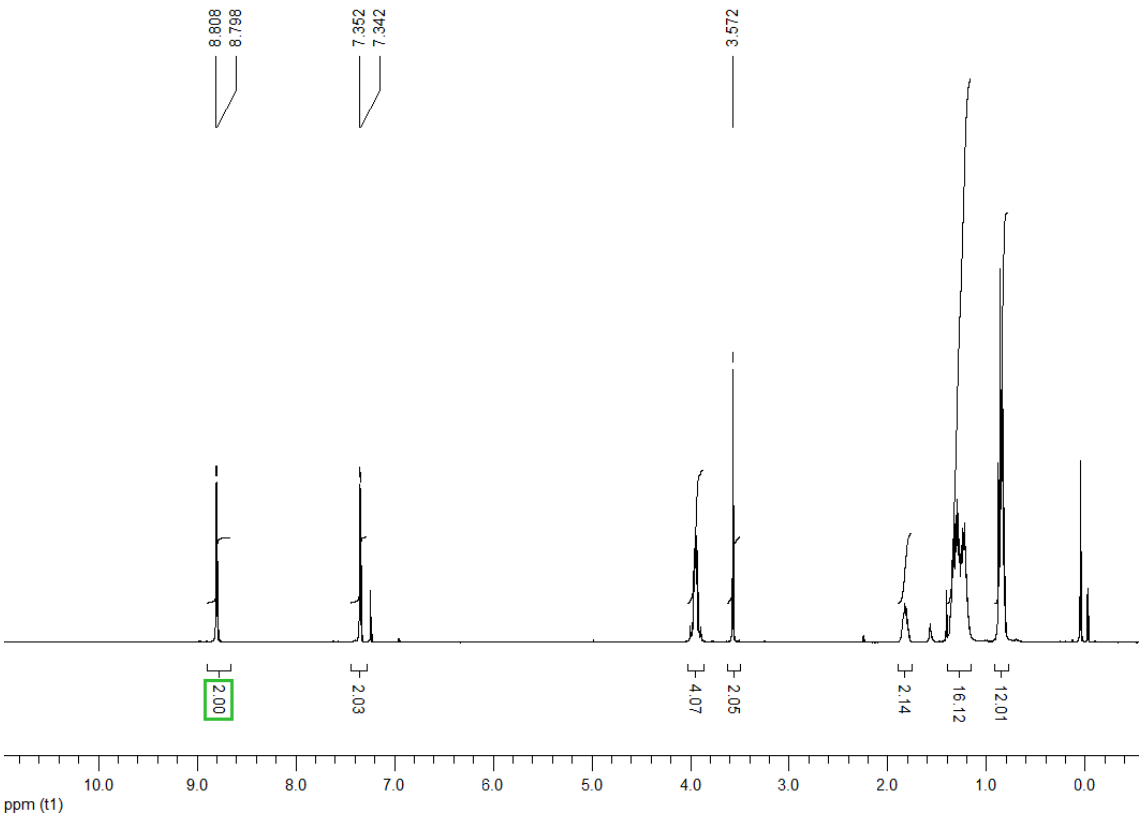


**Figure A19**. [1] H NMR spectrum of compound **4a** (400 MHz, $CDCl_3$).

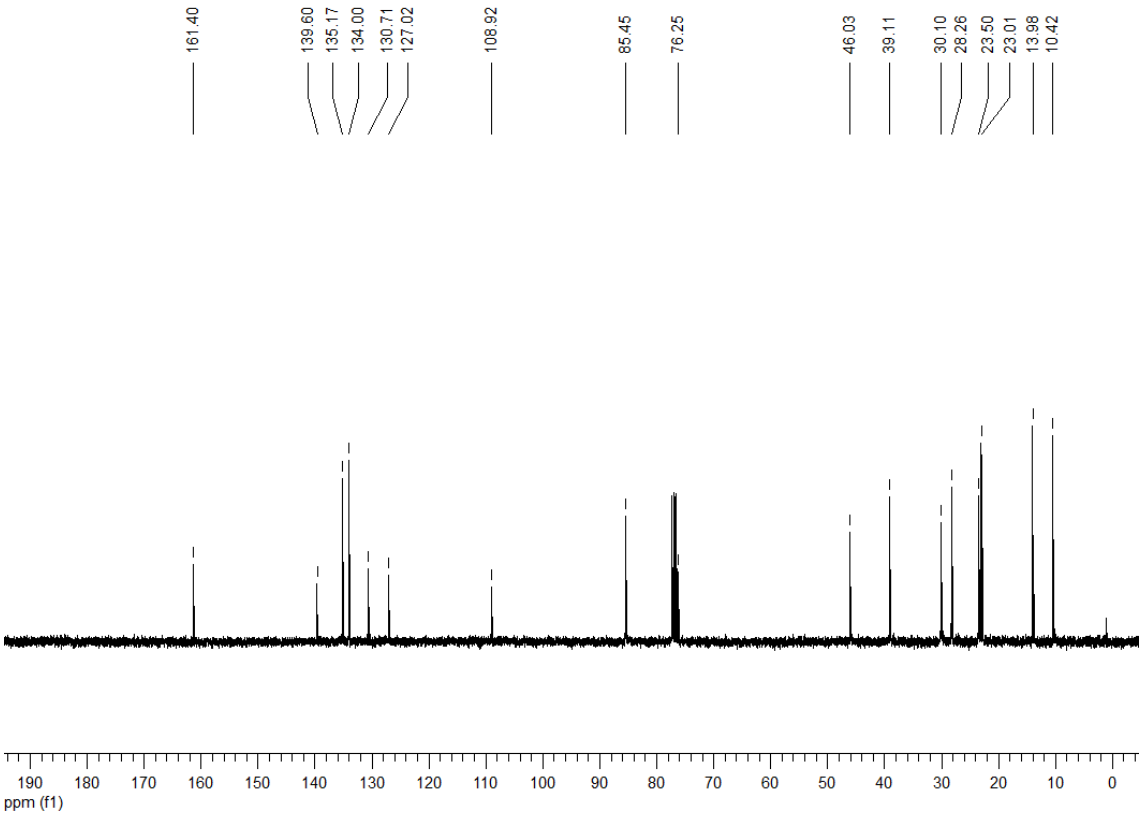


**Figure A20**. [13]C NMR spectrum of compound **4a** (100.6 MHz, $CDCl_3$).

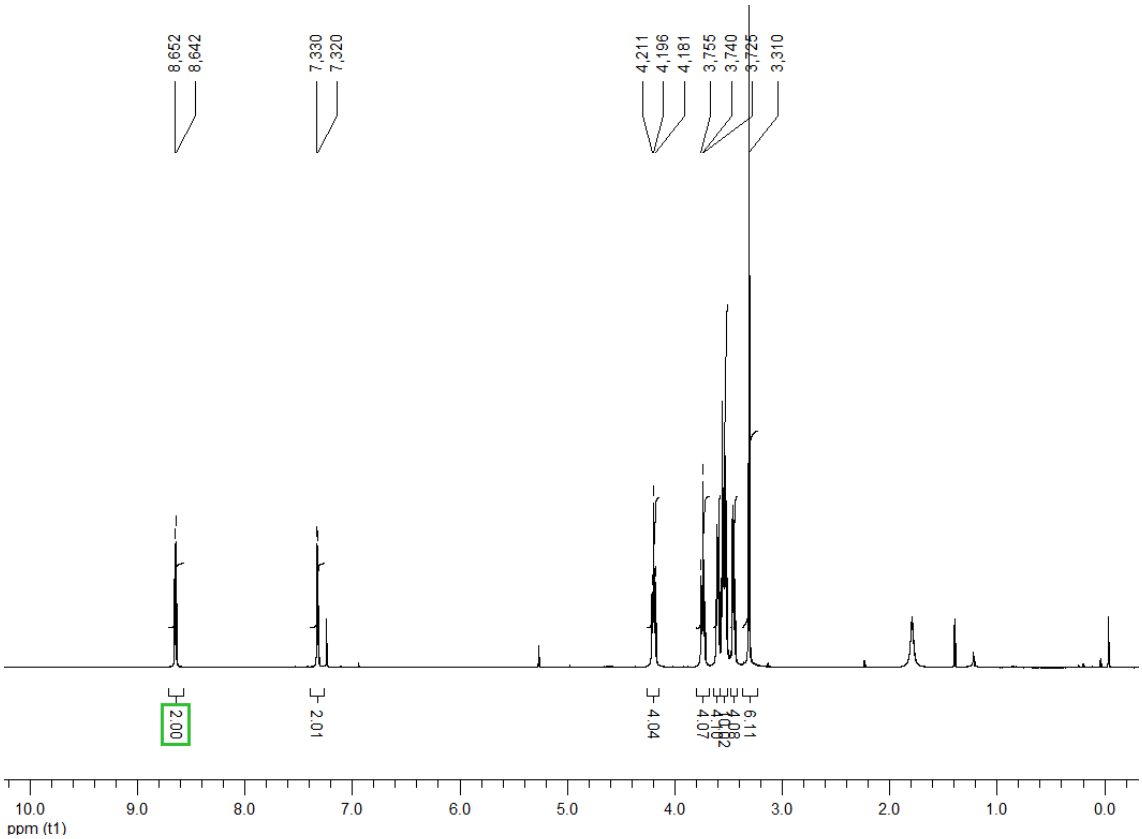


**Figure A21**. [1] H NMR spectrum of compound **4b** (400 MHz, $CDCl_3$).

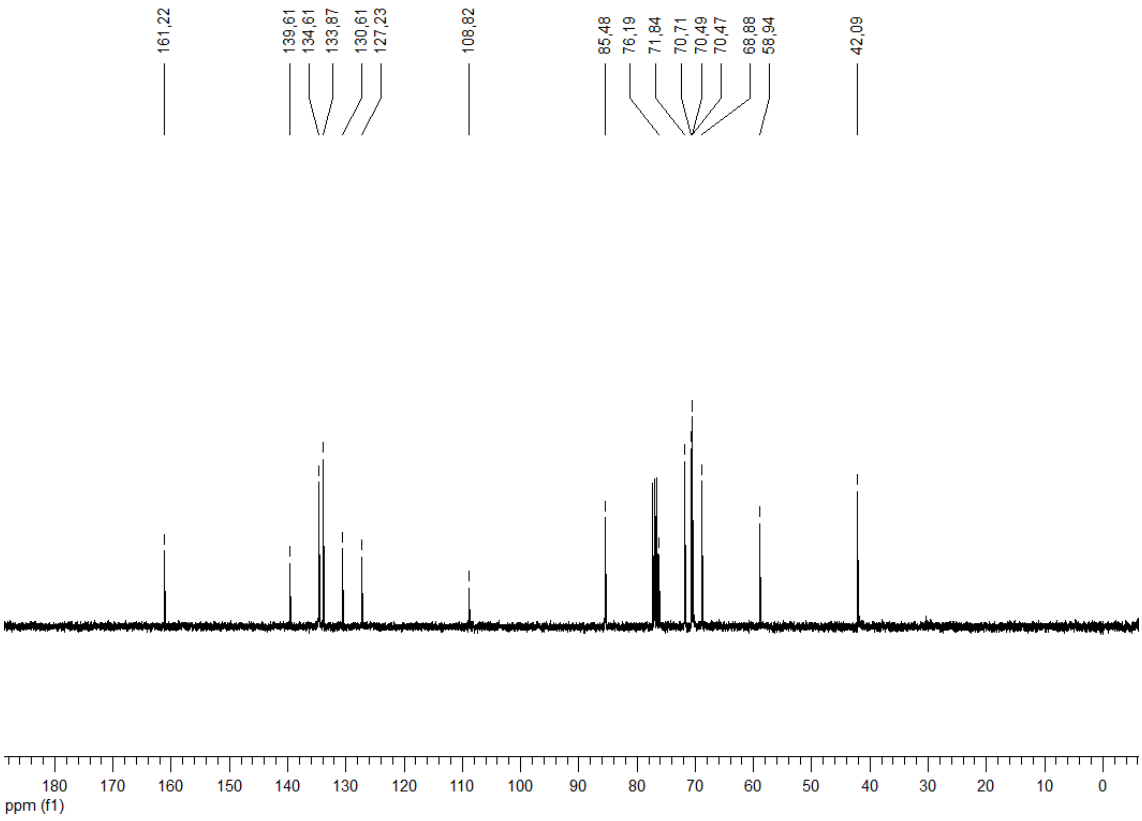


**Figure A22**. [13]C NMR spectrum of compound **4b** (100.6 MHz, $CDCl_3$).

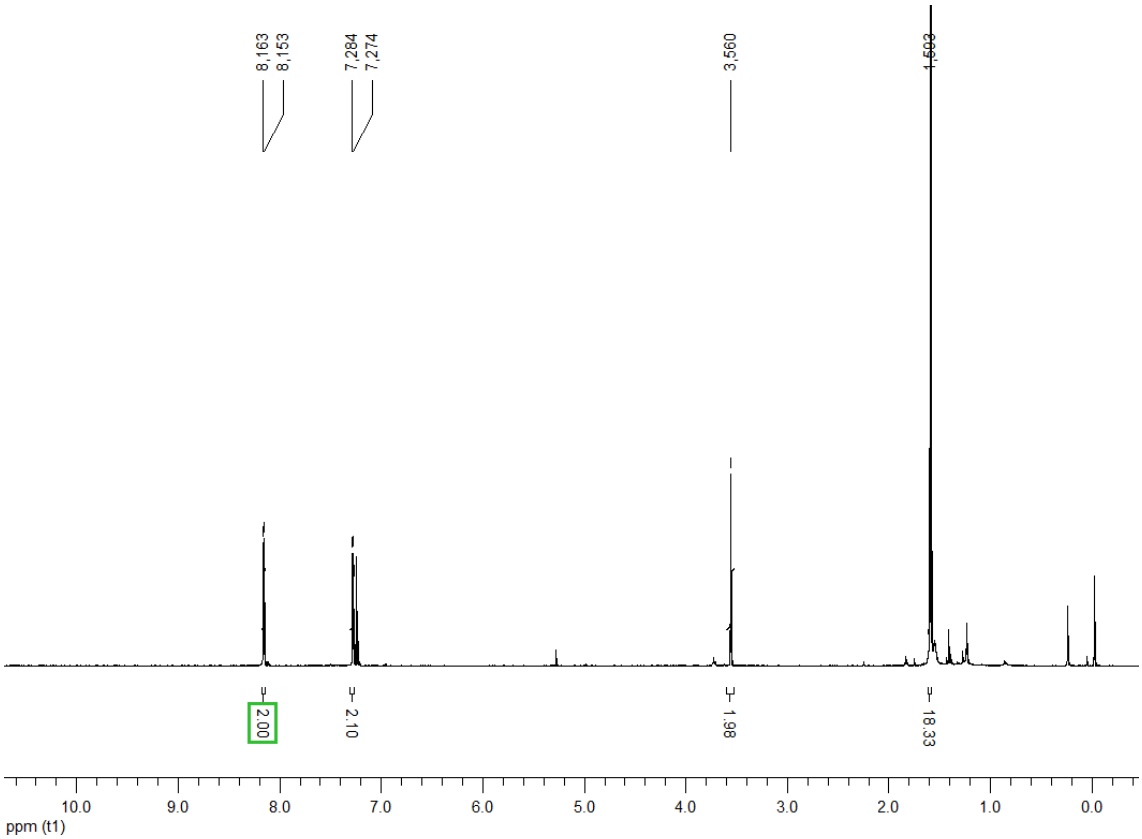


**Figure A23**. [1] H NMR spectrum of compound **4c** (400 MHz, $CDCl_3$).

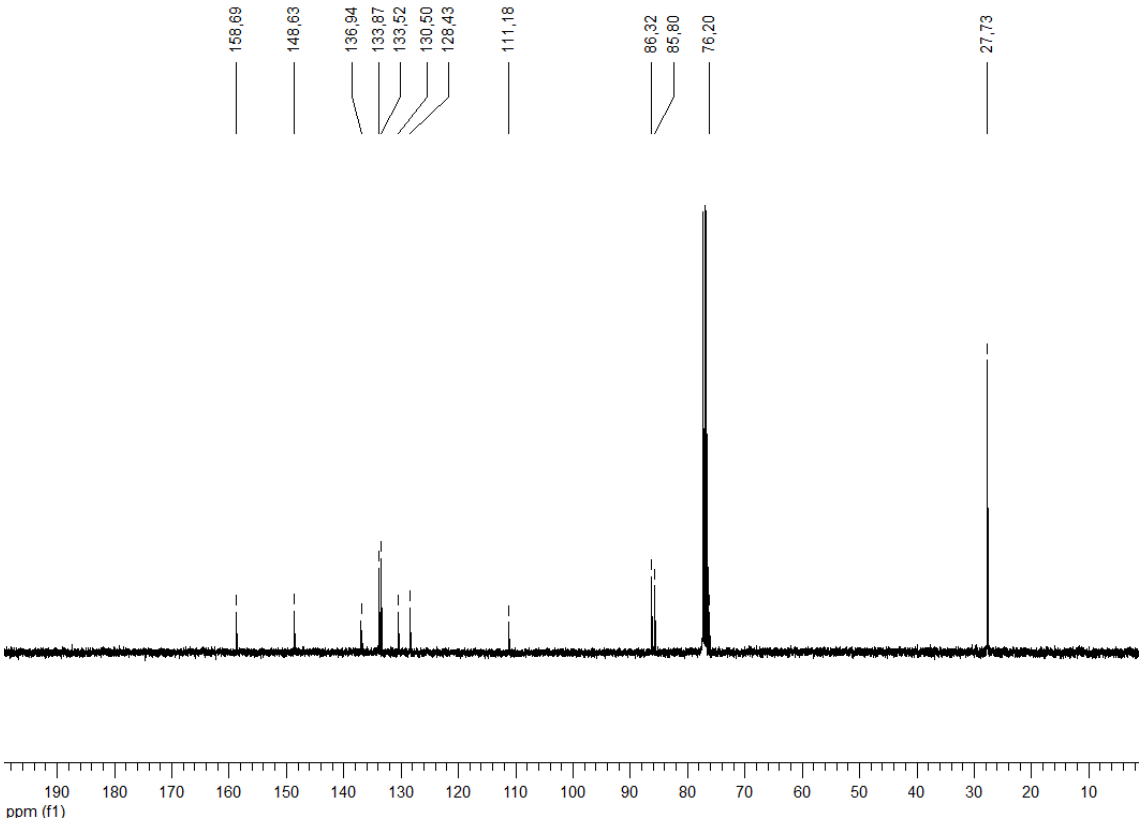


**Figure A24**. [13]C NMR spectrum of compound **4c** (100.6 MHz, $CDCl_3$).

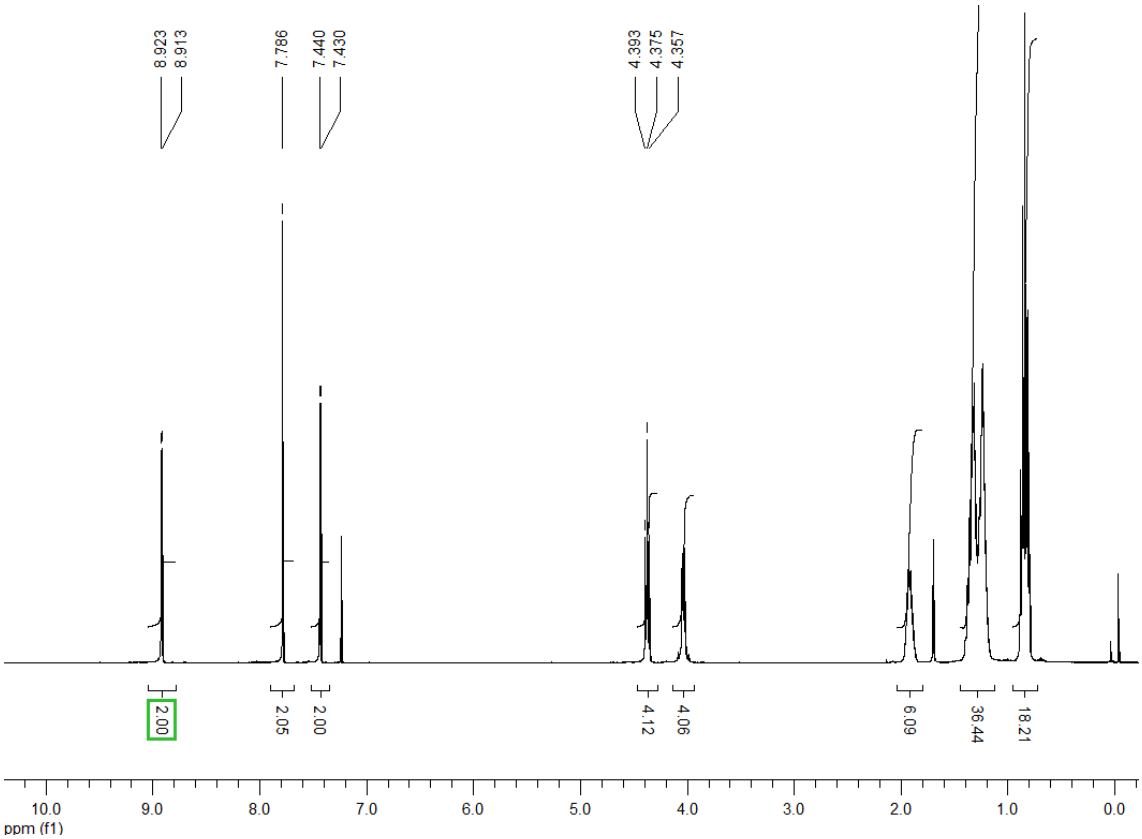


**Figure A25**. [1] H NMR spectrum of compound **5a** (400 MHz, $CDCl_3$).

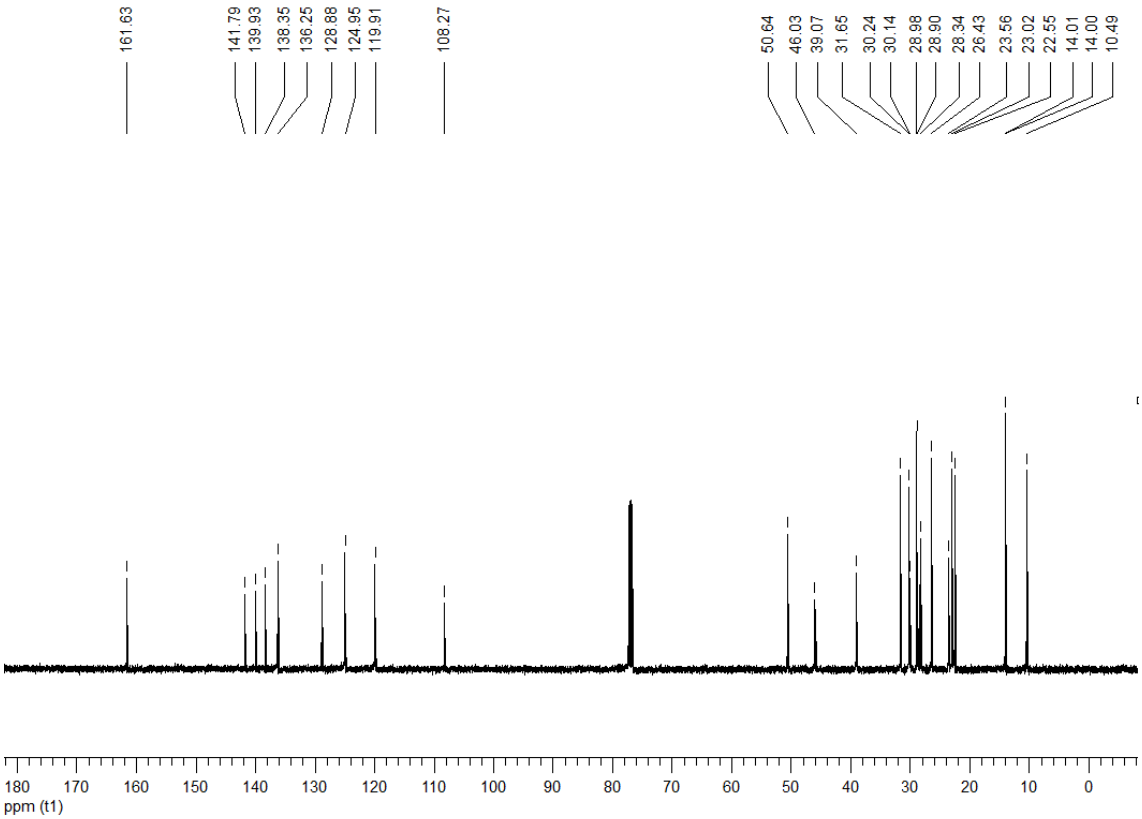


**Figure A26**. [13]C NMR spectrum of compound **5a** (100.6 MHz, $CDCl_3$).

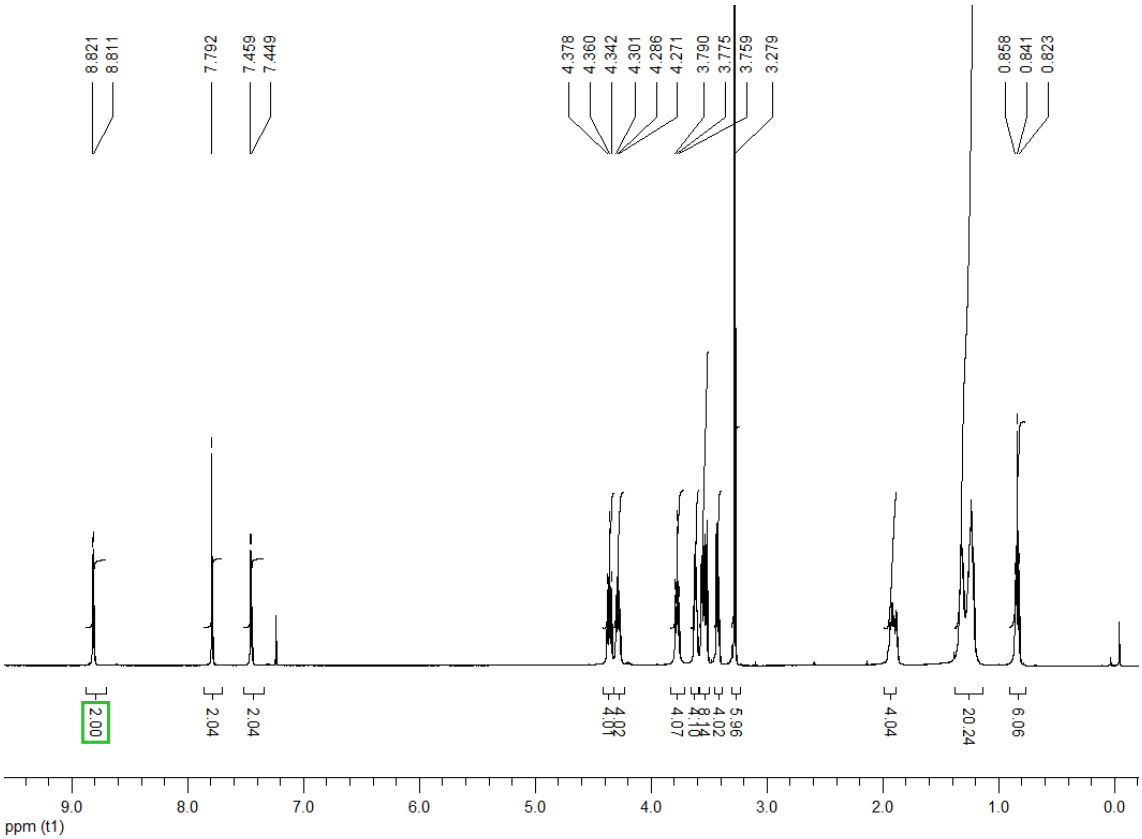


**Figure A27**. [1] H NMR spectrum of compound **5b** (400 MHz, $CDCl_3$).

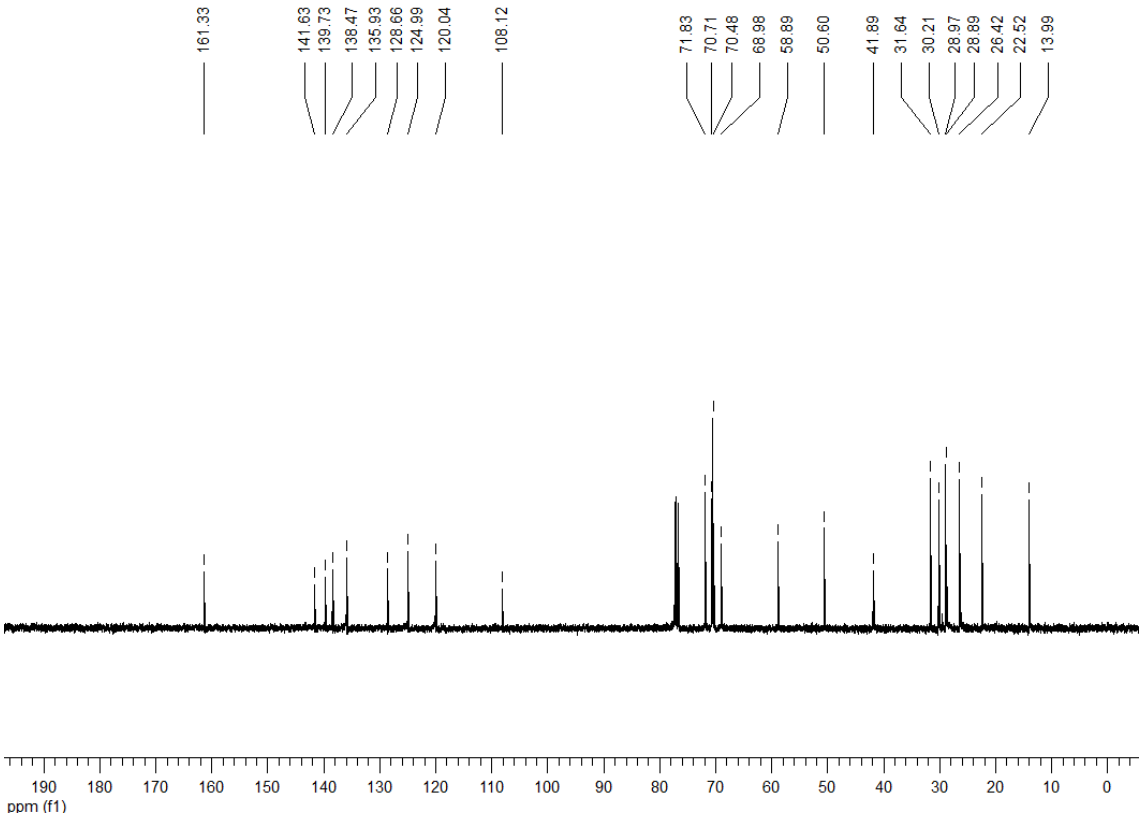


**Figure A28**. [13]C NMR spectrum of compound **5b** (100.6 MHz, $CDCl_3$).

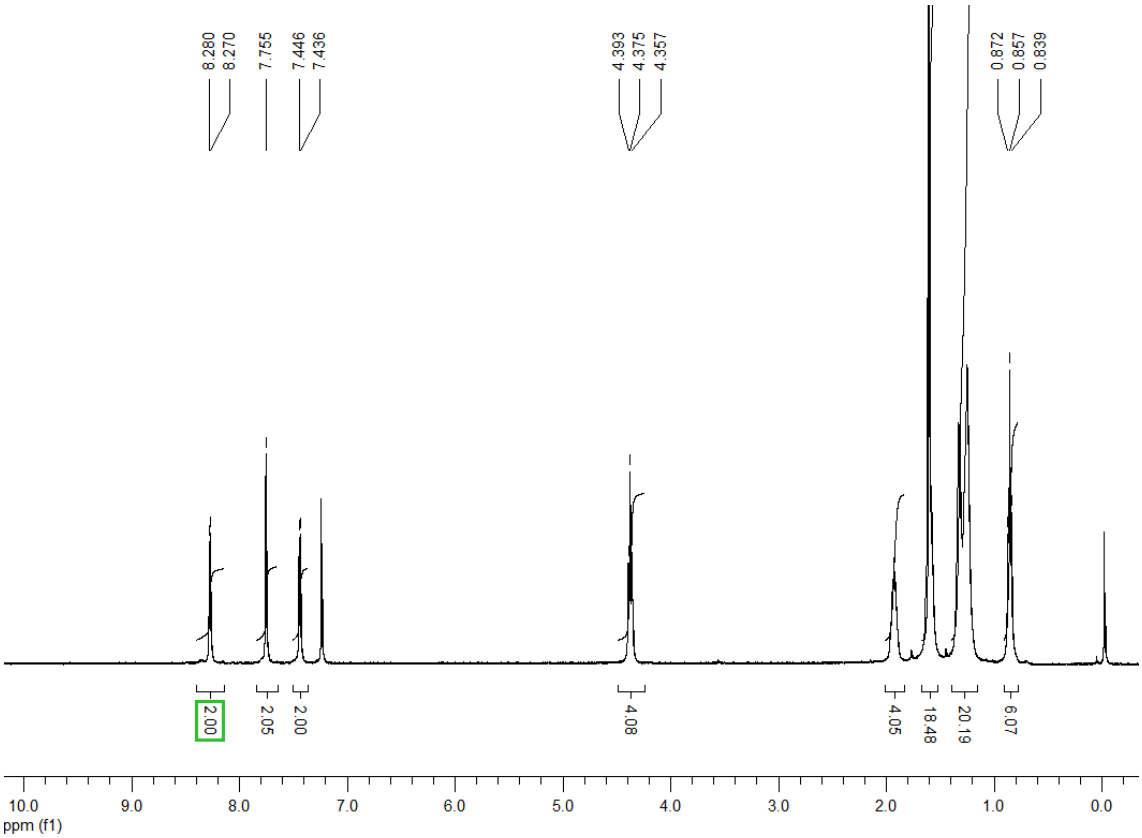


**Figure A29**. [1] H NMR spectrum of compound **5c** (400 MHz, $CDCl_3$).

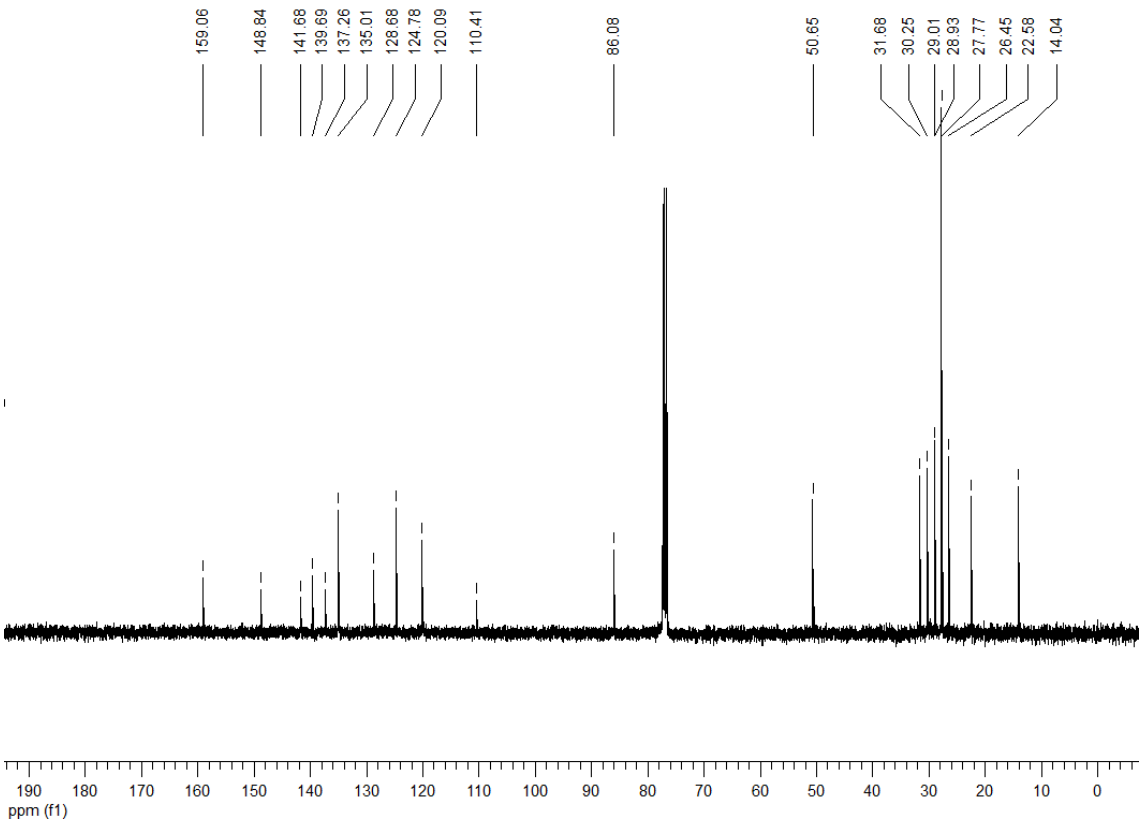


**Figure A30**. [13]C NMR spectrum of compound **5c** (100.6 MHz, $CDCl_3$).

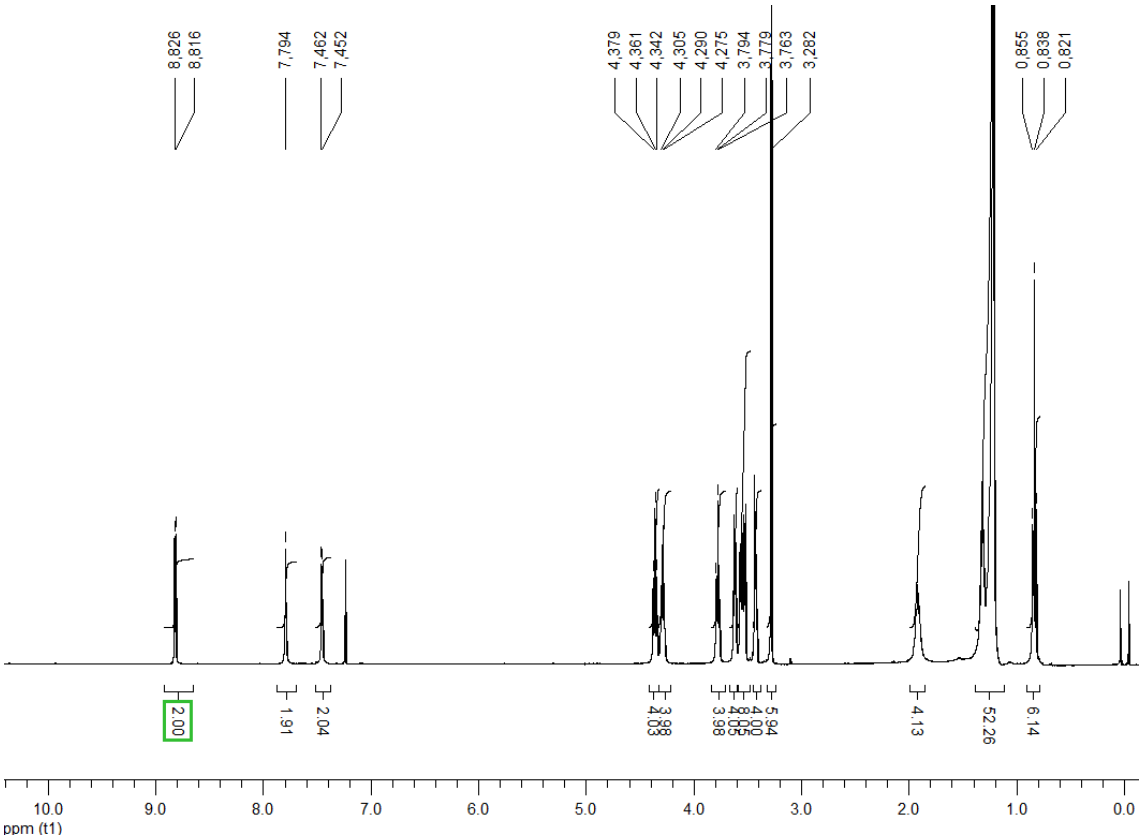


**Figure A31**. [1] H NMR spectrum of compound **5d** (400 MHz, $CDCl_3$).

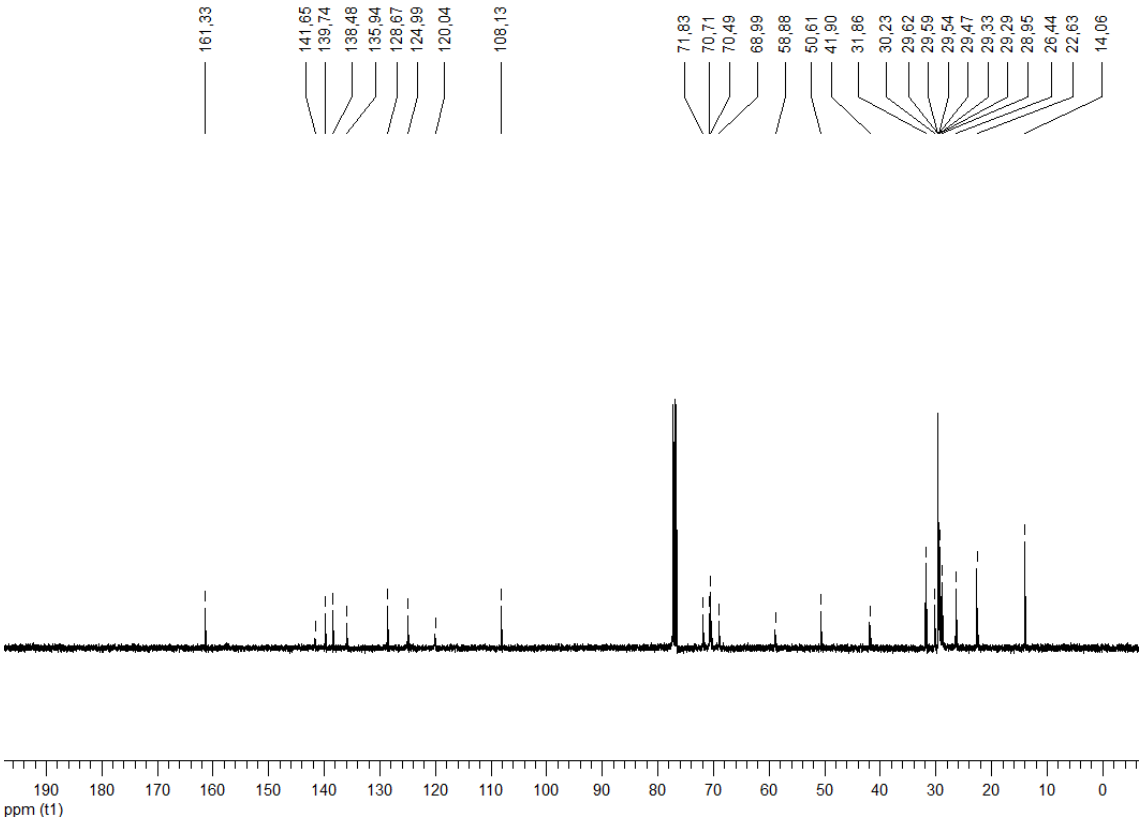


**Figure A32**. [13]C NMR spectrum of compound **5d** (100.6 MHz, $CDCl_3$).

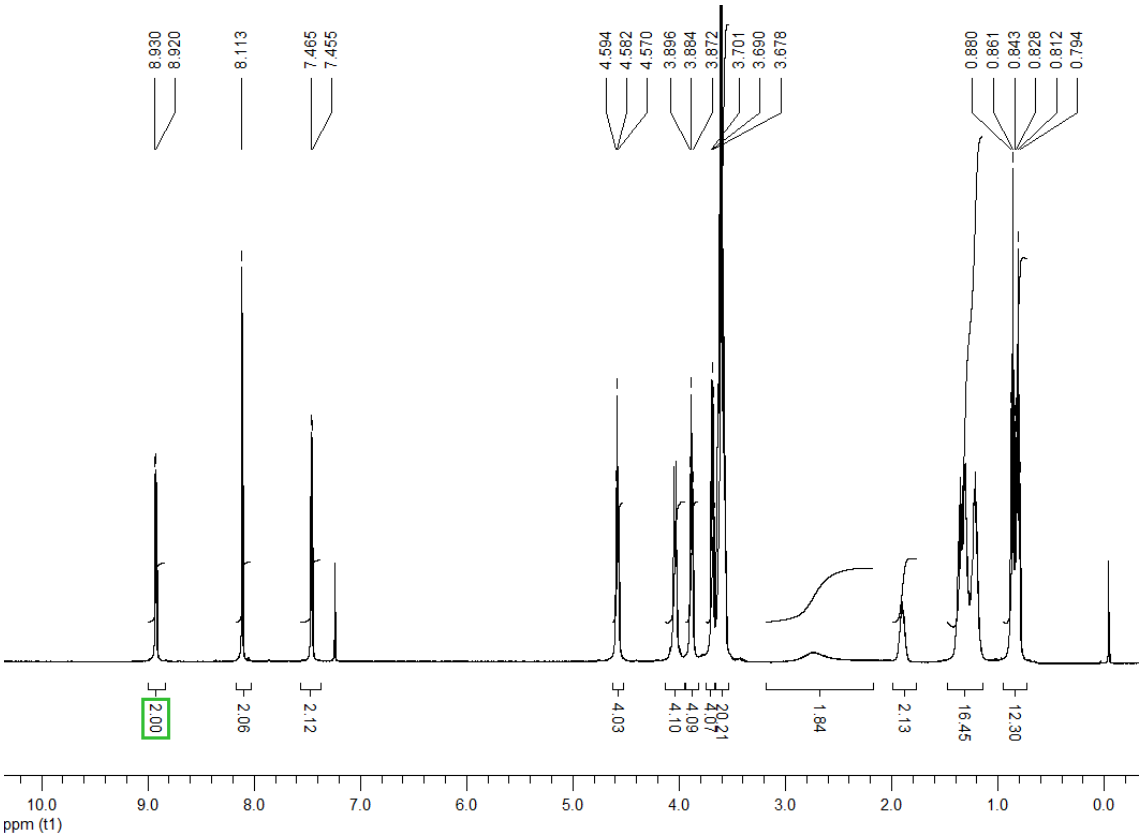


**Figure A33**. [1] H NMR spectrum of compound **5e** (400 MHz, $CDCl_3$).

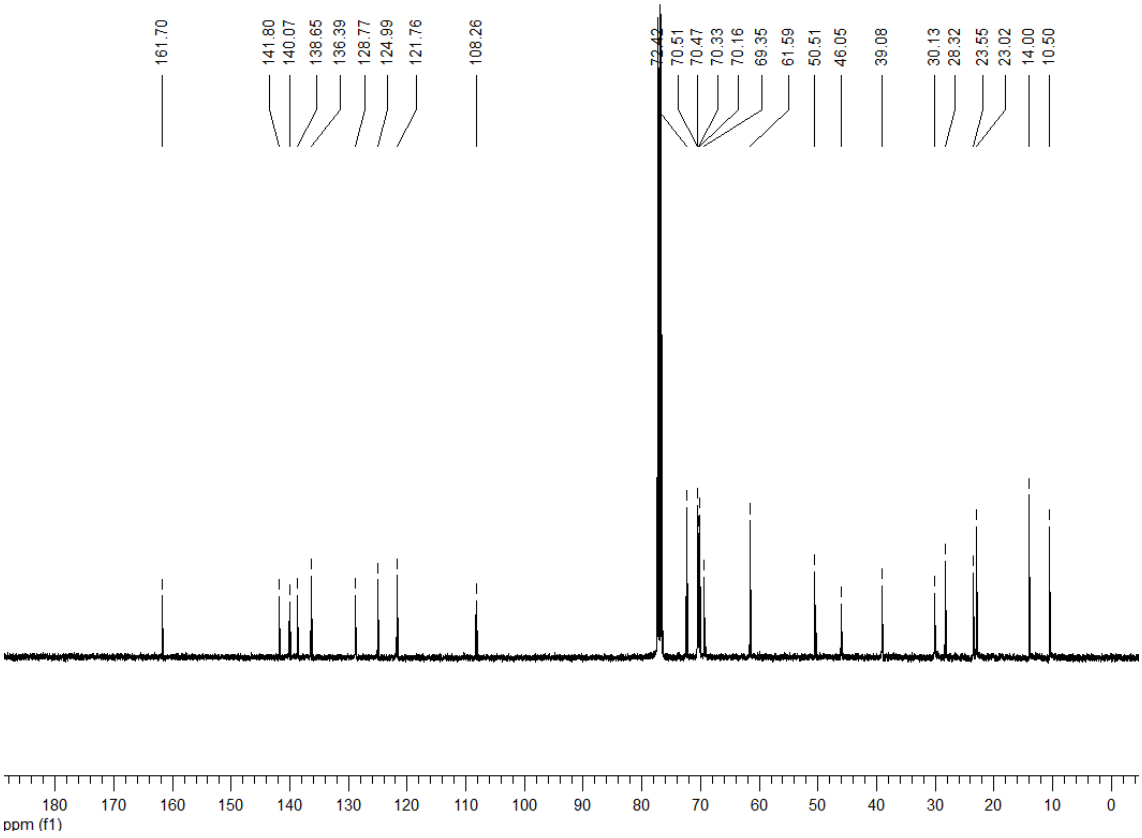


**Figure A34**. [13]C NMR spectrum of compound **5e** (100.6 MHz, $CDCl_3$).

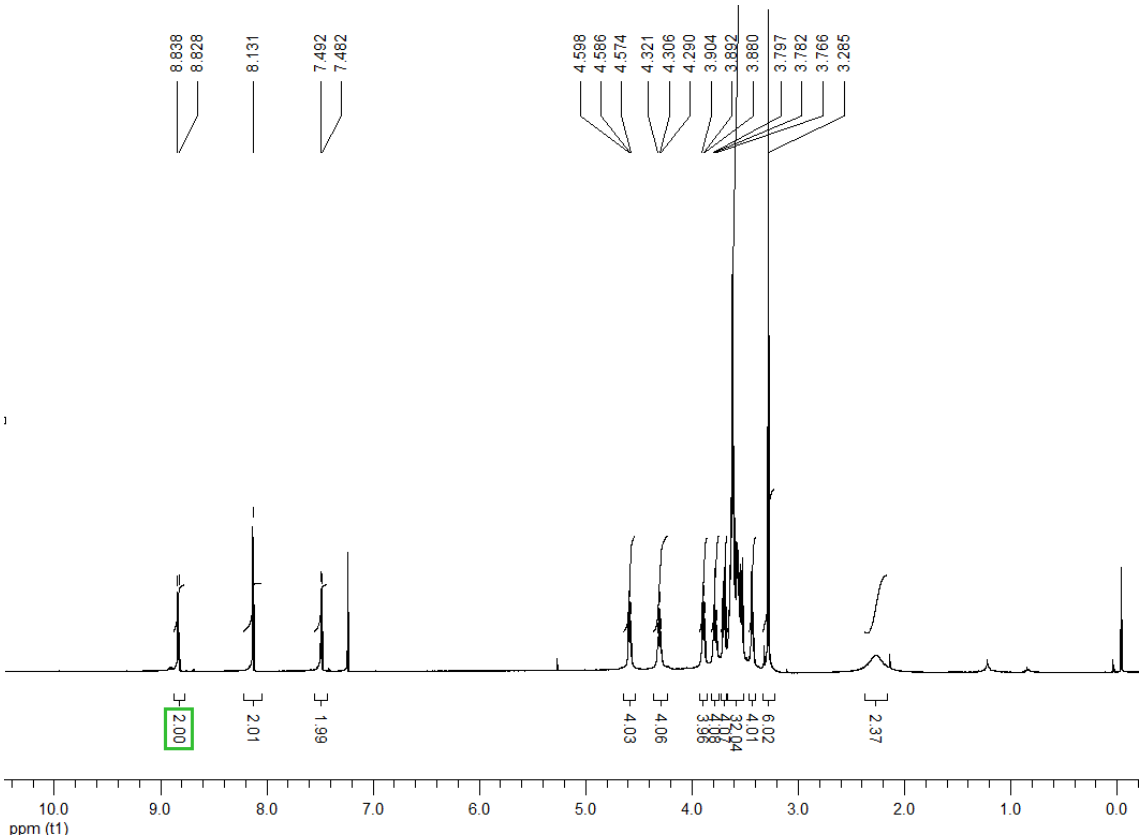


**Figure A35**. [1] H NMR spectrum of compound **5f** (400 MHz, $CDCl_3$).

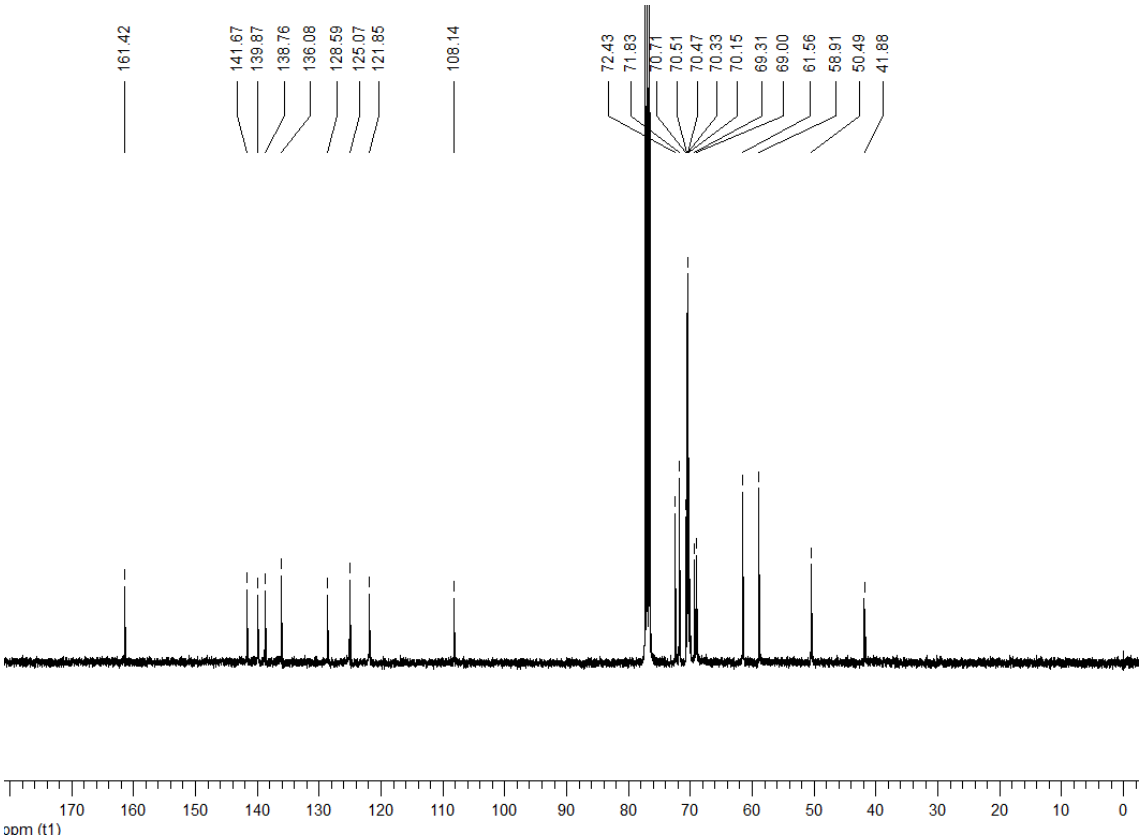


**Figure A36**. [13]C NMR spectrum of compound **5f** (100.6 MHz, $CDCl_3$).

# Bibliography

(1) Brabec, C. J.; Sariciftci, N. S.; Hummelen, J. C. Plastic Solar Cells. *Adv. Funct. Mater.* **2001**, *11* (1), 15–26.

(2) Stokheim, T. A.; Reynolds, J. R. *Handbook of Conducting Polymers*, 3rd Ed.; CRC Press: New York, 2007.

(3) van Mullekom, H. Developments in the Chemistry and Band Gap Engineering of Donor–acceptor Substituted Conjugated Polymers. *Mater. Sci. Eng. R Reports* **2001**, *32* (1), 1–40.

(4) Rostalski, J.; Meissner, D. Photocurrent Spectroscopy for the Investigation of Charge Carrier Generation and Transport Mechanisms in Organic P/n-Junction Solar Cells. *Sol. Energy Mater. Sol. Cells* **2000**, *63* (1), 37–47.

(5) Wöhrle, D.; Meissner, D. Organic Solar Cells. *Adv. Mater.* **1991**, *3* (3), 129–138.

(6) Allemand, P. M.; Koch, A.; Wudl, F.; Rubin, Y.; Diederich, F.; Alvarez, M. M.; Anz, S. J.; Whetten, R. L. Two Different Fullerenes Have the Same Cyclic Voltammetry. *J. Am. Chem. Soc.* **1991**, *113* (3), 1050–1051.

(7) Hoppe, H.; Niggemann, M.; Winder, C.; Kraut, J.; Hiesgen, R.; Hinsch, A.; Meissner, D.; Sariciftci, N. S. Nanoscale Morphology of Conjugated Polymer/Fullerene-Based Bulk-Heterojunction Solar Cells. *Adv. Funct. Mater.* **2004**, *14* (10), 1005–1011.

(8) Müllen, K.; Pisula, W. Donor–Acceptor Polymers. *J. Am. Chem. Soc.* **2015**, *137* (30), 9503–9505.

(9) Kitamura, C.; Tanaka, S.; Yamashita, Y. Design of Narrow-Bandgap Polymers. Syntheses and Properties of Monomers and Polymers Containing Aromatic-Donor and O-Quinoid-Acceptor Units. *Chem. Mater.* **1996**, *8* (2), 570–578.

(10) Markov, D. E.; Amsterdam, E.; Blom, P. W. M.; Sieval, A. B.; Hummelen, J. C. Accurate Measurement of the Exciton Diffusion Length in a Conjugated Polymer Using a Heterostructure with a Side-Chain Cross-Linked Fullerene Layer. *J. Phys. Chem. A* **2005**, *109* (24), 5266–5274.

(11) Stübinger, T.; Brütting, W. Exciton Diffusion and Optical Interference in Organic Donor–acceptor Photovoltaic Cells. *J. Appl. Phys.* **2001**, *90* (7).

(12) Yu, G.; Gao, J.; Hummelen, J. C.; Wudl, F.; Heeger, A. J. Polymer Photovoltaic Cells: Enhanced Efficiencies via a Network of Internal Donor-Acceptor Heterojunctions. *Sci.* **1995**, *270* (5243), 1789–1791.

(13) Yang, C. Y.; Heeger, A. J. Morphology of Composites of Semiconducting Polymers Mixed

with C60. *Synth. Met.* **1996**, *83* (2), 85–88.

(14) Wienk, M. M.; Kroon, J. M.; Verhees, W. J. H.; Knol, J.; Hummelen, J. C.; van Hal, P. A.; Janssen, R. A. J. Efficient Methano[70]fullerene/MDMO-PPV Bulk Heterojunction Photovoltaic Cells. *Angew. Chemie Int. Ed.* **2003**, *42* (29), 3371–3375.

(15) Yao, Y.; Shi, C.; Li, G.; Shrotriya, V.; Pei, Q.; Yang, Y. Effects of C70 Derivative in Low Band Gap Polymer Photovoltaic Devices: Spectral Complementation and Morphology Optimization. *Appl. Phys. Lett.* **2006**, *89* (15).

(16) Packan, P. A. Pushing the Limits. *Science (80-. ).* **1999**, *285* (5436), 2079 LP-2081.

(17) Kingon, A. I.; Maria, J.-P.; Streiffer, S. K. Alternative Dielectrics to Silicon Dioxide for Memory and Logic Devices . *Nature* **2000**, *406* (6799), 1032–1038.

(18) Pierre, A.; Sadeghi, M.; Payne, M. M.; Facchetti, A.; Anthony, J. E.; Arias, A. C. All-Printed Flexible Organic Transistors Enabled by Surface Tension-Guided Blade Coating. *Adv. Mater.* **2014**, *26* (32), 5722–5727.

(19) Gelinck, G. H.; Huitema, H. E. A.; van Veenendaal, E.; Cantatore, E.; Schrijnemakers, L.; van der Putten, J. B. P. H.; Geuns, T. C. T.; Beenhakkers, M.; Giesbers, J. B.; Huisman, B.-H.; et al. Flexible Active-Matrix Displays and Shift Registers Based on Solution-Processed Organic Transistors. *Nat Mater* **2004**, *3* (2), 106–110.

(20) Kronemeijer, A. J.; Gili, E.; Shahid, M.; Rivnay, J.; Salleo, A.; Heeney, M.; Sirringhaus, H. A Selenophene-Based Low-Bandgap Donor–Acceptor Polymer Leading to Fast Ambipolar Logic. *Adv. Mater.* **2012**, *24* (12), 1558–1565.

(21) Xu, J.; Wang, S.; Wang, G.-J. N.; Zhu, C.; Luo, S.; Jin, L.; Gu, X.; Chen, S.; Feig, V. R.; To, J. W. F.; et al. Highly Stretchable Polymer Semiconductor Films through the Nanoconfinement Effect. *Science (80-. ).* **2017**, *355* (6320), 59 LP-64.

(22) Vaklev, N. L.; Müller, R.; Muir, B. V. O.; James, D. T.; Pretot, R.; van der Schaaf, P.; Genoe, J.; Kim, J.-S.; Steinke, J. H. G.; Campbell, A. J. High-Performance Flexible Bottom-Gate Organic Field-Effect Transistors with Gravure Printed Thin Organic Dielectric. *Adv. Mater. Interfaces* **2014**, *1* (3), 1–6.

(23) Berggren, M.; Nilsson, D.; Robinson, N. D. Organic Materials for Printed Electronics. *Nat Mater* **2007**, *6* (1), 3–5.

(24) Sirringhaus, H. Organic Semiconductors: An Equal-Opportunity Conductor. *Nat Mater* **2003**, *2* (10), 641–642.

(25) Luo, C.; Kyaw, A. K. K.; Perez, L. A.; Patel, S.; Wang, M.; Grimm, B.; Bazan, G. C.; Kramer, E. J.; Heeger, A. J. General Strategy for Self-Assembly of Highly Oriented Nanocrystalline Semiconducting Polymers with High Mobility. *Nano Lett.* **2014**, *14* (5), 2764–2771.

(26) Tsao, H. N.; Mullen, K. Improving Polymer Transistor Performance via Morphology Control. *Chem. Soc. Rev.* **2010**, *39* (7), 2372–2386.

(27) Farnum, D. G.; Mehta, G.; Moore, G. G. I.; Siegal, F. P. Attempted Reformatskii Reaction of Benzonitrile, 1,4-Diketo-3,6-diphenylpyrrolo[3,4-C]pyrrole. A Lactam Analogue of Pentalene. *Tetrahedron Lett.* **1974**, *15* (29), 2549–2552.

(28) Grzybowski, M.; Gryko, D. T. Diketopyrrolopyrroles: Synthesis, Reactivity, and Optical Properties. *Adv. Opt. Mater.* **2015**, *3* (3), 280–320.

(29) Wu, P.-T.; Kim, F. S.; Jenekhe, S. A. New Poly(arylene Vinylene)s Based on Diketopyrrolopyrrole for Ambipolar Transistors. *Chem. Mater.* **2011**, *23* (20), 4618–4624.

(30) Qu, S.; Tian, H. Diketopyrrolopyrrole (DPP)-Based Materials for Organic Photovoltaics. *Chem. Commun.* **2012**, *48* (25), 3039–3051.

(31) Hendriks, K. H.; Heintges, G. H. L.; Gevaerts, V. S.; Wienk, M. M.; Janssen, R. A. J. High-Molecular-Weight Regular Alternating Diketopyrrolopyrrole-Based Terpolymers for Efficient Organic Solar Cells. *Angew. Chemie Int. Ed.* **2013**, *52* (32), 8341–8344.

(32) Kim, J.-H.; Lee, M.; Yang, H.; Hwang, D.-H. A High Molecular Weight Triisopropylsilylethynyl (TIPS)-Benzodithiophene and Diketopyrrolopyrrole-Based Copolymer for High Performance Organic Photovoltaic Cells. *J. Mater. Chem. A* **2014**, *2* (18), 6348–6352.

(33) Bürgi, L.; Turbiez, M.; Pfeiffer, R.; Bienewald, F.; Kirner, H.-J.; Winnewisser, C. High-Mobility Ambipolar Near-Infrared Light-Emitting Polymer Field-Effect Transistors. *Adv. Mater.* **2008**, *20* (11), 2217–2224.

(34) Bijleveld, J. C.; Zoombelt, A. P.; Mathijssen, S. G. J.; Wienk, M. M.; Turbiez, M.; de Leeuw, D. M.; Janssen, R. A. J. Poly(diketopyrrolopyrrole−terthiophene) for Ambipolar Logic and Photovoltaics. *J. Am. Chem. Soc.* **2009**, *131* (46), 16616–16617.

(35) Mei, J.; Graham, K. R.; Stalder, R.; Tiwari, S. P.; Cheun, H.; Shim, J.; Yoshio, M.; Nuckolls, C.; Kippelen, B.; Castellano, R. K.; et al. Self-Assembled Amphiphilic Diketopyrrolopyrrole-Based Oligothiophenes for Field-Effect Transistors and Solar Cells. *Chem. Mater.* **2011**, *23* (9), 2285–2288.

(36) Kanimozhi, C.; Yaacobi-Gross, N.; Chou, K. W.; Amassian, A.; Anthopoulos, T. D.; Patil, S.

Diketopyrrolopyrrole–Diketopyrrolopyrrole-Based Conjugated Copolymer for High-Mobility Organic Field-Effect Transistors. *J. Am. Chem. Soc.* **2012**, *134* (40), 16532–16535.

(37) Kanimozhi, C.; Yaacobi-Gross, N.; Burnett, E. K.; Briseno, A. L.; Anthopoulos, T. D.; Salzner, U.; Patil, S. Use of Side-Chain for Rational Design of N-Type Diketopyrrolopyrrole-Based Conjugated Polymers: What Did We Find Out? *Phys. Chem. Chem. Phys.* **2014**, *16* (32), 17253–17265.

(38) Chang, W.-H.; Gao, J.; Dou, L.; Chen, C.-C.; Liu, Y.; Yang, Y. Side-Chain Tunability via Triple Component Random Copolymerization for Better Photovoltaic Polymers. *Adv. Energy Mater.* **2014**, *4* (4), n/a-n/a.

(39) Kaur, M.; Choi, D. H. Diketopyrrolopyrrole: Brilliant Red Pigment Dye-Based Fluorescent Probes and Their Applications. *Chem. Soc. Rev.* **2015**, *44* (1), 58–77.

(40) Søndergaard, R.; Helgesen, M.; Jørgensen, M.; Krebs, F. C. Fabrication of Polymer Solar Cells Using Aqueous Processing for All Layers Including the Metal Back Electrode. *Adv. Energy Mater.* **2011**, *1* (1), 68–71.

(41) Punzi, A.; Maiorano, E.; Nicoletta, F.; Blasi, D.; Ardizzone, A.; Ventosa, N.; Ratera, I.; Veciana, J.; Farinola, G. M. 1,2,3-Triazole–Diketopyrrolopyrrole Derivatives with Tunable Solubility and Intermolecular Interactions. *European J. Org. Chem.* **2016**, *2016* (15), 2617–2627.

(42) Zhang, G.; Li, H.; Bi, S.; Song, L.; Lu, Y.; Zhang, L.; Yu, J.; Wang, L. A New Turn-on Fluorescent Chemosensor Based on Diketopyrrolopyrrole (DPP) for Imaging Zn2+ in Living Cells. *Analyst* **2013**, *138* (20), 6163–6170.

(43) Ftouni, H.; Bolze, F.; de Rocquigny, H.; Nicoud, J.-F. Functionalized Two-Photon Absorbing Diketopyrrolopyrrole-Based Fluorophores for Living Cells Fluorescent Microscopy. *Bioconjug. Chem.* **2013**, *24* (6), 942–950.

(44) Heyer, E.; Lory, P.; Leprince, J.; Moreau, M.; Romieu, A.; Guardigli, M.; Roda, A.; Ziessel, R. Highly Fluorescent and Water-Soluble Diketopyrrolopyrrole Dyes for Bioconjugation. *Angew. Chemie* **2015**, *127* (10), 3038–3042.

(45) Cardona, C. M.; Li, W.; Kaifer, A. E.; Stockdale, D.; Bazan, G. C. Electrochemical Considerations for Determining Absolute Frontier Orbital Energy Levels of Conjugated Polymers for Solar Cell Applications. *Adv. Mater.* **2011**, *23* (20), 2367–2371.

(46) Punzi, A.; Nicoletta, F.; Marzano, G.; Fortuna, C. G.; Dagar, J.; Brown, T. M.; Farinola, G. M. Synthetic Routes to TEG-Substituted Diketopyrrolopyrrole-Based Low Band-Gap Polymers.

*European J. Org. Chem.* **2016**, *2016* (19), 3233–3242.

(47) Marzano, G.; Kotowski, D.; Babudri, F.; Musio, R.; Pellegrino, A.; Luzzati, S.; Po, R.; Farinola, G. M. Tin-Free Synthesis of a Ternary Random Copolymer for BHJ Solar Cells: Direct (Hetero)arylation versus Stille Polymerization. *Macromolecules* **2015**, *48* (19), 7039–7048.

(48) Morin, P.-O.; Bura, T.; Leclerc, M. Realizing the Full Potential of Conjugated Polymers: Innovation in Polymer Synthesis. *Mater. Horizons* **2016**, *3* (1), 11–20.

(49) Grenier, F.; Aïch, B. R.; Lai, Y.-Y.; Guérette, M.; Holmes, A. B.; Tao, Y.; Wong, W. W. H.; Leclerc, M. Electroactive and Photoactive Poly[Isoindigo-Alt-EDOT] Synthesized Using Direct (Hetero)Arylation Polymerization in Batch and in Continuous Flow. *Chem. Mater.* **2015**, *27* (6), 2137–2143.

(50) Mei, J.; Bao, Z. Side Chain Engineering in Solution-Processable Conjugated Polymers. *Chem. Mater.* **2014**, *26* (1), 604–615.

(51) Bijleveld, J. C.; Karsten, B. P.; Mathijssen, S. G. J.; Wienk, M. M.; de Leeuw, D. M.; Janssen, R. A. J. Small Band Gap Copolymers Based on Furan and Diketopyrrolopyrrole for Field-Effect Transistors and Photovoltaic Cells. *J. Mater. Chem.* **2011**, *21* (5), 1600–1606.

(52) Susanna, G.; Salamandra, L.; Ciceroni, C.; Mura, F.; Brown, T. M.; Reale, A.; Rossi, M.; Di Carlo, A.; Brunetti, F. 8.7% Power Conversion Efficiency Polymer Solar Cell Realized with Non-Chlorinated Solvents. *Sol. Energy Mater. Sol. Cells* **2015**, *134*, 194–198.

(53) Sirringhaus, H. 25th Anniversary Article: Organic Field-Effect Transistors: The Path Beyond Amorphous Silicon. *Adv. Mater.* **2014**, *26* (9), 1319–1335.

(54) Liu, C.; Wang, K.; Hu, X.; Yang, Y.; Hsu, C.-H.; Zhang, W.; Xiao, S.; Gong, X.; Cao, Y. Molecular Weight Effect on the Efficiency of Polymer Solar Cells. *ACS Appl. Mater. Interfaces* **2013**, *5* (22), 12163–12167.

(55) Wang, Y.; Yang, F.; Liu, Y.; Peng, R.; Chen, S.; Ge, Z. New Alkylfuranyl-Substituted Benzo[1,2-b:4,5-B']dithiophene-Based Donor–Acceptor Polymers for Highly Efficient Solar Cells. *Macromolecules* **2013**, *46* (4), 1368–1375.

(56) Woong Jung, J.; Woong Jo, J.; Liu, F.; Russell, T. P.; Ho Jo, W. A Low Band-Gap Polymer Based on Unsubstituted benzo[1,2-b:4,5-B[prime or Minute]]dithiophene for High Performance Organic Photovoltaics. *Chem. Commun.* **2012**, *48* (55), 6933–6935.

(57) Intemann, J. J.; Yao, K.; Yip, H.-L.; Xu, Y.-X.; Li, Y.-X.; Liang, P.-W.; Ding, F.-Z.; Li, X.; Jen, A. K.-Y. Molecular Weight Effect on the Absorption, Charge Carrier Mobility, and Photovoltaic

Performance of an Indacenodiselenophene-Based Ladder-Type Polymer. *Chem. Mater.* **2013**, *25* (15), 3188–3195.

(58) Li, K.; Liu, B. Polymer-Encapsulated Organic Nanoparticles for Fluorescence and Photoacoustic Imaging. *Chem. Soc. Rev.* **2014**, *43* (18), 6570–6597.

(59) Naik, M. A.; Venkatramaiah, N.; Kanimozhi, C.; Patil, S. Influence of Side-Chain on Structural Order and Photophysical Properties in Thiophene Based Diketopyrrolopyrroles: A Systematic Study. *J. Phys. Chem. C* **2012**, *116* (50), 26128–26137.

(60) Tamayo, A. B.; Walker, B.; Nguyen*, T.-Q. A Low Band Gap, Solution Processable Oligothiophene with a Diketopyrrolopyrrole Core for Use in Organic Solar Cells. *J. Phys. Chem. C* **2008**, *112* (30), 11545–11551.

(61) Belfield, K. D.; Bondar, M. V; Hernandez, F. E.; Przhonska, O. V; Yao, S. Two-Photon Absorption of a Supramolecular Pseudoisocyanine J-Aggregate Assembly. *Chem. Phys.* **2006**, *320* (2–3), 118–124.